Stony Brook University

In Situ Chemically Crosslinked Carbon Nanomaterial Coatings and Films for Tissue Engineering Applications

A Dissertation Presented

by

Sunny Patel

to

The Graduate School

in Partial Fulfillment of the

Requirements

for the Degree of

Doctor of Philosophy

in

Biomedical Engieering

Stony Brook University

December 2015

Stony Brook University

The Graduate School

Sunny Patel

We, the dissertation committee for the above candidate for the

Doctor of Philosophy degree, hereby recommend

acceptance of this dissertation.

Dr. Balaji Sitharaman– Dissertation Advisor
Associate Professor, Department of Biomedical Engineering

Dr. Yi-Xian Qin - Chairperson of Defense
Professor, Department of Biomedical Engineering

Dr. Eric Brouzes – Committee Member of Dissertation Defense
Assistant Professor, Department of Biomedical Engineering

Dr. Yizhi Meng – Committee Member of Dissertation Defense
Assistant Professor, Department of Materials Science and Engineering

This dissertation is accepted by the Graduate School

Charles Taber
Dean of the Graduate School

Abstract of the Dissertation

***In Situ* Chemically Crosslinked Carbon Nanomaterial Coatings and Films for Tissue Engineering Applications**

by

Sunny Patel

Doctor of Philosophy

in

Biomedical Engieering

Stony Brook University

2015

A current limitation in translating nanotechnology research into the many industries is the assembly of the nanostructural building blocks into complex 2D or 3D structures. Although carbon nanomaterials have shown a great deal of prospect in biomedical engineering, this limitation strongly hinders many translatable biomedical applications for these materials. Weak bonding between the nanoparticles can lead to loose nanomaterial related toxicity and the lack of robustness in devices. In this work we developed a facile and scalable method to develop chemically crosslinked carbon nanomaterial thin films and coatings for biomedical applications. We developed crosslinked coatings of carbon nanotubes and graphene of different diameters and lengths. We present the in vitro cytocompatibility and stem cell differentiation capability of these coatings using human adipose derived stem cells. Our results indicate little or no cellular toxicity on these coatings. We also observed nanoparticle size and chemistry related dependence on the ability for stem cells to differentiate towards osteogenic lineages on these coatings. The results suggest potential for these coatings as surfaces for enhanced osseointegration in orthopedic applications.

Dedication

For my father and my mother –

For their sacrifices, for their love, for which I am eternally grateful

(Chandrakant Patel and Varsha Patel)

Table of Contents

List of Figures/Tables/Illustrations

Figures

Tables

Acknowledgments

As I sit at my desk to write this thesis, a quote which is framed over my desk reads, “Gratitude is not only the greatest of virtues, but the parent of all the others.” I see this quote every day as I sit at my desk to write and contemplate where the next words are going to come from. Truly those words, the ability to disseminate information in this text originates from those I have previously learned from and continue to learn from today. Gratitude is due to all of those people who have influenced me in this process and I can humbly try to extend my gratitude here.

In this process, the most influential figure in my academic career has been my advisor and mentor, Dr. Balaji Sitharaman. I have been a part of his research group since early in my undergraduate career. As a mentor, he provided me the utmost amount of freedom to learn, discover, and try new things with little hesitancy while also providing me with criticism to drive me, to better myself in my academic and professional career. For about the past seven years, I have learned so much from you and I will work hard to honor your name as my advisor in my future endeavors.

I would like to thank my dissertation committee members Dr. Balaji Sitharaman, Dr. Yi-Xian Qin, Dr. Eric Brouzes, and Dr. Yizhi Meng. Each of you brought a unique background and depth of knowledge to this project. The insights and suggestions I have gained from you have truly strengthened this work. I am honored to defend my thesis in front of a group of such well respected and successful professors.

I would like to thank all of my collaborators. From the lab of Dr. Yi-Xian Qin; I would like to thank Tony Zhang and Kartikey Grover for assisting with determining the mechanical properties of the carbon nanomaterial coatings. Your expertise provided foundational work on this project and I appreciate your collaboration. I would also like to thank Gaurav Lalwani, who I started my graduate career collaborating with (and is now Dr. Gaurav Lalwani!). His work on three dimensional carbon nanomaterial architectures inspired the second generation of crosslinked carbon nanoparticle research. I would also like to thank two of my undergraduate students, Kevin Guerrero and Kamal James, for their assistance in these projects. Lastly, but certainly not least, I would like to thank Owais Alam. Very few undergraduates I have seen, ever work so diligently and are driven to contribute to the work with such enthusiasm. I have seen how much you have learned and through that you have contributed to this project in many ways. For all of those hours we sat and systematically troubleshooted the spray coating device, I could not imagine many people who would go through that with such high energy. I am honored to have been your graduate student mentor and I wish you the utmost success in your career and personal life.

I would like to thank all of the people who have supported this work. I would like to thank the support of Dr. Fernando Camino at the Center for Functional Nanomaterials (Brookhaven National Laboratory) and his colleagues who trained me on their high-end characterization resources. Center for Functional Nanomaterials has been an invaluable resource

to this project and I couldn't have done this work with their facility and expertise. I would also like to thank all the other faculty in the Department of Biomedical Engineering who shared their valuable insights on my work and inspired me to pursue my doctoral degree, namely Dr. Richard Clark, Dr. Mary Frame, Dr. Helmut Strey, and Dr. David Rubenstein (for his insights on the immunofluorescence study of this work). I would also like to thank Dr. Guowei Tian at the Central Molecular Imaging Center for assistance with confocal microscopy. I would also like to thank Jesse Kuhn and the team at the OSA Supply Center for constantly providing support, especially when we 'urgently' needed to start experiments.

My lab members and my colleagues are especially ones to acknowledge because they are not only colleagues but also some excellent and dear friends. A special thank you goes to Jason Rashkow, Yahfi Talukdar, Stephen Lee, and Shawn Xie. You have provided me with great suggestions and criticism of my work. However, more than that I remember the fun moments that carried us through these years. While the PhD process seems frightening at times, in retrospect it is because of friends like you that it is one of the most enjoyable times of my life. Dr. Sayan Mullick Chowdhury, thank you for your inputs, help with understanding the cytotoxicity component of my work, and the fun times we had throughout your time here. Dr. Shruti Kanakia thank you for your well spirted nature and always keeping the lab in check. I would also like to thank the other members of Dr. Sitharaman's lab (present and past): Dr. Pramod Avti, Dr. Danielle Green, Cassandra Suhrland, and Saathyaki Rajamani for their support throughout these years.

I am at a loss for words when I have to thank my parents, Chandrakant Patel (my father) and Varsha Patel (my mother). With my parents I have to also thank my sister, Dhara Patel, who I grew up learning from and continue to learning from today. I will try to express my gratitude to you throughout my life for instilling values in me, unconditionally loving me, providing me the opportunity to do everything I want, and for all of those things that words are not cut out to say.

I also appreciate the support of the Stony Brook University community, the Department of Biomedical Engineering, and all of the other individuals I have interacted with throughout my academic career.

This work was sponsored by National Institutes of Health grants (1DP2OD007394 and AR61821). The work at the Center for Functional Nanomaterials at BNL, was supported by the U.S. Department of Energy, Office of Basic Energy Sciences, under Contract No. DE-AC02-98CH10886.

List of Publications

Peer-Reviewed Journal Articles

Sunny C. Patel, Owais Alam, Balaji Sitharaman. "Osteogenic Differentiation of Human Adipose Derived Stem Cells on Chemically Crosslinked Carbon Nanomaterial Coatings." *In Preperation*

Sunny C. Patel, Owais Alam, Tony Zhang, Kartikey Grover, Yi-Xian Qin, Balaji Sitharaman. "Layer-on-Layer Assembly of 2D and 3D Crosslinked Carbon Nanomaterial Architectures by Ultrasonic Spray Deposition." *In Preparation*

Sunny C. Patel, Stephen Lee, Gaurav Lalwani, Cassandra Suhrland, Sayan Mullick-Chowdhury, Balaji Sitharaman. "Graphene Based Platforms for Cancer Therapeutics." *Under Review: Future Science: Therapeutic Delivery 2015*

Sunny C. Patel, Gaurav Lalwani, Kartikey Grover, Yi-Xian Qin, Balaji Sitharaman. "Fabrication and Cytocompatibility of In Situ Crosslinked Carbon Nanomaterial Films." *Nature Scientific Reports,* 2015.

Shawn X. Xie, Fuqiang Gao, Sunny C. Patel, John H. Booske, Susan C. Hagness, Balaji Sitharaman. "Clinically Relevant CNT Dispersions with Exceptionally High Dielectric Properties for Microwave Theranostic Applications." *IEEE Transactions On Biomedical Engineering,* 2014.

Jason T. Rashkow, Sunny C. Patel, Ryan Tappero, Balaji Sitharaman. "Quantification of single-cell nanoparticle concentrations and the distribution of these concentrations in cell population." *Interface,* 2014.

Shawn X. Xie, Fuqiang Gao, Sunny C. Patel, John H. Booske, Susan C. Hagness, Balaji Sitharaman. "Effect of Synthesis and Acid Purification Methods on the Microwave Dielectric Properties of Single-Walled Carbon Nanotube (SWCNT) Aqueous Dispersions." *Applied Physics Letters,* 2013.

Gaurav Lalwani, Andrea Trinward Kwaczala, Shruti Kanakia, Sunny C. Patel, Stefan Judex, Balaji Sitharaman. "Fabrication and Characterization of Three-Dimensional Macroscopic All-Carbon Scaffolds." *Carbon*, 2013.

Textbook Chapters

Pramod Avti, Sunny C. Patel, Pushpinder Uppal, Grace O'Malley, Joe Garlow, Balaji Sitharaman. *Tissue Engineering: Principles and Practices*. "Nanobiomaterials for Tissue Engineering." CRC PRESS, Taylor & Francis Group (ISBN: 9781439874004) 2012.

Pramod Avti, Sunny C. Patel, Balaji Sitharaman. *Nanobiomaterials Handbook*. "Nanobiomaterials: Current and Future Prospects." CRC PRESS, Taylor & Francis Group (ISBN: 9781420094664) 2012.

Chapter 1

Carbon Nanomaterial Films and Coatings for Tissue Engineering and other Biomedical Applications

Introduction

Carbon nanomaterials are sp^2 hybridized, graphitic structures which exist in various shapes and nanoarchitectures (Figure 1.1).[1] The earliest of these nanomaterials are perhaps spherical fullerenes.[2] Planar sheets of sp^2 hybridized carbon are known as graphene; which can be nanosized platelets or large area sheets, single-layer thick or multilayered (<100nm thickness), and pristine, oxidized, or reduced.[3] Most commonly used for biomedical applications are graphene oxide nanoplatelets (GONP) and single layered graphene.[4] Carbon nanotubes are tubular structures of sp^2 hybridized carbon which can consist of single-walled carbon nanotubes (SWCNT), double walled carbon nanotubes (DWCNT) or multiwalled carbon nanotubes (MWCNT).[5] Recently, oxidative unzipping of carbon nanotubes have led to a new graphene structure known as graphene oxide nanoribbons (GONR).[6] Each of these materials exhibit many interesting physicochemical properties[3,7] which has inspired research for many biomedical applications.[8-10] Individual carbon nanoparticles have shown great prospect in many biomedical applications including therapeutic drug delivery,[11,12] bioimaging,[13,14] and reinforcing agents for tissue

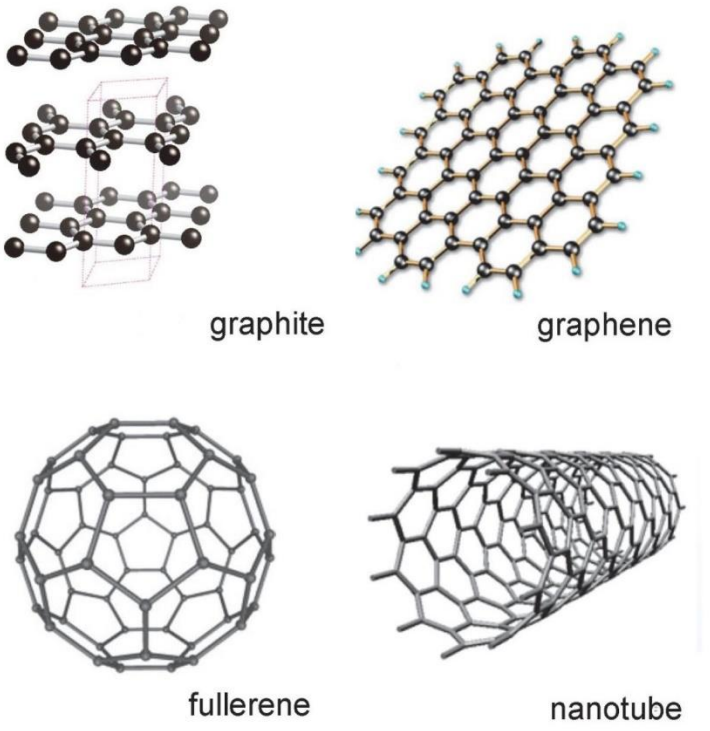

Figure 1.1. Various forms and allotropes of carbon nanomaterials. Adapted with permission from Oganov, et al. "Structure, Bonding, and Mineralogy of Carbon at Extreme Conditions." Reviews in Mineralogy and Geochemistry, 2013. Copyright 2013 GeoScience World.

engineering scaffolds.[15] However, development of larger scale assemblies also provides distinct opportunities for carbon nanomaterials in biomedical applications. Many advances have been made in two-dimensional assemblies of carbon nanomaterials in the past decade, particularly in biomedical research. Two dimensional carbon nanomaterial assemblies include any variation of thin films, coatings, and free-standing films. Figure 1.2 illustrates potential applications of carbon nanomaterials when made into two-dimensional assemblies. Herein, we attempt to summarize and review the progress of two-dimensional carbon nanomaterial assemblies for biomedical applications. To gain a better understanding of the current state-of-art in carbon nanomaterial assemblies, we are only considering all-carbon nanomaterial structures in the scope of this review. Many studies have utilized carbon nanomaterial composites (such as polymers, ceramics, and metals). However comparisons between each composite type is not appropriate due to the effects the secondary material imparts for each application. While majority of these studies are focused on tissue engineering applications, there are other biomedical applications which face similar challenges and they are also reviewed here.

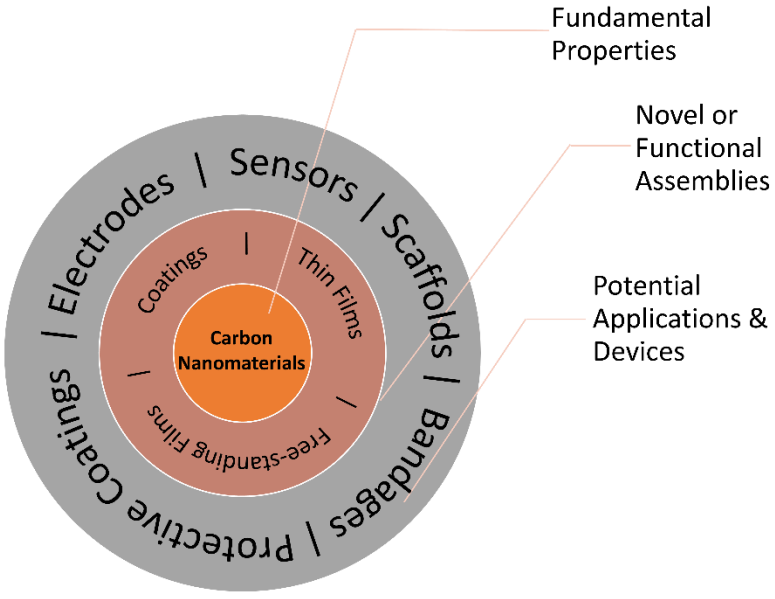

Figure 1.2. Carbon nanomaterials possess many interesting fundamental properties, which are fabricated into novel and functional assemblies. These assemblies in-turn exploit the fundamental properties of the nanomaterials to translatable applications.

Current Fabrication Methods

Two dimensional assemblies of carbon nanomaterials have been previously developed as thin films, coatings and free-standing films. There are many techniques which can be utilized to make two dimensional assemblies of carbon nanomaterials. One of the most commonly used techniques is chemical vapor deposition (CVD) which is a process of chemical growth to produce graphene[16] and carbon nanotubes.[17] Although typically grown on metal catalysts, these coatings can easily be transferred onto a variety of substrates, however, the substrates to transfer to must be relatively flat.[18] In the case of graphene, this method can produce extremely thin, large area coatings down to one-atom layer thick structures.[19] Vacuum filtration is another commonly used method to fabricate carbon nanomaterial coatings.[20,21] A few distinct advantages of this method include: a) the method is simpler than CVD and can create macroscopic free-standing films, b) the surface roughness is self-correcting; as one region of the film becomes dense, the solvent will follow the path of least resistance and auto corrects the thickness of the film,[22] and c) the method is flexible for creating films of various carbon nanomaterials based on the desired application.[20,23] These films can also be robust (due to the vacuum pressure compacting the nanomaterials together), electrically conductive, and cytocompatible.[20] Other methods of making carbon nanomaterial coatings includes dip- and spray-coating. Similar to the vacuum filtration method, these techniques utilize pre-made carbon nanomaterials (either graphene or carbon nanotube powders) and are post assembled by various processes. Dip coating is a process of dipping a pre-treated substrate into a heated liquid suspension of nanomaterial to create graphene films of thicknesses as low as 30nm[24] or carbon nanotube films of thicknesses as low as 12nm.[25] Thicker coatings can be developed by increasing the carbon nanomaterial concentration, repetitive dipping,

and by decreasing the rate of removing the substrate from the dipping solution.[26] This method can be also be used with various types of carbon nanomaterials,[24,26] though not as mechanically robust as vacuum filtered films. Also, this method requires the substrate surface to be linearly symmetrical, like a flat surface or rod, for assembly without aggregated nanoparticles in localized regions.[27] In spray coating, an aerosolized dispersion of carbon nanomaterial is deposited onto a heated substrate to evaporate the carrier solvent and deposit a film of nanomaterials. Spray coating is the most scalable technique of the aforementioned techniques however it also creates the most sparse coatings.[28] Spray coating can create coatings with highly tailorable thicknesses, conductivity, transmittance, and is versatile for various nanomaterials.[28,29] Spray coating can be split into two major groups, airbrushing techniques and ultrasonic spray coating. Airbrushing utilizes compressed gas (e.g. air and nitrogen) to aerosolize the dispersion.[29] Ultrasonic spray coating utilizes an ultrasonic actuated nozzle which creates more uniform droplets while dispersing the nanomaterial solution at the spray head.[30] In each of the following sections, we aim to review the suitability of these methods pertaining to potential biomedical applications for two dimensional carbon nanomaterial assemblies.

Tissue Engineering

Bone Tissue Engineering

Bone tissue engineering may be the most widely studied tissue engineering application of two dimensional carbon nanomaterial coatings. Many groups have studied the effects of carbon nanomaterials on mature osteoblasts and stem cell differentiation.

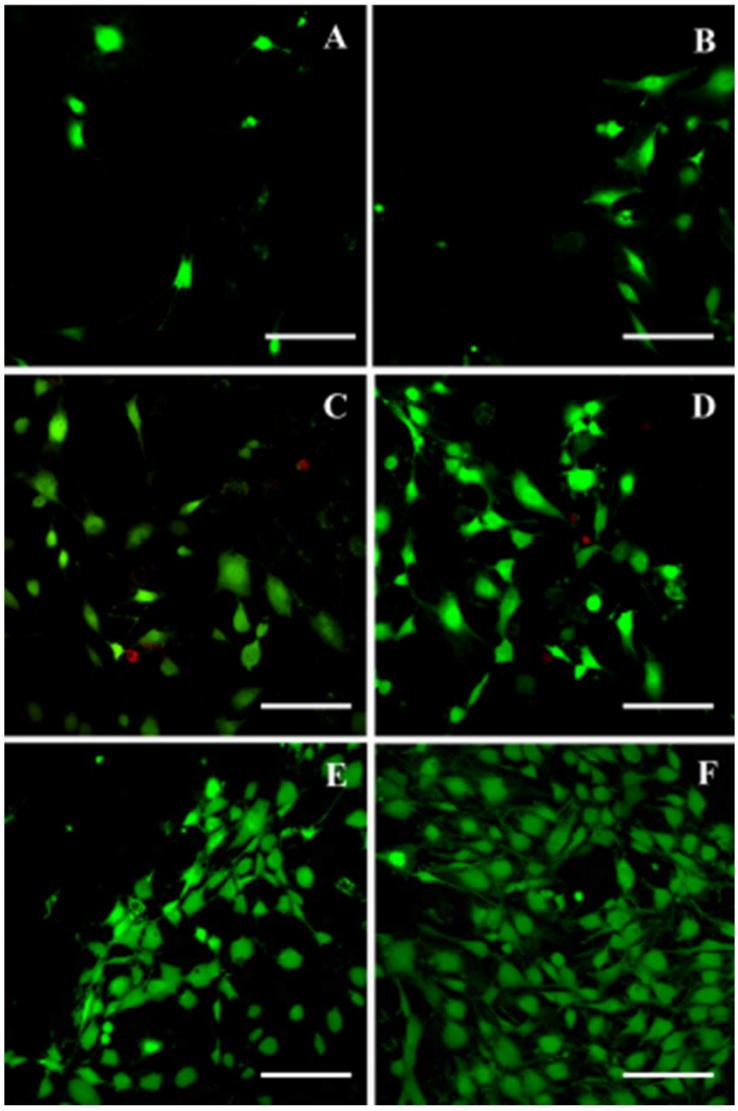

Figure 1.3. Fluorescence images to show cell morphology of osteoblast on graphene coated on different substrates at day 2. [Glass substrate A) without graphene coated layer and B) graphene coated glass substrate. Silicon wafer substrate C) without graphene layer and D) graphene coated silicon wafer. Stainless steel E) without graphene coated layer and F) graphene coated stainless steel substrate.] Scale bars are 200 μm in length. Reproduced with permission from Aryaei, A. et al. "The effect of graphene substrate on osteoblast cell adhesion and proliferation." Journal of Biomedical Materials Research Part A, 2013. Copyright 2013 Wiley Publishing Group.

Osteoblasts are mature, bone matrix depositing cells responsible for rebuilding resorbed or damaged bone tissue.[31] Interfacing native bone tissue with synthetic implant materials; including titanium, stainless steel, and ceramic materials is a key to successful clinical outcomes.[32] Surface coatings can provide a better interface for bone cell adhesion to implant surfaces. Both carbon nanotubes and graphene coatings have been investigated for enhancing preosteoblast and osteoblast adhesion and mineralization on implant surfaces.

The effect of carbon nanotube surface properties on preosteoblast attachment and growth was previously investigated.[33] The group found SWCNT films, made by vacuum filtration, provides optimum preosteoblast growth when surface roughness of the film was about ~ 100 nm r.m.s and hydrophilic due to mild oxidation.[33] Another study shows graphene, fabricated by CVD and transferred onto various substrates (silicon, stainless steel, and soda lime glass), seeded with murine osteoblasts imparts no toxicity to the cells and a 148% improvement in cell spreading on graphene coated stainless steel substrates compared to controls (Figure 1.3).[34]

Adult multipotent stem cells, sourced from bone marrow (MSCs)[35] or adipose tissue (ADSCs)[36], can differentiate into many lineages including osteoblasts, chondrocytes, and adipose tissue. Both carbon nanotubes and graphene have also been investigated for their ability to increase osteogenesis in adult stem cells.

Kroustalli et al. studied the adhesion and biocompatibility of MSCs on MWCNT substrates fabricated by vacuum filtration, finding that the substrates were biocompatible and cell attachment was mediated by proteins adsorbing onto the surface allowing for integrin related attachment.[37] Nayak et al. showed spray coated MWCNT coatings on glass coverslips can also increase MSC differentiation towards osteoblasts with significantly greater expression of osteopontin and calcium deposition (markers for osteogenic stem cell differentiation) than on control substrates.[38] Furthermore, the MWCNT substrates also showed equivalent stem cell differentiation compared to cells treated with bone morphogenic protein-2 (BMP-2), a chemical inducer of osteogenic stem cell differentiation.[38] Graphene substrates, CVD grown, have also shown accelerated osteogenic differentiation and increased calcium deposition compared to substrates without graphene (Figure 1.4).[39] Furthermore, graphene coatings also produce similar calcium deposition to groups treated with BMP-2.[39] Lee, et al. has reported possible reasons behind the enhanced stem cell

differentiation on graphene and graphene oxide coated substrates.[40] They propose osteogenic differentiation of stem cells on graphene substrates is due to the adsorption of osteogenic inducing chemicals such as β-glycerophosphate and dexamethasone and denaturing of adipogenic inducing chemicals such as insulin.[40]

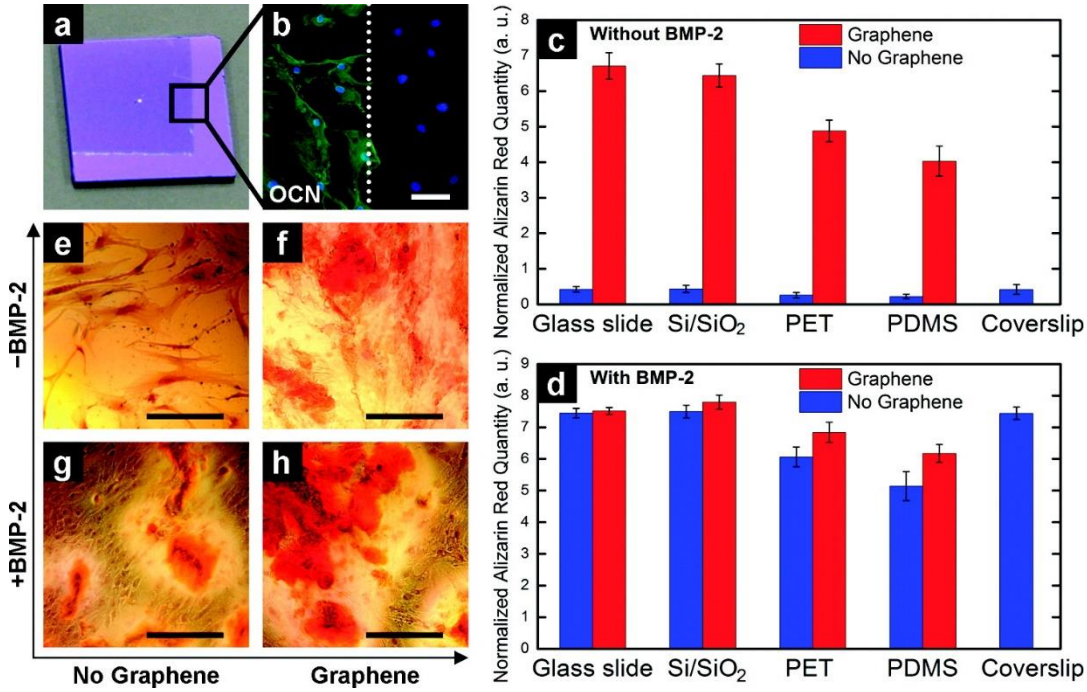

Figure 1.4. Graphene coatings, fabricated by CVD, related accelerated osteogenic differentiation of MSCs. (A) Optical image of partially graphene-coated silicon wafer. (B) Osteocalcin (OCN, green) and DAPI (blue) staining shows osteoblast differentiation on the graphene-coated area with the white line showing the boundary of the graphene coated region. (C) Day 15 alizarin red quantification, measuring calcium deposition, from MSCs grown graphene substrates and controls. (D) BMP-2 treated MSCs grown on graphene substrates and controls. PET substrates seeded with MSCs, stained with alizarin red are shown (E) without BMP-2 and graphene, (F) without BMP-2 but with graphene, (G) with BMP-2 and without graphene and (H) with BMP-2 and graphene. Scale bars are 100 μm in length. Reproduced with permission from Nayak, T., et al. "Graphene for Controlled and Accelerated Osteogenic Differentiation of Human Mesenchymal Stem Cells." ACS Nano, 2011. Copyright 2011 American Chemical Society.

The electromagnetic properties of carbon nanomaterials can also be exploited for tissue engineering applications. Green, et al. reported carbon nanotube derived photoacoustic stimulation enhanced stem cell differentiation towards osteogenic lineages.[41] Laser-stimulated photoacoustic

waves, generated from SWCNT coatings on tissue culture wells, led to a stimulus-responsive enhancement of MSC differentiation. At day 16, the differentiated stem cells treated with the photoacoustic stimulation yielded significantly more (396% increase) calcium deposition compared to chemically induced differentiation controls.[41] Interestingly, graphene materials can impart stronger photoacoustic signal[42] and future studies should investigate the comparative effect of graphene and carbon nanotube coatings on stimulus-responsive differentiation of stem cells.

Neural Tissue Engineering

Neural tissue is perhaps one of the most complex ordered structures, which makes neural tissue engineering an extremely challenging task.[43] Since neurons are highly organized and connected,[44] damaged neurons need to be repaired with similar organization to regain function. Therefore, controlled growth of neurons on carbon nanomaterial coatings is very important.

Drop-casted MWCNT coatings have previously shown ability to host organotypic slice cultures (sectioned, live brain tissue) and induce neuronal outgrowth.[45] Cell SEM also showed membrane-substrate junctions forming between the neurons and the MWCNT substrate.[45] In another study, CVD grown coatings of COOH-functionalized MWCNTs were also found to be biocompatible and allowed for neuronal outgrowth. Tu et al. studied the effects of surface charge of graphene oxide on neuronal growth and branching.[46] Graphene oxide, with various surface charges, were spray coated onto poly ethylene imine coated glass coverslips. Surfaces with positive charges had greater neurite growth than neutral and negatively charged graphene oxide substrates.[46] Graphene films, grown by CVD, have also shown the ability to differentiate neural

stem cells into mature neurons with significantly greater TUJ1, tubulin marker for neuronal differentiation, expression compared to glass coverslip controls.[47]

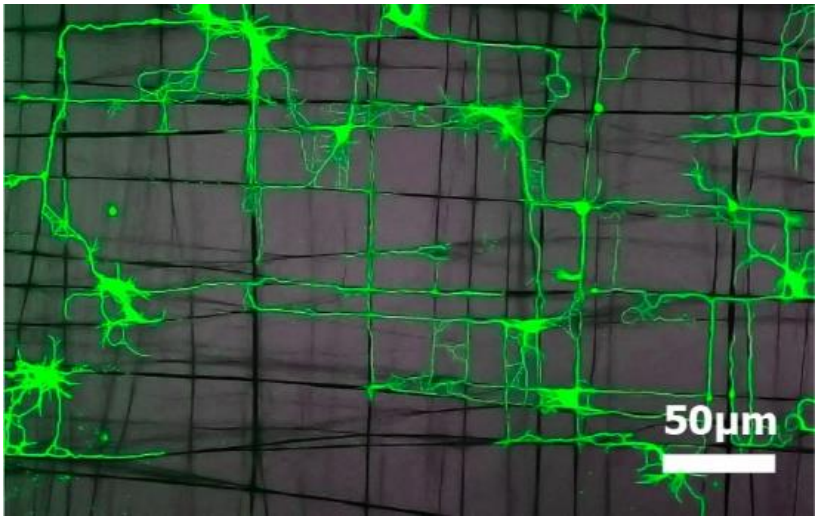

Figure 1.5. Confocal microscopy images of neurite growth on patterned, super-aligned carbon nanotube yarns after 5 days in culture. Reproduced with permission from Fan, L., et al. "Directional Neurite Outgrowth on Superaligned Carbon Nanotube Yarn Patterned Substrate." Nano Letters, 2012. Copyright 2012 American Chemical Society.

To further control neuronal growth directionality, researchers have utilized various patterning methods. In one study, single layer graphene grown by CVD was patterned using a PDMS stamping method to create linear and checkered patterns on the graphene surface.[48] Seeded neurons followed the patterned graphene substrate to create controlled neural networks.[48] In another study, researchers used super-aligned carbon nanotube yarns, fabricated from CVD grown vertically aligned carbon nanotubes substrates, to directionally guide neurite outgrowth on the nanotube yarns (Figure 1.5).[49] Some challenges faced with patterned carbon nanomaterial substrates includes the lack of neurite branching in regions where the carbon nanomaterials are not present.[49] Patterning and controlling neuron growth on carbon nanomaterial substrates opens avenues for repair of the highly organized central nervous system.

Other Tissue Engineering Applications

Graphene oxide substrates, fabricated by dip coating, have shown the ability to differentiate murine C2C12 skeletal myoblasts.[50] Glass substrates coated with graphene oxide showed significantly greater proliferation of skeletal myoblasts at days 2 and 4, than glass substrates and glass coated with reduced graphene oxide. Myoblasts on graphene oxide coated substrates also exhibited significantly greater cell area, myotube length, myosin heavy chain staining, and myogenin positive cells.[50]

Other than adult stem cells, carbon nanomaterial substrates have also been studied for their effects on pluripotent stem cell fate.[51] Pluripotent stem cells are either collected from embryotic sources[52] or induced from adult fibroblasts by chemical methods.[53] Pryzhkova et al. studied carbon nanotubes arrays synthesized by chemical vapor deposition, with tailorable surface roughness, mechanical properties, and topography. Changing these parameters resulted in differentiation and growth of the stem cells into different germ layers. Furthermore, the group found the stem cells can differentiate into all three germ layers; ectoderm, mesoderm, and endoderm, depending on the surface properties of the nanotubes.[52]

Electrodes and Biosensors

Flexible, compact, and robust electrodes are required for next generation biosensors.[54] These nanomaterial based biosensors can be utilized to detect small molecules, proteins,[55] cellular metabolism,[56] diseased tissue,[57,58] etc. The large surface area and tunable electrical properties of carbon nanomaterials make them ideal candidates for novel biosensor development.[59] Multiple reviews have already covered graphene[60,61] and carbon nanotube[62,63] based biosensors, therefore here we will review advances in large-area carbon nanomaterial sensor and electrode development.

Chang et al. developed large area, thick coatings (>1 μm) of carbon nanotubes, grown by CVD, on flexible polyimide surfaces for developing human serum albumin detectors.[64] Variations of serum albumin levels in humans has been previously associated with liver[65] and heart disease.[66] They found the carbon nanotube sensors were extremely sensitive and could detect human serum albumin levels as low as 30 pg/mL using impedance measurements.[64]

Large area graphene substrates have also been investigated for biosensing applications. He et al. fabricated centimeter scale micro-patterns (< 3nm thick) of flexible, reduced graphene oxide on poly ethylene terephthalate (PET) to temporally detecting hormone secretion from neuroendocrine cells.[67] Dopamine secretion, released from PC12 cells, were observed by increases in conductance.[67] Some studies have also studied graphene oxide for biosensor applications. While graphene oxide is not as electrically conductive as graphene, it can be decorated with functionalities to improve analyte detection. Graphene oxide free-standing films can also be a substrate to be further functionalized with gold nanoparticles for high-performance biosensing of analytes like glucose and hydrogen peroxide.[68] The constructs could linearly sense glucose concentrations in solutions as low as 0.01 mM and hydrogen peroxide concentrations as low as 0.005 mM.[68] Similarly, free standing graphene films, fabricated by vacuum filtration, has served as a substrate for gold-platinum nanoparticles to monitor nitric oxide concentrations in media.[69] The assembly could monitor nitric oxide release from live HUVEC cells with visible increases in current density.[69]

Protective Coatings and Antibacterial Substrates

Carbon nanomaterials, because of their sp^2 hybridized chemistry can be utilized for protective coatings in biomedical devices as well. Here the carbon nanomaterials act as a highly flexible and tailorable substrate for solving a multitude of problems including thrombosis and corrosion.

Metal implants and metallic surfaces of biomedical devices can both experience corrosion in saline biological solutions causing adverse effects in patients.[70] For example, copper, and its alloys, are commonly used in many dental applications and toxic copper ions are created in the corrosion of copper.[71] Zhang et al reported single layer, CVD grown graphene on copper substrates, led to a ~23 fold decrease in Cu^{2+} ion release in cell culture media which also resulted in 100% viability in cells compared to no viable cells in the copper control groups.[71]

Functionalized graphene oxide has also been investigated for its antithrombotic properties for vascular implant coating. Kenry, et al. demonstrated a proof of principle study showing albumin functionalized graphene oxide has excellent protein adsorption properties and proposes its use in antithrombotic coatings for biomedical devices which are in contact with blood.[72] This may also be important for scaffolding materials to prevent clot formation at the pores of a scaffold. While many studies propose graphene based anti-thrombogenic coatings, the two dimensional coatings are often fabricated in polymer solutions for extra stability.[71,73]

While graphene substrates can provide protection from oxidation on metallic surfaces, they also possess interesting antibacterial properties. Free-standing graphene oxide substrates, made by vacuum filtration, showed no colony growth of *E. coli* bacteria after overnight incubation.[74] Furthermore, graphene oxide solutions were cytotoxic to *E. coli* at concentrations of 85 μg/mL while shown no toxicity to A549 cells at the same concentration.[74] Another paper showed graphene substrates (both reduced and oxidized) showed more than two times greater *E. coli* toxicity

compared to graphite (both reduced and oxidized) due to the membrane and oxidative stress imparted by graphene particles.[75] Although *E coli* is often studied as a model for antibacterial properties, graphene nano-sheets have also shown toxicity towards pathogenic bacterial like *Salmonella typhimurium*, *Enterococcus faecalis*, and *Bacillus subtillis* at concentrations between 1 – 8 μg/mL.[76]

Challenges

Two dimensional carbon nanomaterial coatings for tissue engineering applications have many challenges which need to be addressed. First, graphene and carbon nanomaterial coatings lack robustness due to the absence of strong chemical bonds between the nanomaterials. A potential work-around this challenge is to use polymer-nanomaterial composite structures.[77,78] While this addresses the lack of robustness of the carbon nanomaterial coatings, it also limits exploiting the unique physicochemical properties which make carbon nanomaterials attractive. Second, while carbon nanotubes and graphene are both excellent candidates for bone tissue engineering substrates, there are no studies which directly compare both nanomaterials for their safety and effectiveness in differentiating stem cells. Thirdly, carbon nanomaterial degradation and wear particle assessment should be studied for each two dimensional coating method. These studies will provide valuable information towards the long-term suitability for the nanomaterial and its assembly. Carbon nanomaterial film degradation is also important for coatings as protective and antibacterial surfaces to prevent loose nanomaterial related toxicity.

Most biosensor and electrode assemblies of carbon nanomaterials require pristine sp^2 hybridized carbon nanoparticles for the greatest electrical conductivity. Therefore chemical vapor

deposition approaches are the most advantageous in fabricating these assemblies. While chemical vapor deposition techniques have become more compatible with non-metallic substrates, the temperatures required for these processes still reach over 400°C and are not compatible for many polymers.[64,79] While reduced graphene oxide materials have also been investigated for biosensing applications,[67] chemical reduction is not 100% efficient and reducing agents are often highly toxic to cells.[80] Additionally, many sensors and protective coatings which require *in vivo* implantation, should also be tested for their robustness over time under fluid flow for vascular devices and mechanical shear for musculoskeletal tissue.

Conclusions

Many techniques have been developed to assemble all-carbon nanomaterial coatings and films for biomedical applications. While the majority of the research for applications of these coatings has been for tissue engineering, other applications have also been investigated. Many of the translational challenges faced in each application is directly related to the fabrication technique utilized to make the coatings, lacking strong bonding between individual nanoparticles. Future studies should focus on improvement of fabrication technologies for more application-appropriate methods and more in-depth assessment of safety and efficacy for two dimensional carbon nanomaterial assemblies.

Specific Aims

With the wide prospect of applications in tissue engineering, biosensing, and protective coatings there is a clear need to develop a suitable method for fabricating carbon nanomaterial thin films with strong bonds, tunable electrical, structural, and mechanical properties. Furthermore, to integrate the technology into industries, it is important that the process is scalable and flexible for multiple applications. Therefore, the overall objective of this work is to develop a technique to assemble carbon nanomaterials into chemically-crosslinked, multifunctional, two-dimensional coatings and evaluating them for bone tissue engineering applications. Towards this objective, the specific aims of the following experiments are as follows:

Specific Aim 1: To develop a proof-of-concept spray coating method for in situ formation of chemical crosslinks between carbon nanoparticles and assess cytocompatibility of the resulting coatings.

Hypothesis: *In situ* crosslinking of carbon nanotubes will result in more robust nanomaterial coatings and will be cytocompatible to human adipose derived stem cells.

Specific Aim 2: To design a coating system and optimize parameters to make reproducible crosslinked carbon nanomaterial coatings of using various materials (SWCNT, MWCNT, GONRs, GONPs).

Hypothesis: Ultrasonic spray coating will allow for fabrication of batch-to-batch consistent films with smoother surface roughness than airbrushing. Also, *in situ* crosslinking of carbon nanomaterials can lead to fabrication of 3D, free standing porous carbon nanomaterial structures.

Specific Aim 3: To compare adipose-derived stem cell differentiation towards osteoblast lineages on various nanoarchitectures in chemically-crosslinked carbon nanomaterial coatings.

Hypothesis: Surface chemistry, roughness, and nanotopography of crosslinked carbon nanomaterial thin films will affect adipose derived stem cell differentiation towards bone cells.

References

1 Oganov, A. R., Hemley, R. J., Hazen, R. M. & Jones, A. P. Structure, bonding, and mineralogy of carbon at extreme conditions. *Rev Mineral Geochem* **75**, 47-77 (2013).

2 Hirsch, A. *The chemistry of the fullerenes*. (Wiley Online Library, 1994).

3 Zhu, Y. *et al.* Graphene and graphene oxide: synthesis, properties, and applications. *Advanced materials* **22**, 3906-3924 (2010).

4 Shen, H., Zhang, L., Liu, M. & Zhang, Z. Biomedical applications of graphene. *Theranostics* **2**, 283 (2012).

5 Cheung, C. L., Kurtz, A., Park, H. & Lieber, C. M. Diameter-controlled synthesis of carbon nanotubes. *The Journal of Physical Chemistry B* **106**, 2429-2433 (2002).

6 Kosynkin, D. V. *et al.* Longitudinal unzipping of carbon nanotubes to form graphene nanoribbons. *Nature* **458**, 872-876 (2009).

7 Dresselhaus, M. S., Dresselhaus, G. & Eklund, P. C. *Science of fullerenes and carbon nanotubes: their properties and applications*. (Academic press, 1996).

8 Yang, W., Thordarson, P., Gooding, J. J., Ringer, S. P. & Braet, F. Carbon nanotubes for biological and biomedical applications. *Nanotechnology* **18**, 412001 (2007).

9 Zhang, Y., Nayak, T. R., Hong, H. & Cai, W. Graphene: a versatile nanoplatform for biomedical applications. *Nanoscale* **4**, 3833-3842 (2012).

10 Partha, R. & Conyers, J. L. Biomedical applications of functionalized fullerene-based nanomaterials. *International journal of nanomedicine* **4**, 261 (2009).

11 Li, N. *et al.* Three-dimensional graphene foam as a biocompatible and conductive scaffold for neural stem cells. *Scientific reports* **3** (2013).

12 Bianco, A., Kostarelos, K. & Prato, M. Applications of carbon nanotubes in drug delivery. *Current opinion in chemical biology* **9**, 674-679 (2005).

13 Liu, Z., Tabakman, S., Welsher, K. & Dai, H. Carbon nanotubes in biology and medicine: in vitro and in vivo detection, imaging and drug delivery. *Nano research* **2**, 85-120 (2009).

14 Sun, X. *et al.* Nano-graphene oxide for cellular imaging and drug delivery. *Nano research* **1**, 203-212 (2008).

15 Harrison, B. S. & Atala, A. Carbon nanotube applications for tissue engineering. *Biomaterials* **28**, 344-353 (2007).

16 Kim, K. S. *et al.* Large-scale pattern growth of graphene films for stretchable transparent electrodes. *Nature* **457**, 706-710 (2009).

17 Cassell, A. M., Raymakers, J. A., Kong, J. & Dai, H. Large scale CVD synthesis of single-walled carbon nanotubes. *The Journal of Physical Chemistry B* **103**, 6484-6492 (1999).

18 Suk, J. W. *et al.* Transfer of CVD-grown monolayer graphene onto arbitrary substrates. *ACS nano* **5**, 6916-6924 (2011).

19 Steirer, K. X. *et al.* Ultrasonic spray deposition for production of organic solar cells. *Solar Energy Materials and Solar Cells* **93**, 447-453 (2009).

20 Chen, H., Müller, M. B., Gilmore, K. J., Wallace, G. G. & Li, D. Mechanically strong, electrically conductive, and biocompatible graphene paper. *Adv. Mater* **20**, 3557-3561 (2008).

21 Dikin, D. A. *et al.* Preparation and characterization of graphene oxide paper. *Nature* **448**, 457-460 (2007).

22 Wu, Z. *et al.* Transparent, conductive carbon nanotube films. *Science* **305**, 1273-1276 (2004).

23 Ng, S. *et al.* Single wall carbon nanotube paper as anode for lithium-ion battery. *Electrochimica Acta* **51**, 23-28 (2005).

24 Wang, X., Zhi, L. & Müllen, K. Transparent, conductive graphene electrodes for dye-sensitized solar cells. *Nano letters* **8**, 323-327 (2008).

25 Jang, E. Y., Kang, T. J., Im, H. W., Kim, D. W. & Kim, Y. H. Single-Walled Carbon-Nanotube Networks on Large-Area Glass Substrate by the Dip-Coating Method. *Small* **4**, 2255-2261 (2008).

26 Mirri, F. *et al.* High-performance carbon nanotube transparent conductive films by scalable dip coating. *ACS nano* **6**, 9737-9744 (2012).

27 Spotnitz, M. E., Ryan, D. & Stone, H. A. Dip coating for the alignment of carbon nanotubes on curved surfaces. *Journal of Materials Chemistry* **14**, 1299-1302 (2004).

28 Geng, H.-Z. *et al.* Effect of Acid Treatment on Carbon Nanotube-Based Flexible Transparent Conducting Films. *Journal of the American Chemical Society* **129**, 7758-7759, doi:10.1021/ja0722224 (2007).

29 Pham, V. H. *et al.* Fast and simple fabrication of a large transparent chemically-converted graphene film by spray-coating. *Carbon* **48**, 1945-1951, doi:http://dx.doi.org/10.1016/j.carbon.2010.01.062 (2010).

30 Weidman, T., Lu, Y., Nault, M. P., Barnes, M. & Moghadam, F. (Google Patents, 2003).

31 Harada, S.-i. & Rodan, G. A. Control of osteoblast function and regulation of bone mass. *Nature* **423**, 349-355 (2003).

32 Puleo, D. & Nanci, A. Understanding and controlling the bone–implant interface. *Biomaterials* **20**, 2311-2321 (1999).

33 Wojtek, T., Manish, C. & Federico, S. The chemical and physical characteristics of single-walled carbon nanotube film impact on osteoblastic cell response. *Nanotechnology* **21**, 315102 (2010).

34 Aryaei, A., Jayatissa, A. H. & Jayasuriya, A. C. The effect of graphene substrate on osteoblast cell adhesion and proliferation. *Journal of Biomedical Materials Research Part A* **102**, 3282-3290 (2014).

35 Pittenger, M. F. *et al.* Multilineage potential of adult human mesenchymal stem cells. *science* **284**, 143-147 (1999).

36 Zuk, P. A. *et al.* Human adipose tissue is a source of multipotent stem cells. *Molecular biology of the cell* **13**, 4279-4295 (2002).

37 Kroustalli, A. A., Kourkouli, S. N. & Deligianni, D. D. Cellular function and adhesion mechanisms of human bone marrow mesenchymal stem cells on multi-walled carbon nanotubes. *Annals of biomedical engineering* **41**, 2655-2665 (2013).

38 Nayak, T. R. *et al.* Thin Films of Functionalized Multiwalled Carbon Nanotubes as Suitable Scaffold Materials for Stem Cells Proliferation and Bone Formation. *ACS Nano* **4**, 7717-7725, doi:10.1021/nn102738c (2010).

39 Nayak, T. R. *et al.* Graphene for Controlled and Accelerated Osteogenic Differentiation of Human Mesenchymal Stem Cells. *ACS Nano* **5**, 4670-4678, doi:10.1021/nn200500h (2011).

40 Lee, W. C. *et al.* Origin of Enhanced Stem Cell Growth and Differentiation on Graphene and Graphene Oxide. *ACS Nano* **5**, 7334-7341, doi:10.1021/nn202190c (2011).

41 Green, D. E., Longtin, J. P. & Sitharaman, B. The Effect of Nanoparticle-Enhanced Photoacoustic Stimulation on Multipotent Marrow Stromal Cells. *ACS Nano* **3**, 2065-2072, doi:10.1021/nn900434p (2009).

42 Lalwani, G., Cai, X., Nie, L., Wang, L. V. & Sitharaman, B. Graphene-based contrast agents for photoacoustic and thermoacoustic tomography. *Photoacoustics* **1**, 62-67 (2013).

43 Griffith, L. G. & Naughton, G. Tissue engineering--current challenges and expanding opportunities. *Science* **295**, 1009-1014 (2002).

44 Gähwiler, B. Organotypic cultures of neural tissue. *Trends in neurosciences* **11**, 484-489 (1988).

45 Fabbro, A. *et al.* Spinal Cord Explants Use Carbon Nanotube Interfaces To Enhance Neurite Outgrowth and To Fortify Synaptic Inputs. *ACS Nano* **6**, 2041-2055, doi:10.1021/nn203519r (2012).

46 Tu, Q. *et al.* Effects of surface charges of graphene oxide on neuronal outgrowth and branching. *Analyst* **139**, 105-115 (2014).

47 Park, S. Y. *et al.* Enhanced differentiation of human neural stem cells into neurons on graphene. *Advanced Materials* **23**, H263-H267 (2011).

48 Hong, D. *et al.* Generation of Cellular Micropatterns on a Single-Layered Graphene Film. *Macromolecular bioscience* **14**, 314-319 (2014).

49 Fan, L. *et al.* Directional Neurite Outgrowth on Superaligned Carbon Nanotube Yarn Patterned Substrate. *Nano Letters* **12**, 3668-3673, doi:10.1021/nl301428w (2012).

50 Ku, S. H. & Park, C. B. Myoblast differentiation on graphene oxide. *Biomaterials* **34**, 2017-2023, doi:http://dx.doi.org/10.1016/j.biomaterials.2012.11.052 (2013).

51 Pryzhkova, M. V. *et al.* Carbon nanotube-based substrates for modulation of human pluripotent stem cell fate. *Biomaterials* **35**, 5098-5109, doi:http://dx.doi.org/10.1016/j.biomaterials.2014.03.011 (2014).

52 Verfaillie, C. Pluripotent stem cells. *Transfusion clinique et biologique* **16**, 65-69 (2009).

53 Takahashi, K. *et al.* Induction of pluripotent stem cells from adult human fibroblasts by defined factors. *cell* **131**, 861-872 (2007).

54 Li, C., Han, J. & Ahn, C. H. Flexible biosensors on spirally rolled micro tube for cardiovascular in vivo monitoring. *Biosensors and Bioelectronics* **22**, 1988-1993 (2007).

55 McAlpine, M. C., Ahmad, H., Wang, D. & Heath, J. R. Highly ordered nanowire arrays on plastic substrates for ultrasensitive flexible chemical sensors. *Nature materials* **6**, 379-384 (2007).

56 Carrara, S. Nano-bio-technology and sensing chips: new systems for detection in personalized therapies and cell biology. *Sensors* **10**, 526-543 (2010).

57 Zheng, G., Patolsky, F., Cui, Y., Wang, W. U. & Lieber, C. M. Multiplexed electrical detection of cancer markers with nanowire sensor arrays. *Nature biotechnology* **23**, 1294-1301 (2005).

58 Kragh-Hansen, U., Chuang, V. T. G. & Otagiri, M. Practical Aspects of the Ligand-Binding and Enzymatic Properties of Human Serum Albumin. *Biological and Pharmaceutical Bulletin* **25**, 695-704, doi:10.1248/bpb.25.695 (2002).

59 Robert, B. Nanosensors: a review of recent progressnull. *Sensor Review* **28**, 12-17, doi:10.1108/02602280810849965 (2008).

60 Kuila, T. *et al.* Recent advances in graphene-based biosensors. *Biosensors and Bioelectronics* **26**, 4637-4648 (2011).

61 Shao, Y. *et al.* Graphene based electrochemical sensors and biosensors: a review. *Electroanalysis* **22**, 1027-1036 (2010).

62 Wang, J. Carbon-Nanotube Based Electrochemical Biosensors: A Review. *Electroanalysis* **17**, 7-14, doi:10.1002/elan.200403113 (2005).

63 Yang, W. *et al.* Carbon nanomaterials in biosensors: should you use nanotubes or graphene? *Angewandte Chemie International Edition* **49**, 2114-2138 (2010).

64 Chang, Y.-T., Huang, J.-H., Tu, M.-C., Chang, P. & Yew, T.-R. Flexible direct-growth CNT biosensors. *Biosensors and Bioelectronics* **41**, 898-902, doi:http://dx.doi.org/10.1016/j.bios.2012.09.049 (2013).

65 Murray, J. F., Dawson, A. & Sherlock, S. Circulatory changes in chronic liver disease. *The American journal of medicine* **24**, 358-367 (1958).

66 Kuller, L. H. *et al.* The Relation between Serum Albumin Levels and Risk of Coronary Heart Disease in the Multiple Risk Factor Intervention Trial. *American Journal of Epidemiology* **134**, 1266-1277 (1991).

67 He, Q. *et al.* Centimeter-Long and Large-Scale Micropatterns of Reduced Graphene Oxide Films: Fabrication and Sensing Applications. *ACS Nano* **4**, 3201-3208, doi:10.1021/nn100780v (2010).

68 Xiao, F. *et al.* Coating Graphene Paper with 2D-Assembly of Electrocatalytic Nanoparticles: A Modular Approach toward High-Performance Flexible Electrodes. *ACS Nano* **6**, 100-110, doi:10.1021/nn202930m (2012).

69 Zan, X. *et al.* Freestanding graphene paper decorated with 2D-assembly of Au@Pt nanoparticles as flexible biosensors to monitor live cell secretion of nitric oxide.

Biosensors and Bioelectronics **49**, 71-78, doi:http://dx.doi.org/10.1016/j.bios.2013.05.006 (2013).

70 Hench, L. L. & Ethridge, E. Biomaterials: an interfacial approach. *Academic Press, Inc., 1972*, 385 (1972).

71 Zhang, W. *et al.* Use of graphene as protection film in biological environments. *Scientific reports* **4** (2014).

72 Loh, K. P. & Lim, C. T. Molecular Hemocompatibility of Graphene Oxide and Its Implication for Antithrombotic Applications. *Small* **11**, 5105-5117 (2015).

73 He, C. *et al.* Graphene oxide based heparin-mimicking and hemocompatible polymeric hydrogels for versatile biomedical applications. *Journal of Materials Chemistry B* **3**, 592-602 (2015).

74 Hu, W. *et al.* Graphene-Based Antibacterial Paper. *ACS Nano* **4**, 4317-4323, doi:10.1021/nn101097v (2010).

75 Liu, S. *et al.* Antibacterial Activity of Graphite, Graphite Oxide, Graphene Oxide, and Reduced Graphene Oxide: Membrane and Oxidative Stress. *ACS Nano* **5**, 6971-6980, doi:10.1021/nn202451x (2011).

76 Krishnamoorthy, K., Veerapandian, M., Zhang, L.-H., Yun, K. & Kim, S. J. Antibacterial Efficiency of Graphene Nanosheets against Pathogenic Bacteria via Lipid Peroxidation. *The Journal of Physical Chemistry C* **116**, 17280-17287, doi:10.1021/jp3047054 (2012).

77 Kuilla, T. *et al.* Recent advances in graphene based polymer composites. *Progress in polymer science* **35**, 1350-1375 (2010).

78 Stankovich, S. *et al.* Graphene-based composite materials. *Nature* **442**, 282-286 (2006).

79 Maruyama, S., Kojima, R., Miyauchi, Y., Chiashi, S. & Kohno, M. Low-temperature synthesis of high-purity single-walled carbon nanotubes from alcohol. *Chemical physics letters* **360**, 229-234 (2002).

80 Vernot, E. *et al.* Long-term inhalation toxicity of hydrazine. *Toxicological Sciences* **5**, 1050-1064 (1985).

Chapter 2

Fabrication and Cytocompatibility of In Situ Crosslinked Carbon Nanomaterial Films

Portions of this chapter have been reproduced from:

Sunny C. Patel, Gaurav Lalwani, Kartikey Grover, Yi-Xian Qin, and Balaji Sitharaman, "Fabrication and Cytocompatibility of In Situ Crosslinked Carbon Nanomaterial Films." *Scientific Reports* **5**, Article Number: 10261, (2015).

*The authors listed in the above manuscript have contributions towards the data reported in this chapter.

Abstract

Assembly of carbon nanomaterials into 2D coatings and films that harness their unique physiochemical properties may lead to high impact energy capture/storage, sensors, and biomedical applications. For potential biomedical applications, the suitability of current techniques such as chemical vapor deposition, spray and dip coating, and vacuum filtration, employed to fabricate macroscopic 2D all carbon coatings or films still requires thorough examination. Each of these methods presents challenges with regards to scalability, suitability for a large variety of substrates, mechanical stability of coating or films, or biocompatibility. Herein we report a coating process that allow for rapid, *in situ* chemical crosslinking of multi-walled carbon nanotubes (MWCNTs) into macroscopic all carbon coatings. The resultant coatings were found to be continuous, electrically conductive, significantly more robust, and cytocompatible to human adipose derived stem cells. The results lay groundwork for 3D layer-on-layer nanomaterial assemblies (including various forms of graphene) and also opens avenues to further explore the potential of MWCNT films as a novel class of nano-fibrous mats for tissue engineering and regenerative medicine.

Introduction

Carbon nanomaterials such as fullerenes, carbon nanotubes (CNTs) and graphene possess unique physiochemical properties,[1-2] and thus, assembly of these nanoscale building blocks into two dimensional (2D) macroscopic coatings and films that harness these properties may lead to high impact biomedical applications. Over the last decade, carbon nanomaterials have been identified as a platform technology for tissue engineering by providing matrix reinforcement to polymeric scaffolds and as substrates for electrically stimulated osteo-conduction and for neuronal network formation.[3] However, compared to 2D macroscopic films and coatings of carbon nanomaterials for electronics and energy storage applications,[4] very few studies (all *in vitro*) have investigated the potential and suitability of carbon nanomaterial thin films for biomedical applications.[5-7] Chemical vapor deposition (CVD), spray (electrospray and air-pressure driven) and dip coatings, and vacuum filtration are few of the methods that have been employed for the fabrication of 2D carbon nanomaterial films.[8] While the suitability of these methods for material science or electronic application has been examined, the adaptation of these techniques for biomedical applications still needs thorough evaluation.

Two issues need to be assessed for biomedical applications of 2D carbon nanomaterial films: 1) the suitability of the fabrication method, and 2) biocompatibility of carbon nanomaterial thin films fabricated using each method. CNT forests, or single layer graphene coatings fabricated using CVD, have been investigated as cell substrates;[9] and have been investigated for its ability to differentiate stem cells to bone lineages.[10,11] However, CVD method requires very specific substrates for nanomaterial film growth or deposition. For instance, direct growth of carbon nanotube forests[12] or graphene[13] coatings by CVD requires substrates that can withstand high

temperatures and pressures. Although, micron-scale thick films of CNTs[14] or graphene, can be fabricated by vacuum filtration,[11] this method requires flat substrates to maintain their structural features, and perhaps cannot be easily applied to irregular or round shapes, such as a hip implant ball head. Spray coating techniques (e.g. airbrushing, electro-spraying, plasma spraying) do allow optimal carbon nanomaterial coatings on irregular, non-flat substrates. A limitation of these spray coating techniques, and indeed all the above techniques, is that in the absence of strong chemical bonds between the individual nanomaterials, the structural integrity of films and coatings relies mainly on physical entanglement of the nanoparticles, or weak Van der Wall forces. Thus, these films and coatings could be prone to disassociation under compressive flexural or shear forces that biomaterials device and implants experience under physiological conditions.

Few studies have also investigated the *in vitro* cytocompatibility of carbon nanomaterials (graphene and carbon nanotubes) thin films for tissue engineering applications fabricated by some of the above methods. Carbon nanotube and graphene substrates, prepared by CVD[5] and spray coating,[15] have been reported to enhance osteogenesis, and upregulate bone matrix mineralization in human mesenchymal stem cell populations. Vacuum filtration-based graphene[11] and carbon nanotubes[16] films have shown cytocompatibility towards mouse fibroblasts and enhanced matrix production by osteoblastic cells, respectively. However, the most densely packed films of carbon nanomaterials, fabricated by vacuum filtration, have been reported to elicit cytotoxic response; attributed to loose nanomaterials that peel away from the films and get uptaken by osteoblasts.[16]

We have recently developed a facile low-cost chemical synthesis protocol that allows the assembly of sp^2 hybridized carbon nanostructures such as fullerenes, carbon nanotubes and graphene into free-standing, chemically-crosslinked macroscopic all-carbon architectures.[17] The protocol involves radical-initiated thermal crosslinking and annealing of sp^2 hybridized carbon

nanostructures. The objective of this study was to adapt an air-pressure driven spray coating technique to develop an innovative *in situ* method to fabricate more robust, chemically-crosslinked all carbon multi-walled carbon nanotube (MWCNT) films. As novel nanofiber mats, we have also evaluated *in vitro* the cytocompatibility of crosslinked MWCNTs films towards their development as scaffolds for tissue engineering applications, and coating for biomedical implants.

Methods

Film Fabrication

Multi-walled carbon nanotubes were purchased from Sigma Aldrich with the outer wall diameters of 110-170 nm and lengths of 5-9μm. Nanoparticle suspensions at 1 mg/ml in anhydrous ethyl acetate were dispersed by sonication for 15 minutes. MWCNT to benzoyl peroxide (BP) mass ratios of 1:1, 1:2, and 1:4 were used for initial characterization. All cell studies were performed on the 1:4 ratio samples. Suspensions were sprayed with an airbrush (Iwata HP-CS) onto 12mm diameter round glass coverslips (Electron Microscopy Sciences). Prior to spraying the coverslips were cleaned with acetone and autoclaved. During the spraying process, the coverslips were heated on a hotplate to ~60˚C to initialize *in situ* crosslinking and prevent the liquid suspension from accumulating on the surface. Samples were further thermally crosslinked in an oven at 60˚C for 12 hours. Excess BP was removed by heating the coated coverslips at 150˚C for 30 minutes.

Surface and Chemical Characterization

Scanning electron microscopy (SEM) was performed using a JEOL 7600F analytical high resolution SEM. Samples were sputter coated with 3nm of Au to prevent surface charge accumulation. Transmission electron microscopy (TEM) samples were prepared by fragmenting crosslinked films by scratching the surface with sharp tweezers and placing them on a conductive carbon TEM porous grid (PELCO, Ted Pella, Redding, CA). TEM was performed using a JEOL JEM2100F high resolution analytical TEM. Both electron microscopy techniques were performed at the Center for Functional Nanomaterials (Brookhaven National Laboratory, New York). For

atomic force microscopy (AFM), crosslinked MWCNT (1:4) were sprayed on smooth, freshly cleaved silicon wafers (Ted Pella, Redding, CA). AFM images were obtained with a NanoSurf EasyScan 2 Flex AFM (NanoScience Instruments Inc., Phoenix AZ), in air by tapping a V-shaped cantilever (APP Nano ACL − 10, frequency fc = 145−230 kHz, L = 225 μm, W= 40 μm, tip radius < 10 nm, spring constant k = 20−95 N/m). NanoSurf Easy Scan 2 Software was utilized to calculate the root mean square (r.m.s.) surface roughness of the coatings. Raman spectroscopy (Enwave Optronics, Irvine, CA) was performed in three regions of each sample (after thermal treatment to remove residual BP) under a 40x objective using a 532nm laser source. Point spectra scanning from 100 to 3,100 cm-1 at room temperature were acquired.

Mechanical Properties

The mechanical properties of spray coated pristine MWCNT and crosslinked MWCNT (MWCNT to benzoyl peroxide (BP) mass ratio of 1:4) were determined using nanoindentation (Triboindenter; Hysitron, Minneapolis, MN) with a Berkovich indenter tip. AFM specimen discs (Ted Pella) of 15mm diameter, which can stick firmly to the magnetic triboindenter base, were coated with either MWCNT or crosslinked MWCNT and mounted into the indenter. After careful analysis of the disks under the imaging system of the triboindenter, points of indentation were selected at a distance no less than 100 μm away from each other. The imaging system of the triboindenter consisted of an objective of magnification 10X and an end zooming lens of magnification 2X. A further zoom of 5X magnification was used to decide the final selection of indentation points through the special electronically controlled magnification of the triboindenter. Samples were indented 7 times to determine elastic modulus (Er) and material hardness (H). Each indentation further comprised of 9 sub-indents in a 3 x 3 pattern and thus, the total number of

indents each sample were 63. Due to the porous nature of the coatings, indents resulting in outlier points were removed individually from each 3*3 indent. Due to the porous nature of the coatings, some of the indents were not made on the thin carbon films but on the pores. Such indentations localized in holes or resulting in poor curves were not included in the analysis. The tip area function was calibrated from indentation analysis on fused quartz, and drift rates in the system were measured prior to each indentation. First, a preload of 3μN was applied to the system followed by a constant loading rate (10μN/second). Next, a hold segment at a fixed system load was applied, followed by a constant unloading rate to retract the tip (−10μN/second), and finally another hold segment was applied (3 μN). Each sample was indented with peak loads ranging from ≈ 15 μN to 100 μN. The elastic response was calculated from the 20–90% portion of the unloading curve using methods previously described.[60] Data is reported in mean (μ), median (mdn.), standard deviation (S.D.) and interquartile range (i.q.r.).

Electrical Characterization

Sheet resistivity was assessed by a four probe resistance measurement technique (Signatone S302-4, SP-4 probe) at Center for Functional Nanomaterials (CFN), Brookhaven National Laboratory, New York. Four spring-loaded probes, spaced equally by 1.25mm distances, were lowered onto glass coverslips coated with crosslinked MWCNT (1:1, 1:2, and 1:4) to measure sheet resistance and resistivity.

Cell Culture

Primary human adipose derived stem cells (ADSCs) were cultured to passage 3 in ADSC basal media supplemented with heat inactivated FBS and ADSC Growth Media Bulletkit™ (Lonza). Cells were grown in tissue culture treated polystyrene at 95% humidity, 5% CO_2, at 37°C with media changes every three days. Nanoparticle coated on coverslips, and plain coverslips (control) were washed with a sterile phosphate buffered saline solution (Gibco, New York) and sterilized under ultraviolet radiation for two hours. Cells were plated on the coverslips (n=6), kept in an un-treated non-adherent 24 well plate, at a density of $4x10^4$ cells per well. Cells were incubated for 24 hours to allow their attachment, after which the coverslips were transferred to a new 24 well plate (considered as the Day 1 time point). Cells were kept plated for three time points; Day 1, 3 or 5. At each time point, the cells were washed twice in phosphate buffered saline solution, and used for viability and cytotoxicity assays.

Cytotoxicity and Cytocompatibility Assays

Cytotoxicity of MWCNT 1:4 films was assessed with ADSCs by measuring lactate dehydrogenase (LDH) release from cells as a function of membrane integrity. (Sigma Aldrich; Missouri, USA). Media was collected from MWCNT films and control coverslips from each cell line at Day 1, 3 and 5. For each sample (n=6), 200µL of the extracted media was incubated for 45 minutes with LDH reagent and absorbance at read at 450 nm. Positive control of 100% dead cells was performed by adding 10 µl of kit-supplied lysis buffer to the control cells. Cell death was calculated from measured optical density of experimental groups, coverslip control, and positive control.

Cell proliferation of ADSCs on MWCNT 1:4 films was assessed using CellTiter 96 Cell Proliferation MTS Assay (Promega; Wisconsin, USA). Briefly, this assay is a water soluble variant of the more commonly used MTT (3-(4,5-dimethylthiazol-2-yl)-2,5-diphenyltetrazolium bromide) assay in which tetrazolium salts are converted to formazan. The colorimetric measurement of formazan (λ=490nm) in the experimental sample, coverslip (live) control, and positive (dead) control allows for the calculation of cell proliferation.

Immunofluorescence / Cell Staining / SEM

Live cells were washed three times with PBS, treated with calcein-AM (0.5mg/ml) for 30 minutes and Hoesct 33342 (2 μg/ml) for 30 minutes. For immunofluorescence microscopy, glutaraldehyde fixed cells were washed with PBS, incubated with 2% glycine for 5 minutes, and permeabilized using 0.5% Triton-X-100 permeabilizing buffer (10.3 g sucrose, 0.4 g Hepes buffer, 0.29 g NaCl, 0.06 g $MgCl_2$, and 0.5 ml Triton-X-100 in 100 ml DI water) for 25 minutes. Samples were washed using immunofluorescence buffer (IFB, 0.1% BSA and 0.1% Triton-X-100 in PBS) and incubated with commercially available monoclonal anti-proliferating Ki-67 antibody raised in mouse (2 μl/ml in IFB, Cat. No. P8825, Sigma Aldrich, New York, USA) for 1 hour. Samples were washed with IFB (3X) and incubated with anti-mouse rhodamine conjugated secondary antibody (2 μl/ml in IFB, Cat. No. SAB3701218, Sigma Aldrich, New York, USA) for 1 hour. Samples were washed with IFB (3X) and stained with FITC conjugated phalloidin (2 μl/ml in PBS) for 1 hour to visualize cytoskeleton (actin filaments). Samples were then imaged using a confocal laser scanning microscope (Zeiss LSM 510 Two-Photon LSCM).

Specimens for scanning electron microscopy (SEM) were prepared as follows. MWCNT 1:4 samples with ADSCs were dehydrated by serial ethanol wetting steps from 50% to anhydrous

ethanol. The samples were then air dried for one day and vacuum dried overnight at room temperature. A 3nm layer of gold sputter was applied prior to SEM. SEM was performed on a high resolution analytical JOEL 7600F SEM at the Center for Functional Nanomaterials (Brookhaven National Laboratories).

Statistical Analysis

All plots for cell studies present a mean and standard deviation. Statistical analysis for cell studies was performed with one-way ANOVA followed by Tukey-Kramer post hoc analysis (Graphpad Prism). Statistical analysis for nanoindentation was performed using Mann-Whitney test (Graphpad Prism). A 95% confidence interval ($p<0.05$) was used for all statistical analysis.

Results and Discussion

Physicochemical Characterization of Crosslinked MWCNT Coatings

Figure 1A depicts the fabrication process. An air pressure driven device sprayed the nanomaterial and benzoyl peroxide solution onto a coverslip heated to 60°C (Figure 1A). The MWCNTs completely coated the coverslips (Figure 1B, top) and were semi-transparent (Figure 1B, bottom). The spraying method leads to the generation of heterogeneously-sized droplets of MWCNT and benzoyl peroxide which deposit onto the heated coverslip. The solvent (ethyl acetate) immediately evaporates, and simultaneously the free radical crosslinking process is initiated which in turn leads to the *in situ* crosslinking of MWCNTs, and fabrication of the films. For all characterization and cell studies, a preset volume and mass of nanomaterial solution was utilized for the fabrication of each film.

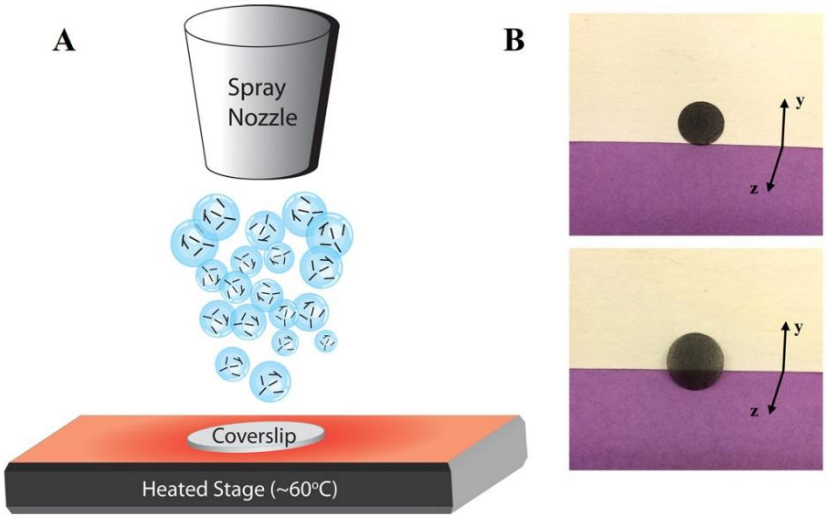

Figure 2.1. Fabrication of crosslinked carbon nanomaterial films. (A) Illustration of *in situ* crosslinking process. (B) Photograph of film standing vertically (top) and tilted to show transparency (bottom).

Low magnification SEM analysis showed that all films created a continuous coating on 12mm diameter glass coverslips with a micro porous network (Figure 2.2A). The films had high surface roughness with a mean height of 75μm (Figure 2.2A inset). Ultra-high resolution SEM showed MWCNT networks with connectivity, micro- and nano-porosity with numerous junctions (Figure 2.2B) of individual MWCNT and bundles crosslinking with each other (Figure 2.2C-D). TEM analysis suggests junctions between two MWCNTs (Figure 2.2E) leading to a checkerboard pattern (Figure 2.2F) similar to previously reported chemically crosslinked MWCNTs[17]. Atomic force microscopy revealed a high root mean square (rms) area surface roughness of 730 nm (S.D. 124 nm, n=3).

Normalized Raman spectra of crosslinked MWCNT films are presented in Figure 3A. Each mass ratio showed the characteristic Raman peaks of MWCNT with D, G, and G' bands at ~ 1345 cm^{-1}, 1560 cm^{-1}, and 2670 cm^{-1}, respectively.[18] Pristine graphitic network is characterized by the G band (intensity represented by I_G) generated by in-plane vibrations of C=C carbon atoms and the D band (intensity represented by I_D) is generated by structural defects or disorder features in graphitic network generate.[18] The I_D/I_G ratio increased with increase in MWCNT: BP ratio (Figure 3B). Further, weakly defined peaks at 802 cm^{-1} to 915 cm^{-1} were observed and assigned to C-O-C bond vibrations and asymmetrical stretching, respectively.[19] These peaks imply presence of covalent carbonyl functional groups most probably formed during the crosslinking reaction.

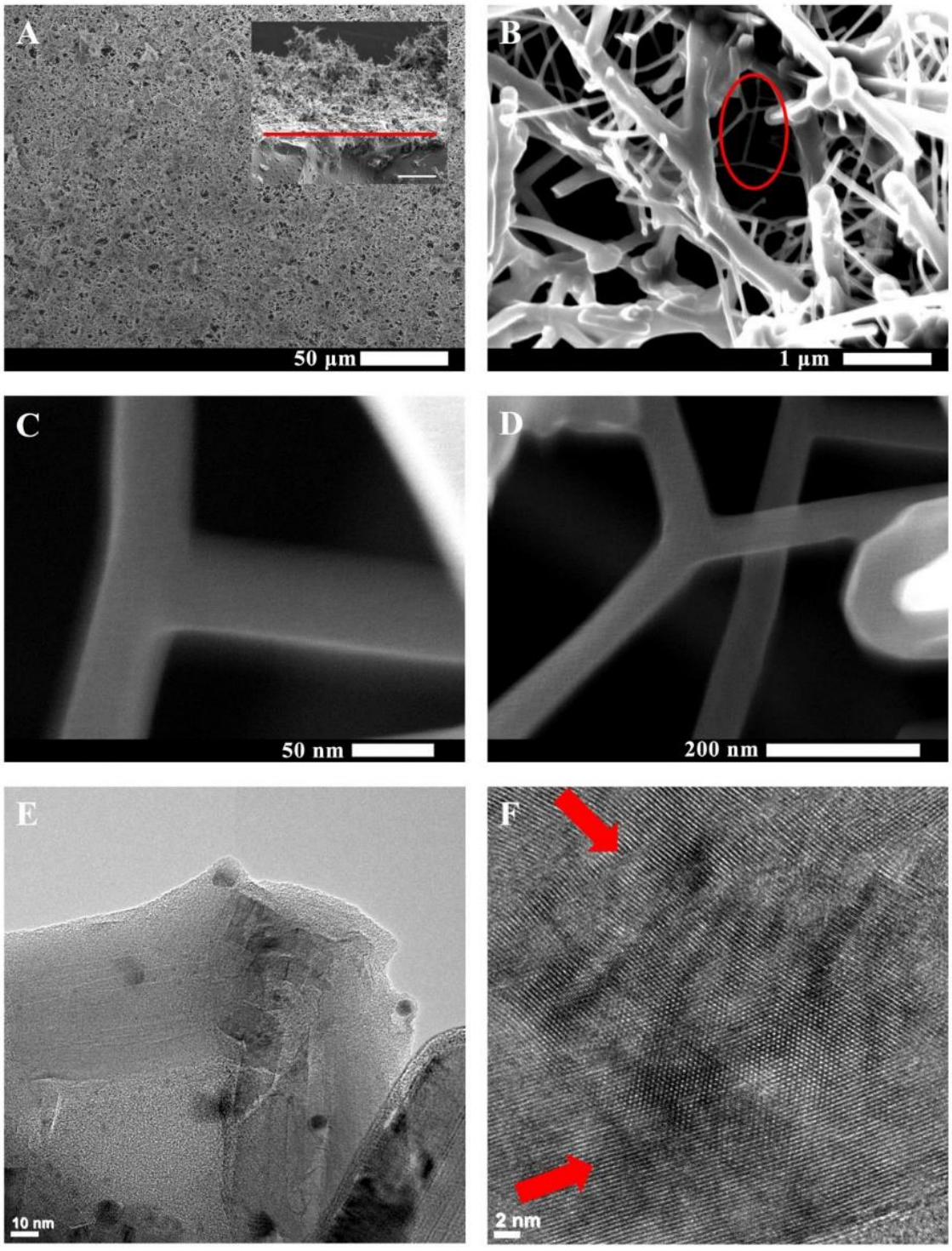

Figure 2.2. Representative SEM and TEM micrographs for 1:4 MWCNT films. (A) Overview micrograph of crosslinked MWCNT coating with a cross-sectional inset in the upper right (scale bar 100µm). Red line denotes the surface-nanomaterial interface. (B) Junctions between nanotubes, shown in red oval (B) and magnified in (C) and (D), suggest crosslinking. (E) TEM image of a single crosslink junction with (F) the directions of intersecting MWCNT lattice shown by red arrows.

Electrical resistivity measurements allow evaluation of the changes in the electrical properties of the MWCNT after the crosslinking reaction. The changes provide surrogate information about the interconnectivity between the MWCNTs.[20] Figure 3B shows the bulk electrical resistivity of the MWCNT films as a function of MWCNT: BP ratio. We found pristine MWCNT coatings to have a resistivity of 29.45 Ω-cm. Adding BP (MWCNT:BP) to samples lead to an initial increased in sheet resistivity to 35.3 Ω-cm for 1:1 (MWCNT:BP) mass ratios and reduction thereafter in sheet resistivity from to 29.2 Ω-cm for 1:4 (MWCNT:BP) mass ratios.

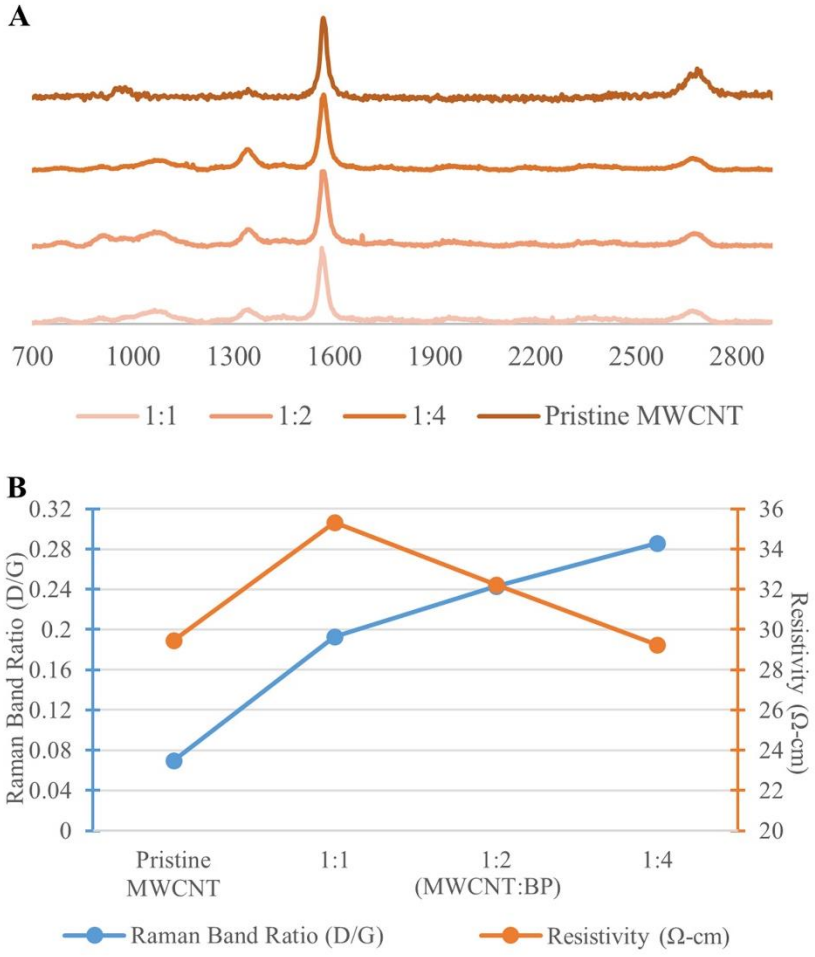

Figure 2.3. A) Representative Raman spectroscopy for MWCNT crosslinked films with three different mass ratios of MWCNT:BP (1:1, 1:2, 1:4). B) MWCNT crosslinked films sheet resistivity and tubular defects analyzed by a four point resistivity system and Raman spectroscopy

Nanoindentation was performed to characterize the mechanical properties of spray-coated chemically-crosslinked MWCNT (1:4) films. Spray coated pristine MWCNT films (without chemical crosslinking) were used as controls. The nanoindentation protocol yielded the values of elastic modulus (Er) and hardness (H) of the films, and are summarized in Table 1. Representative force-displacement curves for the chemically-crosslinked MWCNT and pristine MWCNT films are presented in Figure 2.4. The median Er value of the chemically-crosslinked MWCNT films (mdn=376 MPa, μ=424 MPa, S.D.=287 MPa) were ~232% greater than that of pristine MWCNT (mdn=162 MPa, μ=232 MPa, S.D.=299MPa) ($p < 0.0001$). The crosslinked MWCNT films also exhibited statistically significant ($p<0.0001$) ~242% increase in hardness (mdn=5.15 MPa, μ=5.83 MPa, S.D.=3.84MPa) compared to the pristine MWCNT films (mdn=2.13 MPa, μ=2.37 MPa, S.D.=1.61MPa).

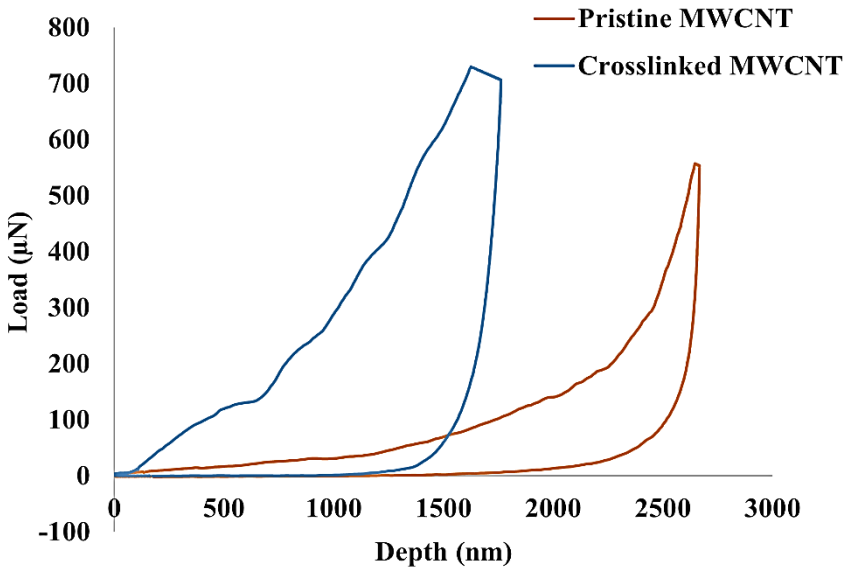

Figure 2.4. Representative load-unloading curve from nanoindentation of spray coated non-crosslinked pristine MWCNT and crosslinked MWCNT (1:4). Elastic modulus (Er) was calculated from the unloading region of each curve.

While the focus of the current study has been on fabrication of all carbon films using MWCNTs as starting material, an advantage to this method lies in its versatility. It can easily be adapted for different sp^2 hybridized allotropes of carbon including, but not limited to, various types of graphene (e.g graphene nano-onions p, nanoribbons and nanoplatelets. See Figure 2.5). This method has four additional advantages: (1) The method should be suitable for a wide variety of substrates (e.g. flexible, irregular or round shaped). The substrates need to be thermally stable up to 60°C and compatible to organic solvents. Comparatively, CVD based films can be grown on a wide variety of substrates, and vacuum filtration films can be fabricated at low temperatures on flat substrates with organic solvents; however, to the best of our knowledge, neither technique allows the flexibility of substrates, solvents and low temperature. (2) This method allows facile control of film thickness. CVD allows deposition of monolayer film of vertically-aligned carbon nanotube forests, or few-layer film of randomly-aligned carbon nanotubes[21] or single and multi-layered graphene.[13] Its capabilities to create thick films still need to be thoroughly explored. Vacuum filtration typically allows maximum film thicknesses of 10-150μm for MWCNT and graphene, since the passage of the filtrate through the filter membrane restricts flow as the film gets deposited on the substrate.[11,22,23] Spray coating of carbon nanotubes onto substrates show sparse network formation[24] which can be a hindrance to create films of controllable thickness.

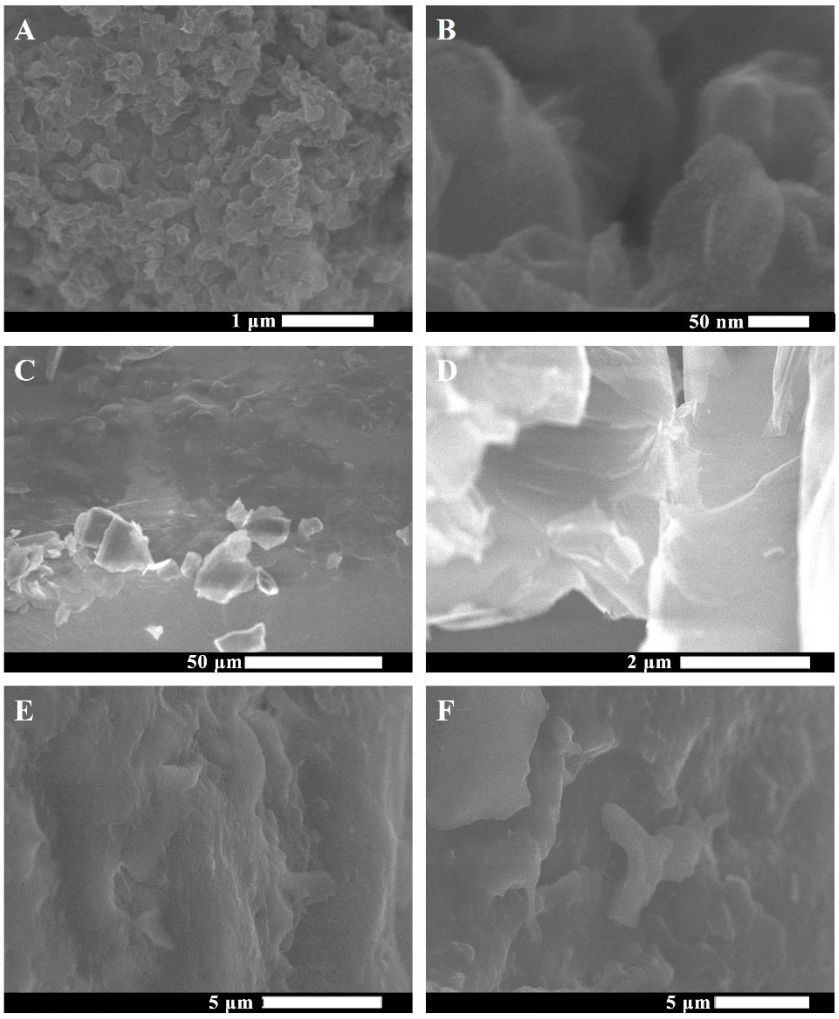

Figure 2.5. Representative low-magnification crosslinked (A, C, E) graphene oxide nanoonions, graphene oxide nanoplatelets, and graphene oxide nanoribbons, (GONO, GONP, and GONR, respectively) and high-magnification crosslinked (B, D, F) GONO, GONP, and GONR SEM images.

Our results indicate that covalent bonding between the MWCNT when combined with spray coating allows for a layer-by-layer assembly of thick coatings (> 100µm in thickness). (3) This method yields coatings with nano- and micro-pores and high surface roughness; advantageous for applications such as biosensing which require high charge storage capacity[25,26] and self-cleaning hydrophobic substrates.[27] Methods such as vacuum filtration and CVD are more suitable for applications that require homogenous roughness coating.[28] Even though spray coating allows coating of irregular shapes, and ability to create a continuous network (Figure 2.2A), the high

surface roughness (~730nm) using the current air spray method warrants exploration of other spray coating techniques. The droplet size inhomogeneity (as depicted in Figure 1A), and nanomaterial aggregation may be responsible for the increased roughness.[29,30] For applications requiring crosslinked MWCNT films with a smoother surface, more homogenous spray coating techniques such as ultrasonic spray coating could be employed. Ultrasonic spray coating has recently shown the ability to create functionalized-MWCNT films of 3 nm average surface roughness. In comparison, vacuum filtration of carbon nanotubes on mixed cellulose ester and transferred to a smooth silicon wafer resulted in 8 nm r.m.s surface roughness.[28] (4) The chemical crosslinking of MWCNTs, substantially enhances the mechanical properties of the films and thus, their structural stability compared to pristine non-crosslinked MWCNT films. This enhancement should prevent the films from disintegration under compressive flexural or shear forces under physiological conditions. Indeed, the crosslinked MWCNT films remained intact during the entire duration (5 days) of static culture experiments. The stability of the films under dynamic conditions still needs to be evaluated. The mean elastic modulus values for crosslinked MWCNT films were comparable and in the same orders of magnitude as polyelectrolyte layer-by-layer SWCNT films,[31] and MWCNTs crosslinked through chemical reaction of functional groups on their surface.[32] However, the elastic modulus of the crosslinked MWCNT is an order of magnitude lower than bucky-paper formed by high pressure compression of CVD synthesized MWCNT films.[33] Though here, the porous structure and control over the porosity of the films also provides a tailorable framework for incorporation of polymers and ceramics to develop novel mechanically-reinforced composites.

Table 2.1. Mechanical properties of spray coated pristine MWCNT and crosslinked MWCNT (MWCNT: BP = 1:4) determined by nanoindentation.

	PRISTINE MWCNT		CROSSLINKED MWCNT	
	Er (MPa)	H (MPa)	Er (MPa)	H (MPa)
MEDIAN	162$^{\#}$	2.13*	376$^{\#}$	5.15*
I.Q.R.	173	1.53	307	5.16
MIN.	20.7	0.452	59.8	0.881
MAX	1762	8.87	1604	22.3

(*represents p<0.0001 between groups and $^{\#}$represents p<0.0001 between groups)

Carbon nanotubes are known to be excellent conductors of electricity, and disruptions (due to functionalization of structural defects) to the sp^2 carbon network are known to decrease electrical conductivity of carbon nanotubes.[34] Although 1:1 (MWCNT:BP) samples showed greater sheet resistivity than pristine MWCNT coatings, we interestingly observed a decrease in sheet resistivity with increase in the defect sites in the MWCNT films to the point of recovery by 1:4 (MWCNT:BP) (Figure 3B). This trend can be attributed to the increased interconnectivity between MWCNT bundles in a less densely packed system.[35] The crosslinked MWCNT films exhibit resistivity similar to previously reported spray coated pristine MWCNT with resistivity values sufficient for applications in electrostatic dissipation and transfer.[36] Although the results suggest that conductivity can be increased by increasing BP concentration for spray coating, high concentrations of BP may cause excessive oxidation of the nanotubes and possible decrease in

conductivity. We observe an increasing amount of sidewall defect formation in the crosslinked carbon nanotube samples and increased electrical resistivity, when compared to the pristine MWCNTs, for 1:1 and 1:2 samples, suggesting that MWCNT interconnectivity and sidewall defects contribute to the electrical properties of these materials. Furthermore, termination reactions involving the benzoyloxyl radicals at MWCNT radical sites may increase as a function of BP concentration as this has been observed in oxidation of olefins by high concentrations of BP.[37] The decrease in conductivity due to oxidation of the nanotubes could be mitigated by treating the MWCNT substrates with reducing agents such as hydrazine hydrate[38] or more biocompatible solutions such as ascorbic acid.[39]

Cytocompatibility and Cytotoxicity

The potential *in vivo* biomedical applications of the MWCNT mats require thorough evaluation of their biocompatibility. *In vitro* cytotoxicity studies are typically the first step before more elaborate and costly *in vivo* animal biocompatibility experiments. Since the MWCNTs mats could be utilized as coatings for orthopedic implants and devices or bone tissue engineering scaffolds, *in vitro* interactions with human adipose derived stem cells (ADSCs) is investigated.[40] Adipose tissue is a good source for multi-potent mesenchymal stem cells; giving greater cell yields with less invasive extraction procedures[41] and good immunosuppressive properties for mitigating graft-host disease.[42] Proliferation and cytotoxicity assays were performed on ADSCs incubated on crosslinked MWCNT films (1:4 of MWCNT:BP) and glass coverslips (control). MTS assay is a measures the conversion of tetrazolium salt to water-soluble formazan crystals by mitochondrial processes in proliferating cells.[43] The release of lactate dehydrogenase (LDH) from compromised cell membranes of dying cells was measured by the LDH toxicity assay. LDH causes oxidation of

lactate to form pyruvate which coverts tetrazolium salt to formazan crystals for colorimetric assessment of LDH release by absorbance spectroscopy.[44] MTS and LDH assays were performed at day 1, 3, and 5 time points. Cytotoxicity of crosslinked MWCNT substrates are normalized to the LDH release of the positive control (100% dead cells by lysis buffer). Live cells on glass coverslips were used as the baseline control for basal LDH release.

Figure 2.6A shows cell proliferation normalized to the control glass coverslips for ADSCs. The initial cell attachment (day 1) on crosslinked MWCNT substrates was approximately 59% of the control group ($p < 0.001$) (Figure 2.6A). At the day 3 time point, there were still significantly less cells on the crosslinked MWNCT substrates (36%, $p < 0.001$) relative to the control group (Figure 2.6A). The cells also proliferated slower from day 1 to day 3 on the crosslinked MWCNT substrates with a 23% decrease in proliferation, compared to the control. Interestingly however, the difference in cell viability at the day 5 timepoint was not significant and recovered to 85% of the value as compared to the control coverslips.

Figure 2.6B shows the cell death on crosslinked MWCNT substrates. The results are normalized to a positive control of 100% dead cells by using an LDH assay lysis buffer. The ADSCs grown on coverslips released approximately 35% and 45% of LDH at days 1 and 3 as compared to the positive control while the cells on the crosslinked MWCNT substrates released approximately 50% and 43% LDH at days 1 and 3 with no statistical differences. A statistical increase by 10% ($p<0.01$) in LDH release was observed at day 5 timepoint LDH assay (Figure 2.6B). This also corresponds to the timepoint where cell proliferation increased as observed by the MTS assay.

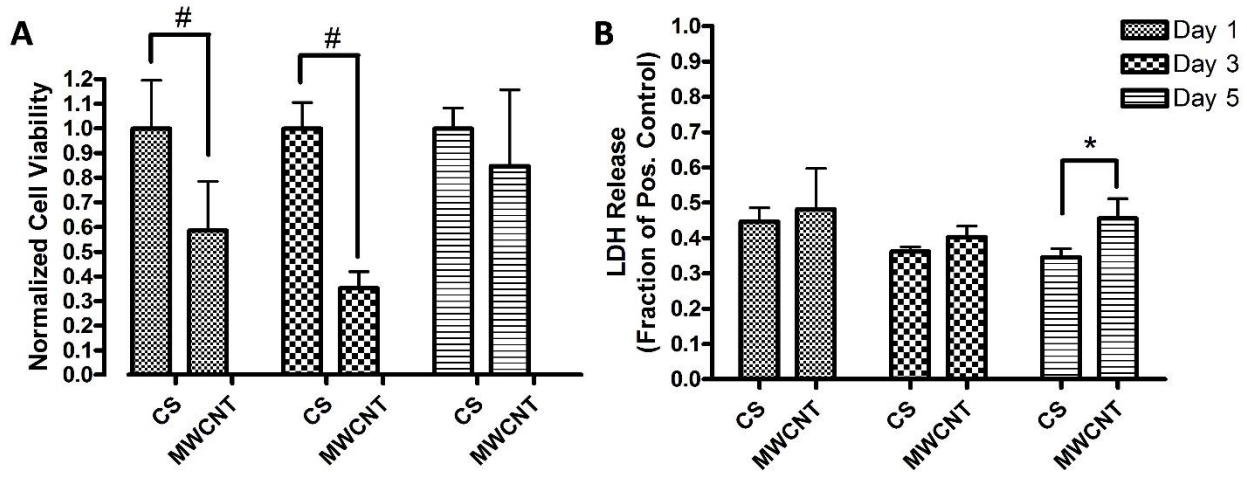

Figure 2.6. (A) Cell proliferation assessed by MTS assay and (B) cytotoxicity assessed by LDH release for ADSCs 1:4 MWCNT:BP crosslinked substrates (MWCNT) and glass coverslips (CS). Data are presented as mean ± SD (n = 6 per group, #indicates $p < 0.001$ and *indicates $p<0.01$)

MTS and LDH assays were employed since they have been validated to be suitable for proliferation and cytotoxicity studies involving carbon nanoparticles.[44,45] MTS proliferation assay (Figure 2.6A,B) indicated decreased cell proliferation at the early time point (day 1 and 3) and recovery to critical density by day 5. Previous studies show that prior to reaching a critical density, a lag phase in cell growth can occur.[46] This effect may be particularly observed when comparing flat 2D substrates, such as coverslips, and thick and rougher substrates, such as the crosslinked MWCNT coatings due to the differences in topography which can hinder proliferation of the cells. LDH cytotoxicity assay (Figure 2.6C,D) indicated that cells remained comparably viable on the MWCNT substrates and the coverslip controls at days 1 and 3. The increase in LDH release at day 5 could be attributed to one of two factors: 1) an increase in basal LDH release for the increasing ADSC proliferation on crosslinked MWCNT substrates or 2) increasing cell death as the cells were

in critical density without media changes for 5 days. The latter may be less likely because we did not observe an increase in LDH release for ADSCs on glass coverslips.

Cell viability was further assessed using calcein AM live cell stain and Hoechst 33342 nuclear stain (Figure 2.7). Cellular uptake of calcein AM by living cells leads to intracellular esterase cleavage, and enhanced green fluorescence due to calcein.[47] Hoechst 33342 is a nucleic acid stain which emits blue fluorescence upon binding to double-stranded DNA (dsDNA), and provides evidence on the presence of dsDNA within intact nuclear membrane of non-apoptotic cells.[48] Calcein AM verified the presence of live cells on glass coverslips (Figure 2.7A) and on crosslinked MWCNT substrates (Figure 2.7B). The Hoechst 33342 stains indicated that dsDNA was indeed confined within the cell in the nucleus. Together the stains provided surrogate confirmation of live cells well spread on the glass coverslips (Figure 2.7A) and MWCNT substrates (Figure 2.7B,C).

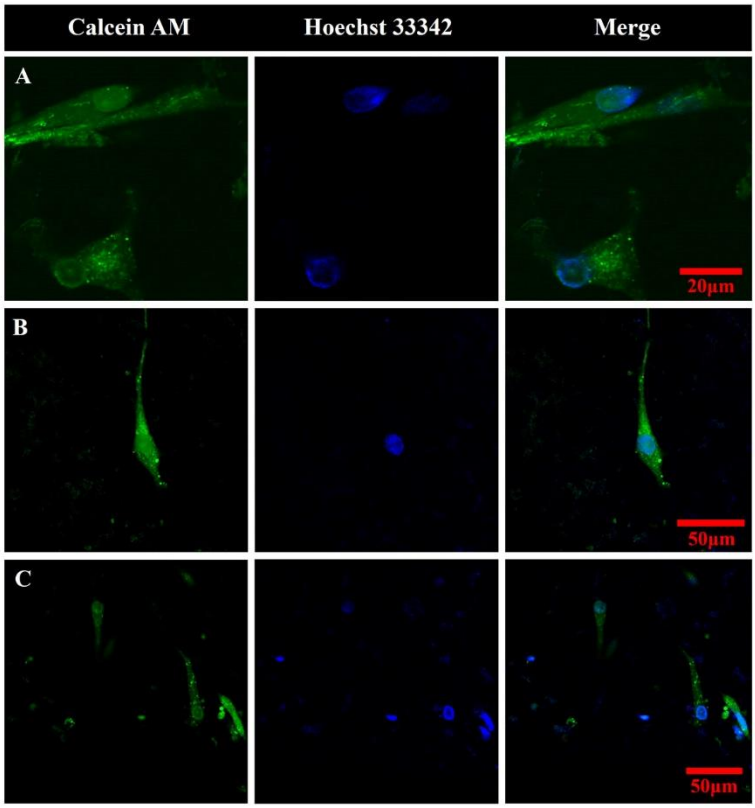

Figure 2.7. Representative confocal fluorescence microscopy of ADSCs stained with Calcein-AM (λ_{ex}=488nm, λ_{em}=505nm) and Hoechst 33342 (two-photon λ_{ex}=800nm, λ_{em}=465nm) grown on glass coverslips (A) and MWCNT crosslinked substrates (B and C) for 5 days at 37°C.

Immunochemistry studies were conducted to investigate whether cell division was arrested in cells seeded on the MWCNT substrates. In these experiments, ADSCs grown on coverslips and MWCNT films for five days were stained with fluorescently labeled antibodies for cellular proliferation marker protein, Ki-67, and probed for fluorescence (Figure 2.8, center column). Ki-67 protein is present in all phases of cell growth, and can therefore be employed to evaluate whether the ADSCs are still dividing while cells that enter a G_0 resting phase would not express Ki-67 protein.[49] Additionally, cells were stained for β-actin (Figure 2.8, left column) to identify the cytoskeleton of the ADSCs. The merged images of Ki-67 and β-actin (Figure 2.8, right column) show the presence of Ki-67 throughout the cell cytoplasm and nucleus for cells seeded on glass coverslips (Figure 2.8A,B) or MWCNT (Figure 2.8C,D) substrates implying that the cells were proliferating and metabolically active. Actin staining, also showed a more elongated cellular morphology on the MWCNT substrates (Figure 2.8D) compared to the control coverslips (Figure 2.8B).

Immunohistochemistry analysis (Figure 2.8) also showed cell spreading and proliferation on the MWCNT mats and provided further evidence that these mats did not affect the various phases of cell growth cycle. For further investigation, SEM was used to characterize the cellular morphology and cellular adhesion to the substrates. Figure 2.9 shows representative SEM images of ADSCs on the MWCNT substrates. The images shows uniaxially elongated cells (double-sided arrows in Figure 2.9C,E,F) on the MWCNT substrates. The images suggested that cells interfaced well with MWCNT substrate. Cells had cytoplasmic prolongations (Figure 2.9A,C red circles) that seemed to attach to the MWCNT fibers (Figure 2.9B, indicated by red arrows) by wrapping over or under the fiber bundles (Figure 2.9D, indicated by red arrows).

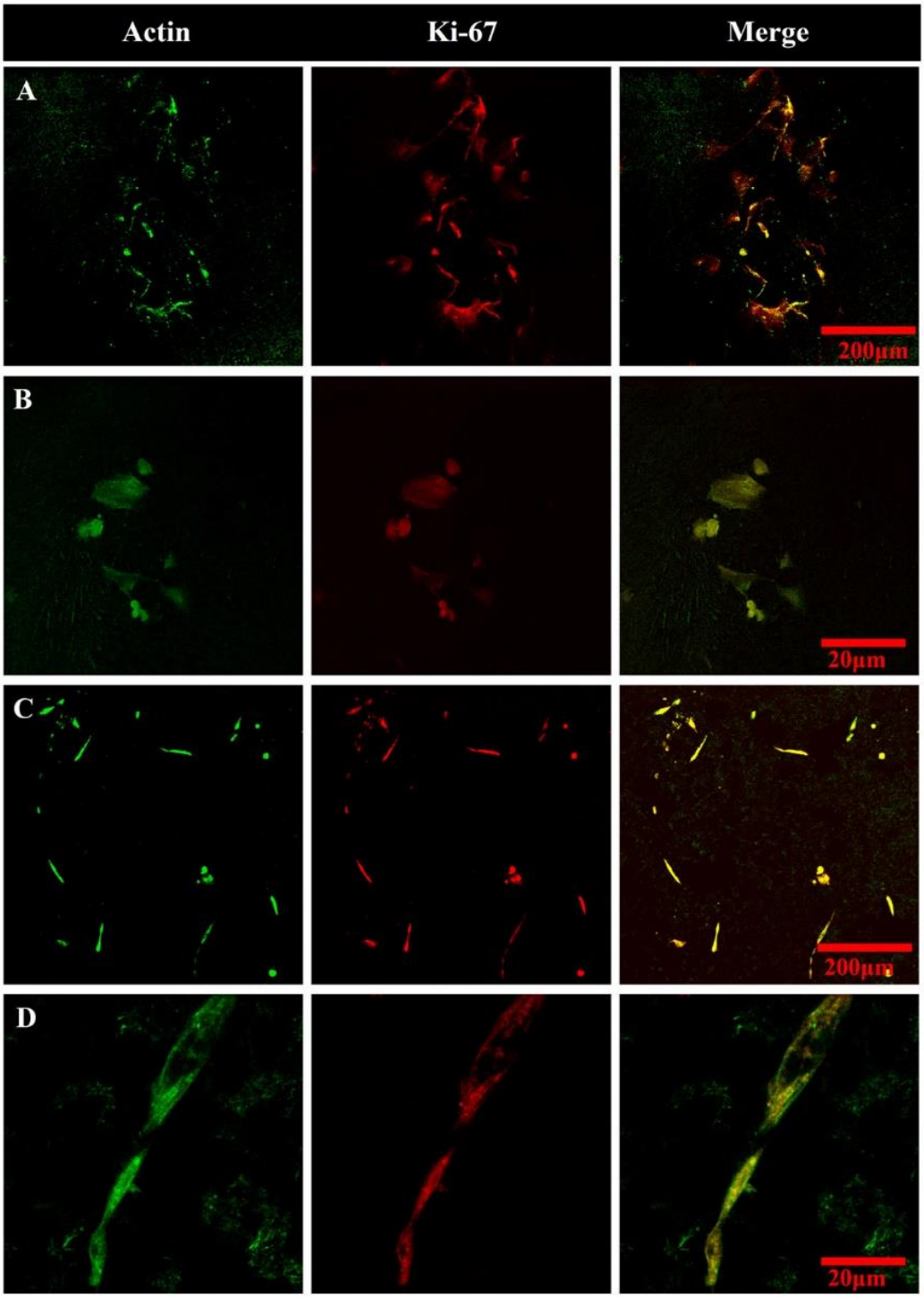

Figure 2.8. Representative confocal immunofluorescence microscopy of ADSCs for actin (λ_{ex}=488nm, λ_{em}=550nm) and proliferation marker Ki-67 (λ_{ex}=543nm, λ_{em}=560nm). Images taken for ADSCs grown for 5 days on glass coverslips at 10x (A) and 20x (B) magnification and MWCNT crosslinked substrates at 10x (C) and 20x magnification (D).

The assays, immunochemistry and SEM analysis together clearly showed that, even though the initial cell proliferation rates on the MWCNT substrates were slower compared to coverslip controls, the MWCNTs were not cytotoxic and allowed cell attachment and proliferation over the 5 day period. Harnessing the potential of carbon nanotechnology for biomedical applications often requires the 2D and 3D macroscopic assembly of nanoscale building-blocks. The results of this work introduce a novel, facile, cheap, and scalable method to fabricate robust carbon nanotube mats with chemically cross-linked junctions between sp^2 carbon atoms, which can be easily adapted for other carbon nanostructures such as graphene and a variety of substrates with different shapes. Furthermore, with the advent of commercialized 3D printing, the mechano-structural benefits provided by the chemical crosslinks should allow for 3D-printed all-carbon nanomaterial structures.

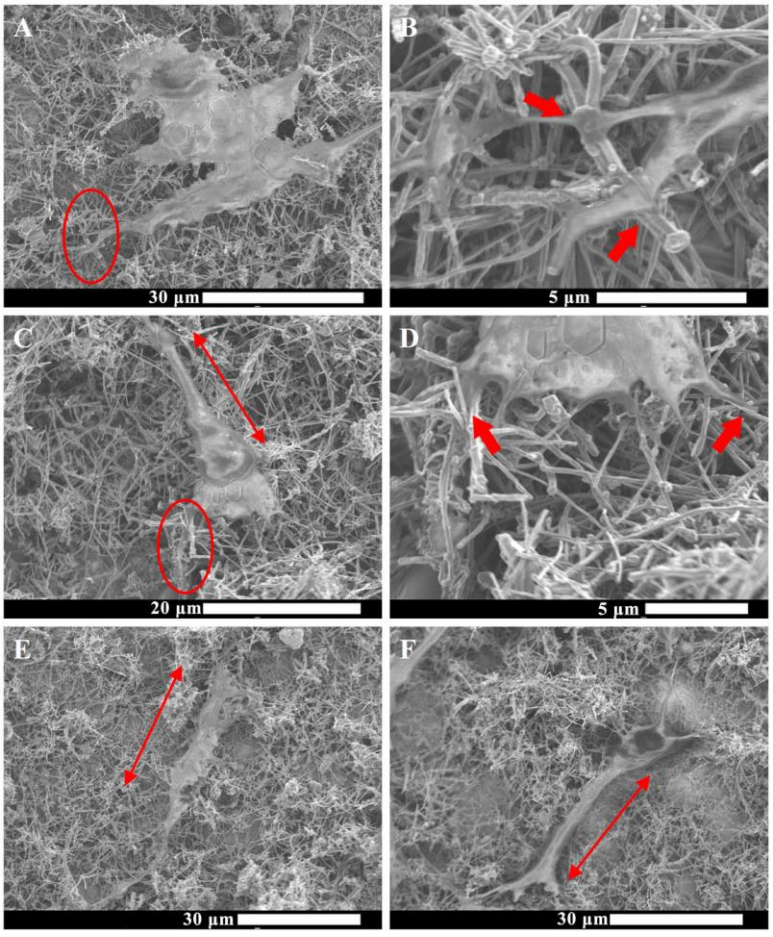

Figure 2.9. Representative SEM images of adipose derived stem cells grown on MWCNT substrates. Red circles in (A) and (C) are magnified in (B) and (D) respectively with red arrows showing cell adhesion by wrapping around nanotubes (B) or cell protrusions going underneath nanotube structures (D).

The results open avenues further *in vitro* and *in vivo* studies to the further explore the potential of MWCNT films as a novel class of nano-fibrous mats for tissue engineering and regenerative medicine applications. The nano-fibrous MWCNT mats could be beneficial over conventional polymeric electrospun films and other methods to create nanofibrous mats[50] for tissue engineering application. Even though nanofibrous substrates have numerous advantages as synthetic extracellular matrix scaffolds of various tissue,[51] techniques employed to fabricate nanofibrous mats, such as molecular self-assembly, face severe commercialization and scale-up issues including expensive processing and poor control of fiber diameter.[50] Electrospinning, the current gold standard method to fabricate nanofiber requires very precise control of humidity, viscosity, and solvent volatility to produce consistent nanofibers. Marginal increases in humidity can cause large inhomogeneity in fiber diameter and clotting at the electrospray source.[52] Assembly of engineered nanomaterials such as MWCNT could overcome these fabrication challenges and allow the consistent fabrication of synthetic nanofiber mats with narrow size distribution. Further, the dense packing of electrospun fibers, and consequent lack of macro-porosity,[53] prohibiting cell infiltration into these scaffolds.[54] The method discussed herein allows fabrication of MWCNT substrates with micro- and macro porous architecture, which should allow cell infiltration. Additionally, carbon nanotubes assembled in 2D films and substrates, may exhibit multifunctional capabilities for regenerative medicine applications. The electromagnetic and electrical properties of these carbon nanostructures could be exploited to develop stimulus responsive scaffolds for electroceuticals,[55] control the fate of progenitor cells,[56-58] and non-invasively image the scaffolds and the regenerative process.[59]

Conclusions

Radical initiated thermal crosslinking of carbon nanomaterials combined with air-pressure driven spray coating technique, allows rapid in situ assembly of MWCNTs into chemically-crosslinked and mechanically robust MWCNT films. This protocol can be easily adapted for other carbon nanostructures such as graphene (e.g graphene nano-onions, graphene nanoribbons and graphene nanoplatelets). The crosslinked MWCNT films were found to be cytocompatible for human ADSCs. The results introduce a novel, facile, cheap, and scalable method to fabricate robust carbon nanotubes nanofiber mats and open avenues further in vitro and in vivo exploration their multifunctional potential for tissue engineering and regenerative medicine applications.

Acknowledgements

This work was sponsored by National Institutes of Health grants (1DP2OD007394 and AR61821). Electrical measurements and SEM were conducted at Center for Functional Nanomaterials at BNL, supported by the U.S. Department of Energy, Office of Basic Energy Sciences, under Contract No. DE-AC02-98CH10886.

References

1 Lalwani, G. & Sitharaman, B. Multifunctional fullerene-and metallofullerene-based nanobiomaterials. *Nano LIFE* **3** (2013).

2 Zhang, Y., Nayak, T. R., Hong, H. & Cai, W. Graphene: a versatile nanoplatform for biomedical applications. *Nanoscale* **4**, 3833-3842 (2012).

3 Harrison, B. & Atala, A. Carbon nanotube applications for tissue engineering. *Biomaterials* **28**, 344-353 (2007).

4 Jariwala, D., Sangwan, V. K., Lauhon, L. J., Marks, T. J. & Hersam, M. C. Carbon nanomaterials for electronics, optoelectronics, photovoltaics, and sensing. *Chem. Soc. Rev.* **42**, 2824-2860 (2013).

5 Nayak, T. R. *et al.* Graphene for controlled and accelerated osteogenic differentiation of human mesenchymal stem cells. *ACS Nano* **5**, 4670-4678 (2011).

6 Ryoo, S.-R., Kim, Y.-K., Kim, M.-H. & Min, D.-H. Behaviors of NIH-3T3 fibroblasts on graphene/carbon nanotubes: proliferation, focal adhesion, and gene transfection studies. *ACS Nano* **4**, 6587-6598 (2010).

7 Hirata, E. *et al.* Multiwalled carbon nanotube-coating of 3D collagen scaffolds for bone tissue engineering. *Carbon* **49**, 3284-3291 (2011).

8 Hu, L., Hecht, D. S. & Gruner, G. Carbon nanotube thin films: fabrication, properties, and applications. *Chem. Rev.* **110**, 5790-5844 (2010).

9 Lobo, A. *et al.* Cell viability and adhesion on as grown multi-wall carbon nanotube films. *Mater. Sci. Eng., C* **28**, 264-269 (2008).

10 Kalbacova, M., Broz, A., Kong, J. & Kalbac, M. Graphene substrates promote adherence of human osteoblasts and mesenchymal stromal cells. *Carbon* **48**, 4323-4329 (2010).

11 Chen, H., Müller, M. B., Gilmore, K. J., Wallace, G. G. & Li, D. Mechanically strong, electrically conductive, and biocompatible graphene paper. *Adv. Mater.* **20**, 3557-3561 (2008).

12 Lau, K. K. *et al.* Superhydrophobic carbon nanotube forests. *Nano Lett.* **3**, 1701-1705 (2003).

13 Reina, A. *et al.* Large area, few-layer graphene films on arbitrary substrates by chemical vapor deposition. *Nano Lett.* **9**, 30-35 (2008).

14 Wu, Z. *et al.* Transparent, conductive carbon nanotube films. *Science* **305**, 1273-1276 (2004).

15 Nayak, T. R. *et al.* Thin films of functionalized multiwalled carbon nanotubes as suitable scaffold materials for stem cells proliferation and bone formation. *ACS Nano* **4**, 7717-7725 (2010).

16 Tutak, W. *et al.* Toxicity induced enhanced extracellular matrix production in osteoblastic cells cultured on single-walled carbon nanotube networks. *Nanotechnology.* **20**, 255101 (2009).

17 Lalwani, G. *et al.* Fabrication and characterization of three-dimensional macroscopic all-carbon scaffolds. *Carbon* **53**, 90-100 (2012).

18 Dresselhaus, M. S., Dresselhaus, G., Saito, R. & Jorio, A. Raman spectroscopy of carbon nanotubes. *Phys. Rep.* **409**, 47-99 (2005).

19 Sahoo, S., Chakraborti, C., Mishra, S., Naik, S. & Nanda, U. FTIR and Raman Spectroscopy as a Tool for Analyzing Sustained Release Hydrogel of Ciprofloxacin/Carbopol Polymer. *J. Adv. Pharm. Technol. Res.* **2**, 195-204 (2011).

20 Nirmalraj, P. N., Lyons, P. E., De, S., Coleman, J. N. & Boland, J. J. Electrical Connectivity in Single-Walled Carbon Nanotube Networks. *Nano Lett.* **9**, 3890-3895, (2009).

21 Murakami, Y. *et al.* Growth of vertically aligned single-walled carbon nanotube films on quartz substrates and their optical anisotropy. *Chem. Phys. Lett.* **385**, 298-303 (2004).

22 Dikin, D. A. *et al.* Preparation and characterization of graphene oxide paper. *Nature* **448**, 457-460 (2007).

23 Xu, G., Zhang, Q., Zhou, W., Huang, J. & Wei, F. The feasibility of producing MWCNT paper and strong MWCNT film from VACNT array. *App. Phys. A* **92**, 531-539 (2008).

24 Kaempgen, M., Duesberg, G. & Roth, S. Transparent carbon nanotube coatings. *App. Surf. Sci.* **252**, 425-429 (2005).

25 Keefer, E. W., Botterman, B. R., Romero, M. I., Rossi, A. F. & Gross, G. W. Carbon nanotube coating improves neuronal recordings. *Nat. Nanotechnol.* **3**, 434-439 (2008).

26 Collaert, N. *et al.* In vitro recording of neural activity using carbon nanosheet microelectrodes. *Carbon* **67**, 178-184, (2014).

27 Wang, Z., Koratkar, N., Ci, L. & Ajayan, P. M. Combined micro-/nanoscale surface roughness for enhanced hydrophobic stability in carbon nanotube arrays. *App. Phys. Lett.* **90**, 143117 (2007).

28 Tenent, R. C. *et al.* Ultrasmooth, Large-Area, High-Uniformity, Conductive Transparent Single-Walled-Carbon-Nanotube Films for Photovoltaics Produced by Ultrasonic Spraying. *Adv. Mater.* **21**, 3210-3216 (2009).

29 Yang, J., Zhang, Z., Men, X. & Xu, X. Fabrication of stable, transparent and superhydrophobic nanocomposite films with polystyrene functionalized carbon nanotubes. *App. Surf. Sci.* **255**, 9244-9247 (2009).

30 Geng, H.-Z. *et al.* Effect of acid treatment on carbon nanotube-based flexible transparent conducting films. *J. Am. Chem. Soc.* **129**, 7758-7759 (2007).

31 Xue, W. & Cui, T. Characterization of layer-by-layer self-assembled carbon nanotube multilayer thin films. *Nanotechnology* **18**, 145709 (2007).

32 Cha, S. I. *et al.* Mechanical and electrical properties of cross-linked carbon nanotubes. *Carbon* **46**, 482-488 (2008).

33 Zhang, L., Zhang, G., Liu, C. & Fan, S. High-Density Carbon Nanotube Buckypapers with Superior Transport and Mechanical Properties. *Nano Lett.* **12**, 4848-4852, (2012).

34 Dai, H., Wong, E. W. & Lieber, C. M. Probing electrical transport in nanomaterials: conductivity of individual carbon nanotubes. *Science* **272**, 523-526 (1996).

35 Zhang, M. *et al.* Strong, transparent, multifunctional, carbon nanotube sheets. *Science* **309**, 1215-1219 (2005).

36 Kaempgen, M., Duesberg, G. S. & Roth, S. Transparent carbon nanotube coatings. *App. Surf. Sci.* **252**, 425-429 (2005).

37 Bateman, L. Olefin oxidation. *Q. Rev. Chem. Soc.* **8**, 147-167 (1954).

38 Stankovich, S. *et al.* Synthesis of graphene-based nanosheets via chemical reduction of exfoliated graphite oxide. *Carbon* **45**, 1558-1565 (2007).

39 Fernandez-Merino, M. *et al.* Vitamin C is an ideal substitute for hydrazine in the reduction of graphene oxide suspensions. *J. Phys. Chem. C* **114**, 6426-6432 (2010).

40 Talukdar, Y., Rashkow, J. T., Lalwani, G., Kanakia, S. & Sitharaman, B. The effects of graphene nanostructures on mesenchymal stem cells. *Biomaterials* **35**, 4863-4877 (2014).

41 Kern, S., Eichler, H., Stoeve, J., Klüter, H. & Bieback, K. Comparative analysis of mesenchymal stem cells from bone marrow, umbilical cord blood, or adipose tissue. *Stem Cells* **24**, 1294-1301 (2006).

42 Yanez, R. *et al.* Adipose Tissue-Derived Mesenchymal Stem Cells Have In Vivo Immunosuppressive Properties Applicable for the Control of the Graft-Versus-Host Disease. *Stem Cells* **24**, 2582-2591 (2006).

43 Lewinski, N., Colvin, V. & Drezek, R. Cytotoxicity of nanoparticles. *Small* **4**, 26-49 (2008).

44 Mullick Chowdhury, S. *et al.* Cell specific cytotoxicity and uptake of graphene nanoribbons. *Biomaterials* **34**, 283–293 (2012).

45 Avti, P. K., Caparelli, E. D. & Sitharaman, B. Cytotoxicity, cytocompatibility, cell-labeling efficiency, and in vitro cellular magnetic resonance imaging of gadolinium-catalyzed single-walled carbon nanotubes. *J. Biomed. Mater. Res. A* **101**, 3580-3591 (2013).

46 Bensaïd, W. *et al.* A biodegradable fibrin scaffold for mesenchymal stem cell transplantation. *Biomaterials* **24**, 2497-2502 (2003).

47 Sayes, C. M. *et al.* The differential cytotoxicity of water-soluble fullerenes. *Nano Lett.* **4**, 1881-1887 (2004).

48 Allen, S., Sotos, J., Sylte, M. & Czuprynski, C. Use of Hoechst 33342 staining to detect apoptotic changes in bovine mononuclear phagocytes infected with Mycobacterium avium subsp. paratuberculosis. *Clin. Diagn. Lab. Immunol.* **8**, 460-464 (2001).

49 Scholzen, T. & Gerdes, J. The Ki-67 protein: from the known and the unknown. *J. Cell. Physiol.* **182**, 311-322 (2000).

50 Luo, C., Stoyanov, S. D., Stride, E., Pelan, E. & Edirisinghe, M. Electrospinning versus fibre production methods: from specifics to technological convergence. *Chem. Soc. Rev.* **41**, 4708-4735 (2012).

51 Stevens, M. M. & George, J. H. Exploring and engineering the cell surface interface. *Science* **310**, 1135-1138 (2005).

52 Subbiah, T., Bhat, G., Tock, R., Parameswaran, S. & Ramkumar, S. Electrospinning of nanofibers. *J. Appl. Polym. Sci.* **96**, 557-569 (2005).

53 Baker, B. M. *et al.* The potential to improve cell infiltration in composite fiber-aligned electrospun scaffolds by the selective removal of sacrificial fibers. *Biomaterials* **29**, 2348-2358 (2008).

54 Hollister, S. J. Porous scaffold design for tissue engineering. *Nat. Mater.* **4**, 518-524 (2005).

55 Famm, K., Litt, B., Tracey, K. J., Boyden, E. S. & Slaoui, M. Drug discovery: A jump-start for electroceuticals. *Nature* **496**, 159-161 (2013).

56 Supronowicz, P. *et al.* Novel current-conducting composite substrates for exposing osteoblasts to alternating current stimulation. *J. Biomed. Mater. Res. A* **59**, 499-506 (2002).

57 Harrison, B. S. & Atala, A. Carbon nanotube applications for tissue engineering. *Biomaterials* **28**, 344-353 (2007).

58 Sitharaman, B., Avti, P. K., Schaefer, K., Talukdar, Y. & Longtin, J. P. A novel nanoparticle-enhanced photoacoustic stimulus for bone tissue engineering. *Tissue Eng. Part A* **17**, 1851-1858 (2011).

59 Pramanik, M., Swierczewska, M., Wang, L. V., Green, D. & Sitharaman, B. Single-walled carbon nanotubes as a multimodal-thermoacoustic and photoacoustic-contrast agent. *J. Biomed. Opt.* **14**, 034018-034018-034018 (2009).

60 Ozcivici, E., Ferreri, S., Qin, Y.-X. & Judex, S. Determination of bone's mechanical matrix properties by nanoindentation. *Osteoporosis* 323-334 (Springer, 2008).

Chapter 3

Layer-on-Layer Assembly of 2D and 3D Crosslinked Carbon Nanomaterial Architectures by Ultrasonic Spray Deposition

Contributions by: Sunny C. Patel, Owais Alam, Tony Zhang, Kartikey Grover, Yi-Xian Qin, Balaji Sitharaman

Abstract

Two and three dimensional assemblies of carbon nanomaterials are required to utilize their remarkable physicochemical properties in many applications. Spray coating of carbon nanomaterials is a facile method to fabricate macroscopic coatings but the coatings lack structural robustness and bonding between the individual nanoparticles. Herein we report a method to spray uniform, chemically crosslinked coatings of various allotropes of carbon nanotubes and graphene using ultrasonic spray coating. The method produces robust macroscopic carbon nanoparticle coatings, while maintaining their nanoarchitecture and sp^2 hybridized chemistry. Furthermore, we fabricated free-standing, porous, three dimensional SWCNT structures as a proof of concept of layer-on-layer assembled 3D structures. This technique opens avenues for creating more robust carbon nanomaterial assemblies and the potential for 3D printing of all-carbon nanomaterial structures.

Introduction

Carbon nanomaterials such as graphene, carbon nanotubes, fullerenes, etc., possess many interesting and unique physicochemical properties[1] which have led to their investigation for energy,[2] optical,[3] and biomedical[4] fields. While many of the specific applications for each field exists for individual nanoparticles, larger macroscopic assemblies of the nanoparticles are also required for many specific applications. Two- and three- dimensional carbon nanomaterial assemblies have been developed for applications including sensor development,[5,6] solar cells,[7] electromagnetic shielding,[8,9] fuel cells,[10] and scaffolding.[11]

Spray coating of carbon nanomaterials is one of the most inexpensive and flexible methods for creating surface coatings. Unlike other coating modalities, such as chemical vapor deposition and vacuum filtration of carbon nanomaterials, spray coating does not require a flat substrate, impose specific substrate chemistries for chemical growth of the nanomaterial, or exert high pressures and temperatures on the substrates.[12-14] The layer-on-layer approach of spray coating allows for fine control of coating thickness and recent advances have also significantly improved surface homogeneity[15] and the mechanical properties of spray coated carbon nanomaterial coatings.[16]

Spray coating has been previously used to fabricate large surface area graphene[17] and carbon nanotube[15,18] films. Two main methods of spray coating includes airbrushing techniques and ultrasonic spray coating. Airbrushing is the application of an aerosolized dispersion of particles using a pressurized gas carrier. Airbrushed coatings have been fabricated for stem cell differentiation on carbon nanotube coatings,[19] carbon nanotube solar cell counter electrodes,[18] and graphene based semiconductors.[20] Ultrasonic spray coating is a newer method which utilizes a high frequency actuated nozzle creating more homogenous droplets than airbrushing, with

individual droplet volumes as low as the picoliter range.[21] In contrast to airbrush methods, ultrasonic spray nozzles also disperses the nanomaterials as the ultrasonic vibrations can disrupt particle aggregates and self-cleans at the nozzle to prevent nanomaterial accumulation at the spray head. Ultrasonic spray coating of carbon nanomaterials has been investigated for assembly of graphene-carbon nanotube composite electrochemical cells[22] and carbon nanotube photovoltaics.[15] While these techniques have proved to be efficacious at laboratory scales, many real-world applications of these assemblies are still severely hindered by their limitation. One of the greatest limitations of spray coating carbon nanomaterials is the lack of strong physical (compaction) and chemical (covalent) bonding between the particles. For example, while graphene and carbon nanotube coatings show prospect for orthopedic devices, they lack of physical and chemical bonds between individual particles which can lead to loose nanoparticle related toxicity.[23] Also for some photovoltaic applications, such as solar panels, components need to be durable and able to withstand various mechanical stressors.[24]

Recently, we have reported a method to fabricate robust, *in situ* chemically-crosslinked multiwalled carbon nanotubes (MWCNT) coatings using a simple free radical crosslinking protocol.[25] We reported a method to fabricate high surface roughness coatings using MWCNTs and benzoyl peroxide, a free radical initiator, by a facile airbrushing technique. However, with airbrushing, there are some severe limitations. First, the pressure required to carry the solvent and create droplets can reach over 20 psi, which can disrupt the coating and cause inhomogeneity on the surface. Second, the droplets created by the airbrush are more inhomogeneous in size and volume when compared to ultrasonic spray coating. Therefore we believe smoother and more uniform coatings of the carbon nanomaterials are achievable by adopting a more appropriate coating system.[26]

Herein we present a technique to create chemically crosslinked carbon nanomaterial coatings by a layer-on-layer ultrasonic spray coating approach. The chemical crosslinking continues to be an *in situ* process which allows us to fabricate thick, macroscopic coatings. In this study we also explore and compare coatings made with different diameter carbon nanotubes and graphene allotropes. Lastly we show a proof of concept to utilize this technique and build layer-on-layer assembled, free-standing, three dimensional crosslinked carbon nanotube structures.

Materials and Methods

Materials

Multi-walled carbon nanotubes of high diameter (MWCNT-H) and multi-walled carbon nanotubes of low diameter (MWCNT-L) were purchased from Sigma Aldrich (St. Louis, MO. USA). The free radical initiator, benzoyl peroxide (BP) and anhydrous ethyl acetate was also purchased from Sigma Aldrich (St. Louis, MO. USA). Single-walled carbon nanotubes (SWCNT) and research-grade graphene oxide nanoplatelets (GONP) were purchased from CheapTubes (Cambridgeport, VT. USA). Graphene oxide nanoribbons (GONR) were provided by AZ Electronic Materials (Branchburg, NJ, USA).

Film Fabrication

For each carbon nanomaterial geometry, 0.4-1.0 mg/ml dispersions were made in anhydrous ethyl acetate and subsequently treated by bath sonication for 1 hour to disperse aggregated particles. In order to initiate *in situ* crosslinking of nanomaterials, BP was added to each solution at a 1:4 mass ratio of nanomaterial to BP shortly before spraying. Spray coating was conducted in a rastering pattern utilizing an automated XYZ gantry with an ultrasonic spray nozzle (Sonaer Ultrasonics, Farmingdale, NY. USA). The nanomaterial and BP were fed to the nozzle by a syringe pump with flow rates varying according to the speed of the x-y motion and nanoparticle concentration. The suspensions were coated onto 12mm diameter commercially pure (Grade 2) titanium circles fabricated by Wyoming Machine (Stacy, MN. USA). Additionally inert nitrogen gas was fed into the spray nozzle to shape the spray into a conical shape as it exits the spray head. While spray coating, the titanium circles were affixed to a custom fabricated aluminum vacuum

chuck. The vacuum chuck was placed directly onto an aluminum hotplate with a set point temperature of 135°C. The temperature at the surface of the titanium was found to be around 90°C as measured by a laser guided heat gun (Fluke, Everett, WA. USA).

Layer-on-Layer Fabrication of 3D Structures

Three dimensional structures were fabricated using a dispersion of 1.0 mg/ml SWCNT in chloroform which were dispersed via bath sonication for 1 hour prior to spraying. Similar to the 2D coatings, BP was added to the solution at a 1:4 mass ratio of SWCNT to BP shortly before spraying. The solution was sprayed into a cylindrical well made by drilling a 3/16" diameter hole in an aluminum block. The ultrasonic spray nozzle rasterized between three wells above the mold. While spraying the mold was placed on an aluminum hotplate with a set point temperature of 105°C. The resultant 3D carbon nanotube architecture was removed from the well by gently dislodging it using a sharp 27 gauge needle and sharp tweezers.

Electron Microscopy

Scanning electron microscopy (SEM) analysis was performed at Brookhaven National Lab on a JEOL 7600 analytical high-resolution SEM. Carbon nanomaterial films on titanium discs were sputter coated with 3nm of silver to prevent surface charge accumulation and provide higher resolution imaging.

Transmission electron microscopy (TEM) of crosslinked thin films were performed on lacey carbon TEM grids (Ted Pella, Redding, CA, USA). Each coating surface was scratched with sharp tweezers and the fragmented coating was placed over the lacey carbon grid. TEM was

performed at Brookhaven National Lab on a JOEL 1400F analytical TEM at 80kV accelerating voltage.

Atomic Force Microscopy

For atomic force microscopy (AFM), the crosslinked films on titanium substrates were probed with a NanoSurf EasyScan 2 Flex AFM (NanoScience Instruments Inc., Phoenix AZ). AFM was performed in tapping-mode by a V-shaped cantilever (APP Nano ACL − 10, frequency fc = 145−230 kHz, L = 225 μm, W= 40 μm, tip radius < 10 nm, spring constant k = 20−95 N/m) mounted on a 10μm x 10μm scan head. NanoSurf Easy Scan 2 software was utilized to calculate the root mean square (r.m.s.) area surface roughness of the coatings.

Raman Spectroscopy

Raman spectroscopy (Enwave Optronics, Irvine, CA) was performed in five regions of each sample under a 40x objective using a 532nm laser source. Point spectra scanning from 100 to 3,100 cm^{-1}, at room temperature, were acquired for analysis.

Mechanical Testing- Nanoindentation

Quasi-static nanoindentaiton was used to find the elastic modulus and hardness of the various carbon nanoparticle coatings. The coated titanium disks were subsequently attached to AFM specimen disks (Ted Pella, of 15 mm diameter), which were finally mounted on the magnetic base of the nanoindenter (Hysitron, Minneapolis, MN USA). Points of indentation were chosen using the imaging system of the triboindenter (with an objective of 10X magnification and eyepiece of 2X magnification), after careful analysis. The selection of the indentation took account

of the porous structure of the samples. Each point was selected at a distance no less than 100 μm away from the others. Each indentation further comprised of 9 sub-indents in a 3 × 3 pattern. The tip area function was calibrated from indentation analysis on fused quartz, and drift rates in the system were measured prior to each indentation. For each indentation, first, a preload of 3 μN was applied to the system followed by a constant loading rate (10 μN/second). Next, a hold segment at a fixed system load was applied, followed by a constant unloading rate to retract the tip (−10 μN/second), and finally another hold segment was applied (3 μN). Each sample was indented with a peak load of 50 μN. The elastic response was calculated from the 20–90% portion of the unloading curve using methods previously described.[27] Indentation depth of less than 500nm were rejected as an exclusion criteria, due to the possibility of probing the titanium substrate. Statistical analysis was performed using GraphPad Prism 4 using a non-parametric analysis of variance (Kruskal-Wallis test) with multiple comparisons post hoc test (Dunn's multiple comparison test).

In order to determine the nanoscale viscoelastic properties of crosslinked carbon nanomaterial coatings, nanoscale dynamic mechanical analysis (nanoDMA) was carried out by using a nanoindenter (Hysitron, Minneapolis, MN USA) with a Berkovich indenter tip.[28] The specimens were fixed on AFM specimen discs (Ted Pella) and firmly mounted onto the magnetized base of the nanoindenter. Samples were indented 10 single indents each time to determine the average loss modulus, storage modulus and subsequently the respective phase angle (δ). The indentations were performed at room temperature. After calibration, frequency mode were used for the nanoDMA testing. A quasistatic load of 1 μN at a loading rate of 10 μN/s was applied to the sample. Superposed on the load was a 0.1 μN dynamic load with a frequency range of 10 Hz to 250 Hz. The quasistatic load was determined to limit the depth of the indentation to be within

1000 nm so that the tip of the indenter did not puncture the carbon film and engage with the titanium substrate. The storage and loss modulus were determined by:[29]

$$E' = \frac{K_S\sqrt{\pi}}{2\sqrt{A}} \quad \textbf{(1)}$$

$$E'' = \frac{\omega \cdot C_S\sqrt{\pi}}{2\sqrt{A}} \quad \textbf{(2)}$$

Where K_s is the dynamic stiffness and C_s is the dynamic damping coefficient, A is the projected contact area of the Berkovich tip used in this study and ω is the frequency in radians per second. Tan (δ), or the damping from the material, was determined by E"/E'.

Micro-Computed Tomography

A high-resolution micro computed tomography (μCT) scanner (μCT-40, SCANCO Medical AG, Bassersdorf, Switzerland) was used for scanning of the macroscopic 3D SWCNT structures to characterize the porosity and 3-D structure of the material. The samples were placed cylinder, with rigid foam supports in the sample holder, and scanned with a spatial resolution of 6 μm. Specific Gaussian sigma, support, lower threshold and upper threshold were set to be 0.3, 1, 28 and 60, respectively, for image smoothing purposes.

Thermogravimetric Analysis

Thermogravimetric analysis (TGA) was performed on three-dimensional structures made by chemically crosslinking SWCNT in a layer-on-layer approach. The porous three dimensional structure was placed in an aluminum pan and the mass was recorded using a Perkin Elmer TGA

(Waltham, MA USA) while heating the sample from 100°C to 550°C at a rate of 5°C/min with oxygen purging.

Results and Discussions

Two-Dimensional Coatings

Carbon nanomaterials of various sizes and architectures, dispersed in ethyl acetate, were coated onto titanium substrates heated to approximately 90°C. We utilized carbon nanotubes of varying diameters, as specified by the producer, including SWCNT (1-4nm diameter), MWCNT-L (40-70nm diameter), and MWCNT-H (110-170nm diameter). For graphene coatings, two allotropes of graphene were used: GONP (few layer, 1-2μm grain size) and GONR (~400-700nm in width as measured by TEM). BP was used as a free radical initiator to create crosslinks between the nanoparticles as the ethyl acetate droplets evaporated at the heated titanium surface. Many parameters of the spray coating process had to be optimized for this process, as summarized in Table 3.1. Of these parameters, the most essential parameters to optimize were flow rate and hotplate temperature. Adequate flow rate was required for the ultrasonic nozzle to continuously aerosolize the nanoparticle dispersions. Hotplate temperature optimization was required to prevent droplet accumulation at the surface, for the free radical crosslinking reaction to occur, and avoid Leidenfrost temperature which causes the droplets to randomly travel across the surface.[30]

Table 3.1. Parameters optimized for ultrasonic spray coating of chemically crosslinked carbon nanomaterial coatings.

Parameter	Test Ranges	Key Observations	Optimal Conditions
Flow Rate	0.1 - 3 ml min^{-1}	Low flow rates (<1ml min^{-1}) leads to poor aerosolization.	1 - 2 ml min^{-1}
Hot Plate Temperature	80-150°C	Low temperatures leads to longer solvent dissipation time and higher temperatures cause Leidenfrost Effect	120-140°C
Z-Height	1-5 cm from surface	Lower heights cause droplets to splatter and striations in the coatings. Droplets move in air flow at greater heights	~3 cm
Nanoparticle Concentration	0.1- 1mg ml^{-1}	Lower concentrations lead to more sparse coatings, higher concentrations do not maintain good dispersion	0.4 - 1 mg ml^{-1}
# of Passes	5 – Continuous	Lower passes lead to more sparse coatings	30 to Continuous

Photographs of the titanium substrates and the coatings for each type of nanomaterial are shown in Figure 3.1A. An illustrated schematic of the ultrasonic spray coating process is shown in Figure 3.1B. GONP coated as a dark grey color while the remainder of the materials coated to form a dark black coating. We believe this is attributed to the GONP making more transparent coatings due to the few-layer thickness of these particles and their stacking in a planar fashion as seen in Figure 3.2e, revealing the color of the underlying titanium substrate. Each coating was observed under scanning and transmission electron microscopy (Figure 3.2). Low magnification (Figure 3.2, left panel) SEM images show the continuity of the coatings. High magnification (Figure 3.2, middle panel) SEM images show the relative size scales of the particles as well as the crosslink junctions observed in the MWCNT-H. The crosslinks for the other materials are better

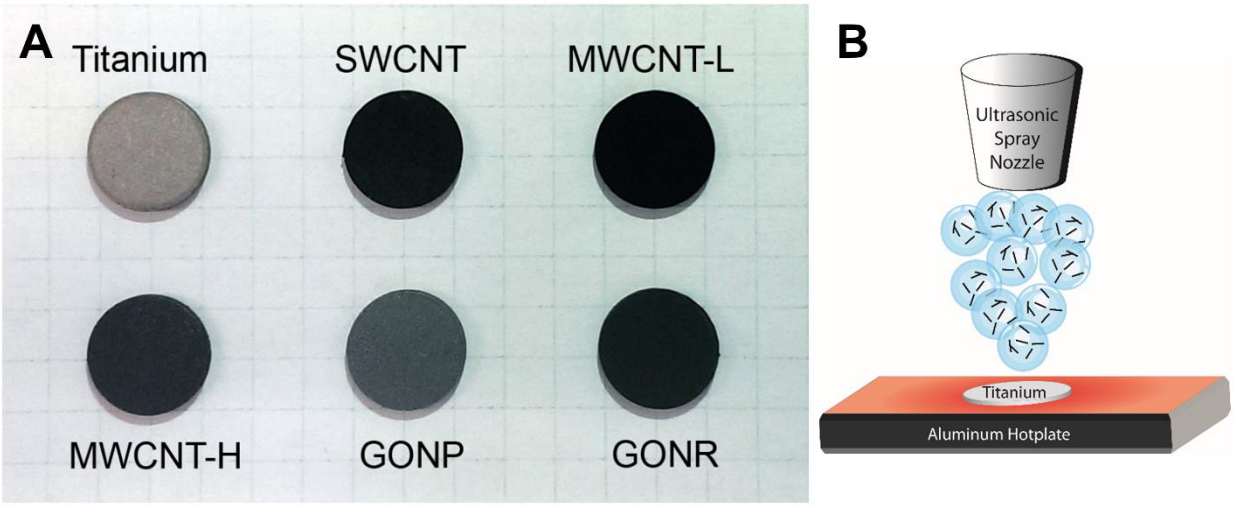

Figure 3.1. (A) Photographs of titanium substrates coated with *in situ* chemically crosslinked SWCNT, MWCNT-L, MWCNT-H, GONP, and GONR. (B) An illustrated schematic of ultrasonic spray coating process.

visualized by TEM as shown by the red arrows in the figure (Figure 3.3, right panel). For SWCNT (Figure 3.2a) the nanotubes form dense rope structures, characteristic of SWCNT which are not treated to harsh, oxidizing acidic solutions to separate the bundles.[31] As the nanotubes become thicker in diameter, the structures are also visibly more rigid and linear as SWCNT exist as entangling ropes while MWCNT-H are more like rigid rods. While the tubular nanoparticles form networks of tubes stacked upon each other, we observed the graphene allotropes are stacked on their planar surfaces as they are sprayed onto the titanium (Figure 3.2d,e left column). TEM of the fragmented coatings (Figure 3.2, right column) was performed to observe the crosslinks between the nanoparticles. By inspection under TEM, SWCNTs existed in ropes but still had a few noticeable junctions which suggest crosslinking, while MWCNT-L, MWCNT-H, and GONR had more obvious junctions between the individual particles as indicated by the red arrows. Corroborating with SEM images, TEM observation of GONP indicates planar stacking and crosslinking of the graphene sheets to create larger sized graphitic fragments with crosslinks forming between one or more sheets as indicated by the red arrows.

Surface roughness and topography was studied using AFM. Representative AFM images of each crosslinked carbon nanomaterial coating is presented in Figure 3.3. Samples were probed

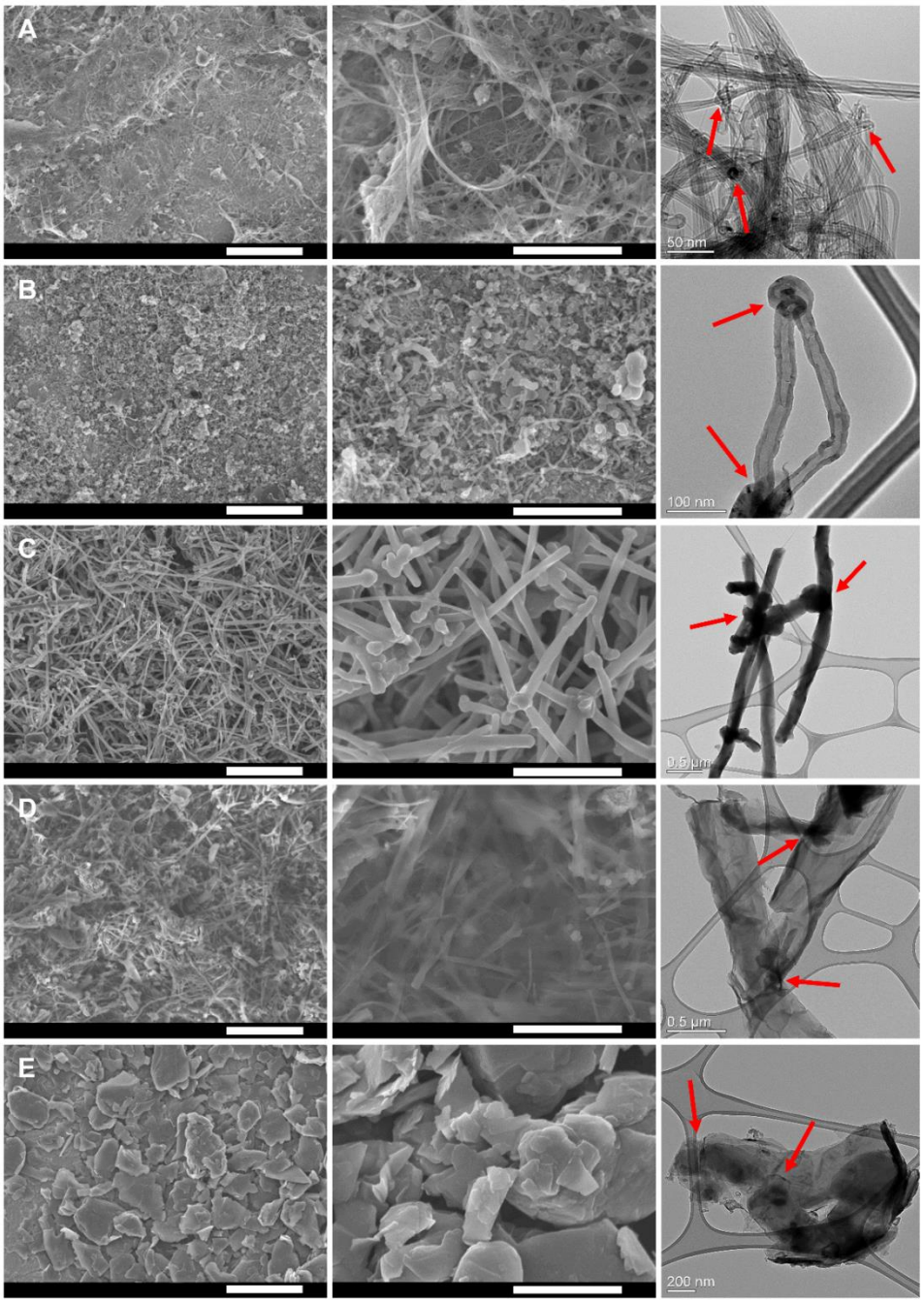

Figure 3.2. Electron microscopy of chemically crosslinked carbon nanomaterial films. The left column shows low magnification SEM images (scale bars: 5µm) and the middle column shows higher magnification SEM images (scale bars 2µm). The right column shows TEM images of fragmented carbon nanomaterial films and junctions (red arrows) between nanoparticles. Each carbon nanomaterial is shown in the following corresponding rows: (A) SWCNT, (B) MWCNT-L, (C) MWCNT-H, (D) GONR, and (E) GONP.

in AFM tapping mode in multiple regions of multiple coatings (n=10). Surface roughness measurements were determined from a total of 10 regions for each group. Each of the nanomaterials showed regions of dense packing as shown in Figure 3.3. Line plots of SWCNT (Figure 3.3a) show small peaks nested inside larger topographical features while fewer nested peaks are observed in the MWCNT-L (Figure 3.3b), and even fewer in MWCNT-H (Figure 3.3c). GONP had large planar sheet-like structures which had high intrinsic topography shown in the line plot of Figure 3.3d. GONR were visibly planar with long (Figure 3.3e), flat structures randomly oriented in the x-y direction. Surface roughness (r.m.s) measurements were performed on the titanium substrates and the crosslinked carbon nanomaterial coatings (Table 3.2).

The titanium substrates had surface roughness of 110.79nm. The additional coating of the crosslinked carbon nanomaterials increased the overall surface roughness to 125.56 – 225.45 nm. Increasing the diameter of the carbon nanotubes from SWCNT to MWCNT-H showed an expected increase in surface roughness due to the diameter of the tubes. However MWCNT-L (125.56nm) had a lower surface roughness than SWCNT (179.65nm). This may be due to the SWCNT existing in large rope-like bundles unless pre-treated with acidic solutions.[31] Both graphene structures, GONP and GONR, both showed comparable surface roughness, between 162.63 – 172.81 nm.

Table 3.2. Surface roughness (r.m.s) of titanium substrates and crosslinked carbon nanomaterial coatings as measured by AFM (n=10 for each group).

	Surface Roughness (nm)					
	Titanium	SWCNT	MWCNT-L	MWCNT-H	GONP	GONR
Average	110.79	179.65	125.56	225.45	162.63	172.81
Std. Dev.	54.21	68.65	43.51	81.98	78.66	63.94

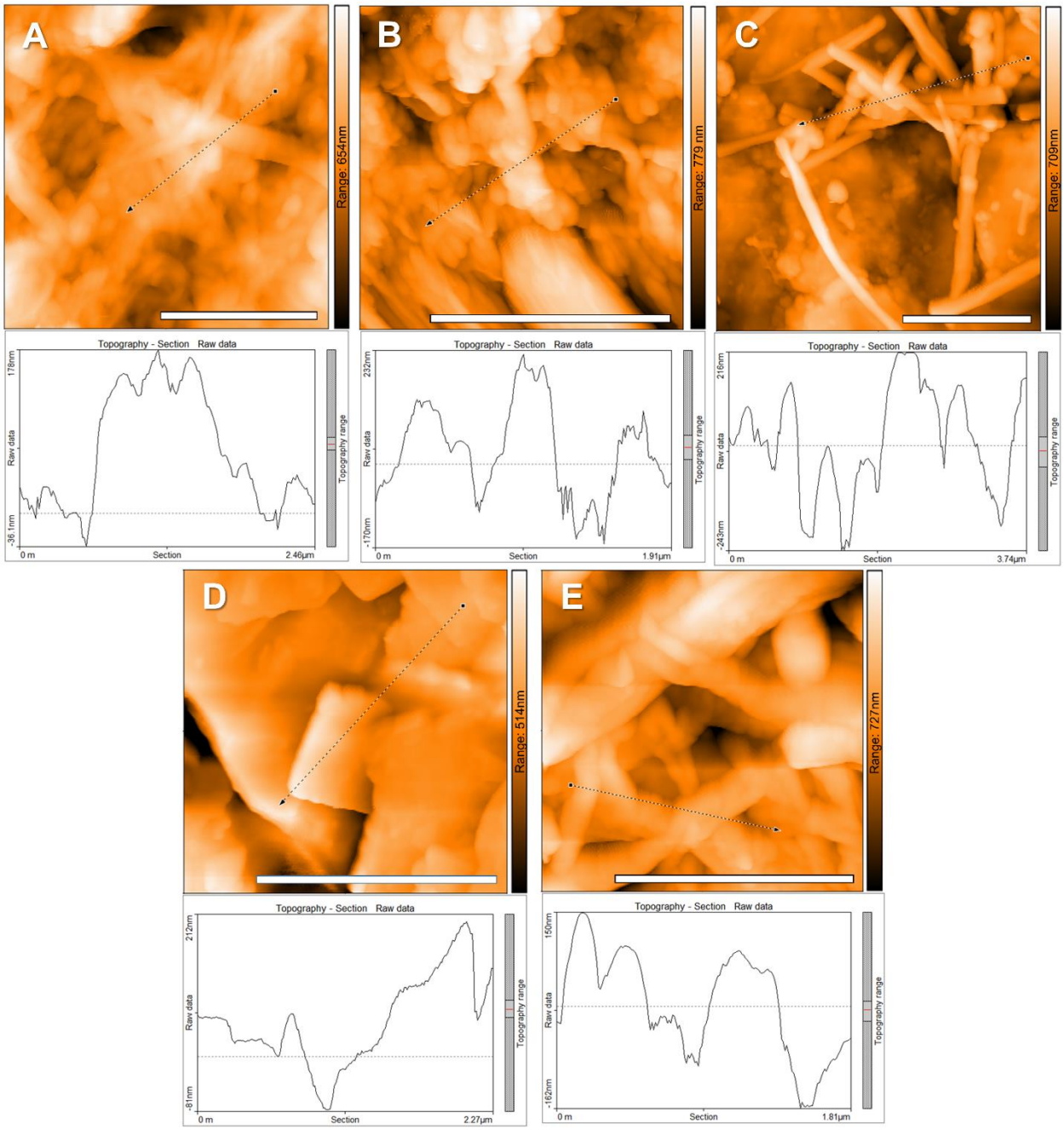

Figure 3.3 Representative AFM images and line graphs showing regions of interest of ultrasonic spray coated, chemically crosslinked (A) SWCNT, (B) MWCNT-L, (C) MWCNT-H, (D) GONP, and (E) GONR coatings on titanium substrates. Each scale bar is 2µm in width.

Spray coating of carbon nanomaterial dispersions provides a lot of heterogeneity in the film surface roughness. While airbrushing techniques can make carbon nanomaterial films, it requires the nanomaterials to be dispersed with a surfactant like carboxymethyl cellulose or sodium

dodecyl sulfate.[15] While the smoothest carbon nanotube films (~3 nm r.m.s. surface roughness)[15] were spray coated using ultrasonic spray coating, these also required an amphiphilic surfactant to disperse the materials. In this technique we refrained from using any such dispersants for two primary reasons: 1) we wanted to fabricate coatings of only carbon nanomaterials to better exploit their physicochemical properties and 2) the usage of any surfactant could have resulted in the radical initiator forming chemical functionalities on the nanomaterials and inert surfactants would compete with surface area available for radical sites to form on the carbon nanoparticles. Nevertheless, we observed significantly smoother and more uniform coatings utilizing ultrasonic spray coating to fabricate crosslinked MWCNT-H coatings (225.45 nm) then our previous reports of fabricating such films using an airbrush techniques (730 nm).[25] Also, although we cannot directly subtract a baseline surface roughness from the titanium substrate, some of the surface roughness of the crosslinked carbon nanomaterial coatings may also be attributed to the underlying titanium substrate.

Although spray coating can be optimized by using highly sensitive and precise inlet flow and axial motion, the coatings created by spray coating are usually more inhomogeneous then both CVD and vacuum filtration techniques. In the case of CVD, the growth of the graphene or carbon nanotubes is well controlled and relatively homogenous on the surface of the catalyst material.[32] Vacuum filtration allows for homogenous film fabrication because the technique can auto-correct itself. The permeation of the solvent containing nanoparticles would be more hindered in regions where there is more accumulation, forcing the solvent to flow through less densely packed areas.[14] However these techniques have limited versatility. While CVD can produce highly homogenous coatings of carbon nanotubes or graphene, it requires the substrate to be heated to high temperatures and requires particular surface chemistries for growth to occur[33,34] while spray

coating only requires mild heating depending on the carrier solvent chosen. Vacuum filtration requires a flat porous membrane to fabricate films and can be made into a free standing film,[14,35,36] however the surface these films are transferred to must also be flat to prevent wrinkling of the film while spray coating allows for coating on many substrate geometries.

Raman spectroscopy was utilized to characterize the chemical properties of the carbon nanomaterial crosslinked coatings. Raman spectra of each pristine nanomaterial (nanomaterial drop casted onto a silicon wafer without any treatments) and chemically crosslinked coatings (on titanium discs) are presented in Figure 3.4a and Figure 3.4b, respectively. Characteristic Raman peaks of carbon nanomaterials include three prominent peaks at ~ 1345 cm^{-1}, 1560 cm^{-1}, and 2670 cm^{-1}, identified as the D, G, and G' bands respectively.[37] Pristine sp^2 hybridized carbon nanomaterials share a characteristic G band (intensity of which is I_G) generated by in-plane vibrations of double bonded carbon atoms.[38]

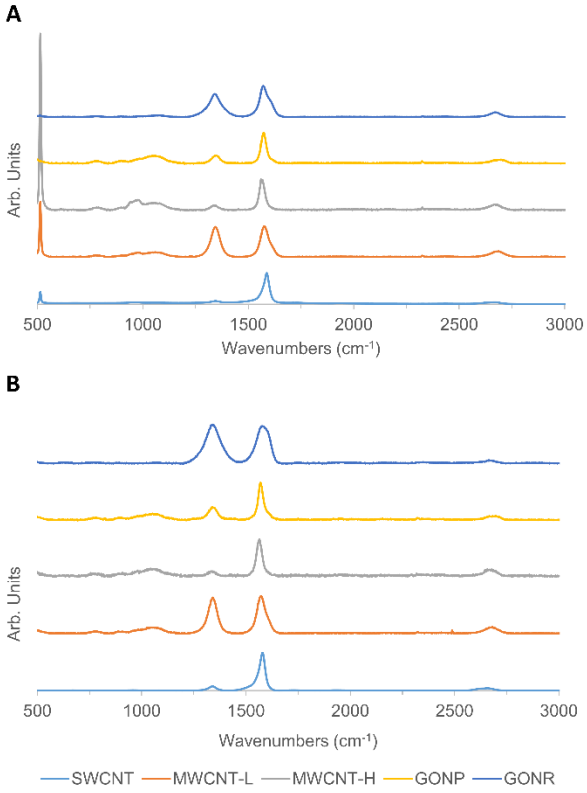

Figure 3.4 Representative Raman spectrographs of (A) pristine carbon nanomaterials drop casted on silicon substrates and (B) chemically crosslinked carbon nanomaterial coatings on titanium substrates.

Defect structures, identified by the D band (intensity of which is I_D), are caused by structural defects or sp^3 bonds in the graphitic network.[37] The relative amounts of defect structures between groups can be identified by the I_D/I_G ratio. We found an increase in the I_D/I_G ratio for each group

(n=3) of chemically crosslinked carbon nanoparticle when compared to its pristine counterpart (Table 3.3). This may be attributed to the radical initiated crosslinking forming junctions on the surface of adjoining nanoparticles. Notably, the I_D/I_G ratio of the crosslinked SWCNT and GONP groups nearly doubled as compared to their pristine counterparts. Along with the chemical crosslinking, this may be attributed to the sonicating of the nanoparticles for extended duration of time to debundle the aggregated SWCNT and exfoliate larger GONP to fewer layer particles as sonication has shown the ability to damage sp^2 hybridized carbon nanoparticles.[39]

Table 3.3. Normalized Raman I_D/I_G ratios for pristine carbon nanoparticles on silicon substrates and chemically crosslinked carbon nanoparticles on titanium substrates (n=3 for each group).

		I_D/I_G Ratio				
		SWCNT	MWCNT-L	MWCNT-H	GONP	GONR
Pristine	Average	0.049	0.96	0.14	0.23	0.76
	Std. Dev.	0.0027	0.015	0.0016	0.034	0.026
Crosslinked	Average	0.13	0.99	0.18	0.43	1.10
	Std. Dev.	0.013	0.043	0.0088	0.098	0.014

Nanoindentation was performed on the crosslinked carbon nanomaterial coatings to characterize the mechanical properties of the coatings. For many applications of carbon nanomaterials, including solar cells, personal devices, medical devices and implants, etc., mechanical analysis of the carbon nanomaterial assembly is required. Quasistatic indentation was performed to measure the elastic modulus (Table 3.4) and hardness (Table 3.5) from the unloading curve of the indentation. Quasistatic indentation revealed SWCNT groups to have the lowest elastic modulus (79 MPa), two orders of magnitude less than all other groups, and significantly less than MWCNT-L, GONP, and GONR groups. MWCNT-H also had a significantly lower elastic modulus (1.18 GPa) compared to MWCNT-L and GONR.

Table 3.4. Elastic modulus determined by quasi-static nanoindentation of chemically crosslinked carbon nanomaterial coatings. All data is reported in median, interquartile range (I.Q.R), average, and standard deviation (significant differences are observed as follows: *p<0.01, **p<0.001).

	Elastic Modulus (GPa)				
	SWCNT	MWCNT-L	MWCNT-H	GONP	GONR
Median	0.07932	5.522	1.182	3.214	5.258
(Sig. Differences)	***MWNCT-L, GONP, GONR*		**MWCNT-L, GONR*		
I.Q.R	0.08548	6.191	0.5743	2.819	4.303
Average	0.09525	6.925	1.147	3.738	6.723
Std. Dev.	0.06168	4.905	0.5176	1.682	2.271

Table 3.5. Mechanical hardness determined by quasi-static nanoindentation of chemically crosslinked carbon nanomaterial coatings. All data is reported in median, interquartile range (I.Q.R), average, and standard deviation (significant differences are observed as follows: *p<0.05, **p<0.01, ***p<0.001).

	Hardness (MPa)				
	SWCNT	MWCNT-L	MWCNT-H	GONP	GONR
Median	1.843	41.63	10.07	25.26	97.52
(Sig. Differences)	**MWNCT-H ***MWNCT-L, GONP, GONR*		***GONR*	**GONR*	
I.Q.R	2.024	44.25	17.748	30.06	29.63
Average	2.417	41.57	20.1	27.93	91.39
Std. Dev.	1.885	25	22.19	17.89	20.61

The nanoindentation also measured hardness revealing similar results. Measured hardness of SWCNT (1.843 MPa) was significantly less than all other groups. Here, however there was only one order of magnitude difference between SWCNT and other groups. GONR showed the greatest hardness (97.52 MPa), significantly greater than both MWCNT-H and GONP groups. An exclusion criteria of contact depth was imposed on the quasistatic indentation. We wanted to measure the mechanical properties of the crosslinked coating, rather than effects due to the substrate. In-plane Young's modulus of the sp^2 hybridized lattice of carbon nanomaterials can

theoretically be as great as 1 TPa,[40] therefore shallow indentations would effectively also probe the surface underneath the carbon nanoparticles. To avoid this, we only collected data from points where contact depth was greater than 500nm.

Nanoscale dynamic mechanical analysis (nanoDMA) was utilized to understand the viscoelastic properties of the coatings. Repeated loading and unloading frequency sweeps, from 10 Hz to 250 Hz, were performed on the samples. For SWCNT and MWCNT-H, the storage modulus (G') increased 44% and 22%, respectively when scanning from 10 Hz to 250 Hz (Figure 3.5a). MWCNT-L and GONP, only observed marginal increases in G' (14% and 7.8% respectively) from 10 Hz to 250 Hz. Interestingly for GONR, the G' decreased 104% in the same frequency sweep (Figure 3.5a). The loss modulus of each increased by 77% to 96% for any group (Figure 3.5b). Tan (δ), a measure of energy dissipation as a function of G"/G', increased for each group from 10 Hz to 250 Hz, with GONR having the greatest rate of increase from all of the groups and MWCNT-H having the lowest rate of increase (Figure 3.5c).

Carbon nanotube based damping observed through nanoDMA suggests higher viscoelastic response in SWCNT and MWCNT-L coatings compared to MWCNT-H (Figure 3.5c). Previous work nanoDMA work with carbon nanotubes and boron nitride nanotubes suggests thicker diameter tubes are more constricted in their ability to slide in a network because of their intrinsic stiffness.[41] Constricted sliding in these networks of nanotubes can be also be attributed to the chemical crosslinking at the surface of the nanotubes, which would be greater in MWCNT-H since there would be more theoretically more crosslinks per nanotube than in SWNCT or MWCNT-L.

Previous work with CVD grown graphene, transferred to a silicon substrate, demonstrated how few layer (~5 layers) and multi-layered (~10 layers) graphene also indicate a dominant role in frequency dependent damping behavior.[40] They reported this effect is due to ripple formation and propagation in the graphene layers and energy adsorption by the stacking of layers (by van der

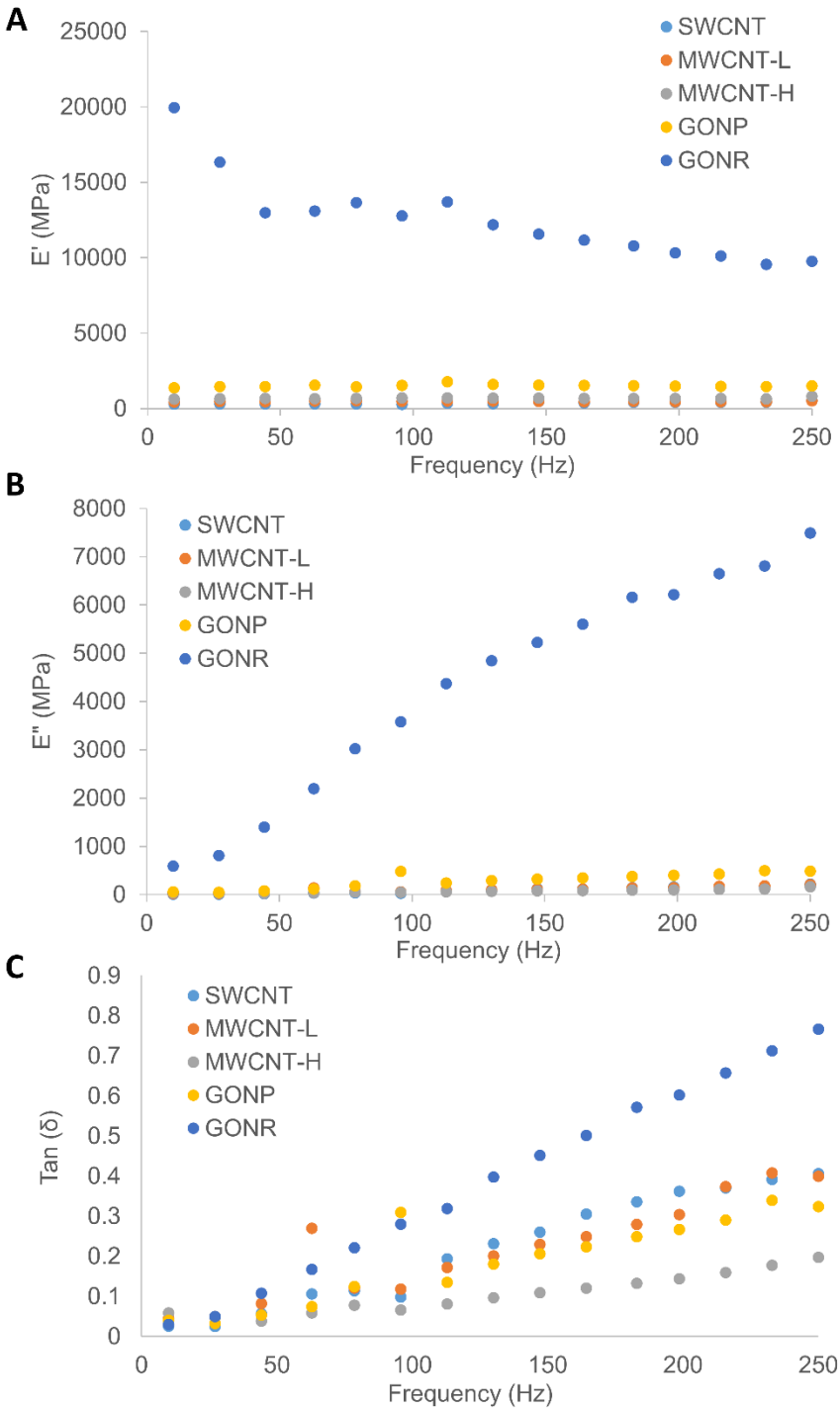

Figure 3.5. Nanoscale dynamic mechanical analysis of crosslinked carbon nanoparticles coatings. Frequency sweep measurements of (A) storage modulus, (B) loss modulus, and (C) tan (δ) are presented for each group.

Waals forces). Thicker (10 layer) graphene had a more pronounced increase in tan (δ) after 150 Hz, with the increased damping due to the increased accommodation of ripple propagation in the z-direction.[40] Still, this does not explain why tan (δ) increased faster in GONR than GONP in our studies. Perhaps this is because of the intrinsic folding of the GONR during synthesis,[42] theoretically increasing the space for z-axis ripple propagation, and further increasing the spring like behavior of the GONR matrix.

An interesting comparison would have been with coatings of pristine carbon nanomaterial coatings to see if the chemical crosslinking was making more robust coatings. However, we were not able to fabricate coatings of appreciable thicknesses without the crosslinking method. Thinner coatings (<1 μm) would not be acceptable for mechanical analysis since the probing method may also include the mechanical properties of the underlying titanium substrate.

Three Dimensional Assemblies

Since the layer-on-layer *in situ* crosslinking of the carbon nanoparticles lead to macroscopic coatings, we also wanted to examine if this technique could be utilized for creating free standing macroscopic 3D architectures. As a proof of concept, we used SWCNT to fabricate the 3D structures. Using the same SWCNT:BP ratio (1:4), we spray coated the dispersion in three aluminum wells fabricated in an aluminum block. Aluminum was chosen because it is inert to the reagents utilized, while provides good heat conduction to the structures as they are built up three-dimensionally. The three dimensional structures were removed from the wells after being heat treated in an oven at 150°C for about one hour to remove excess benzoyl peroxide, as suggested in previous reports.[43] Photographs of the 3D structures are shown in Figure 3.6a. The structures maintained the conical shape of their wells and even structures which break apart maintained

macroscopic 3D structures (Figure 3.6b). The 3D all-carbon structures were visibly porous and the porosity / microstructure was further investigated by μCT analysis. Three-dimensional reconstructions of the μCT slices were rendered to visualize the porosity of the 3D assemblies (Figure 3.6c). A rectangular prism section from inside the scaffold structure was chosen to evaluate for porosity measurements to prevent subjective contouring on the irregular edges of the porous

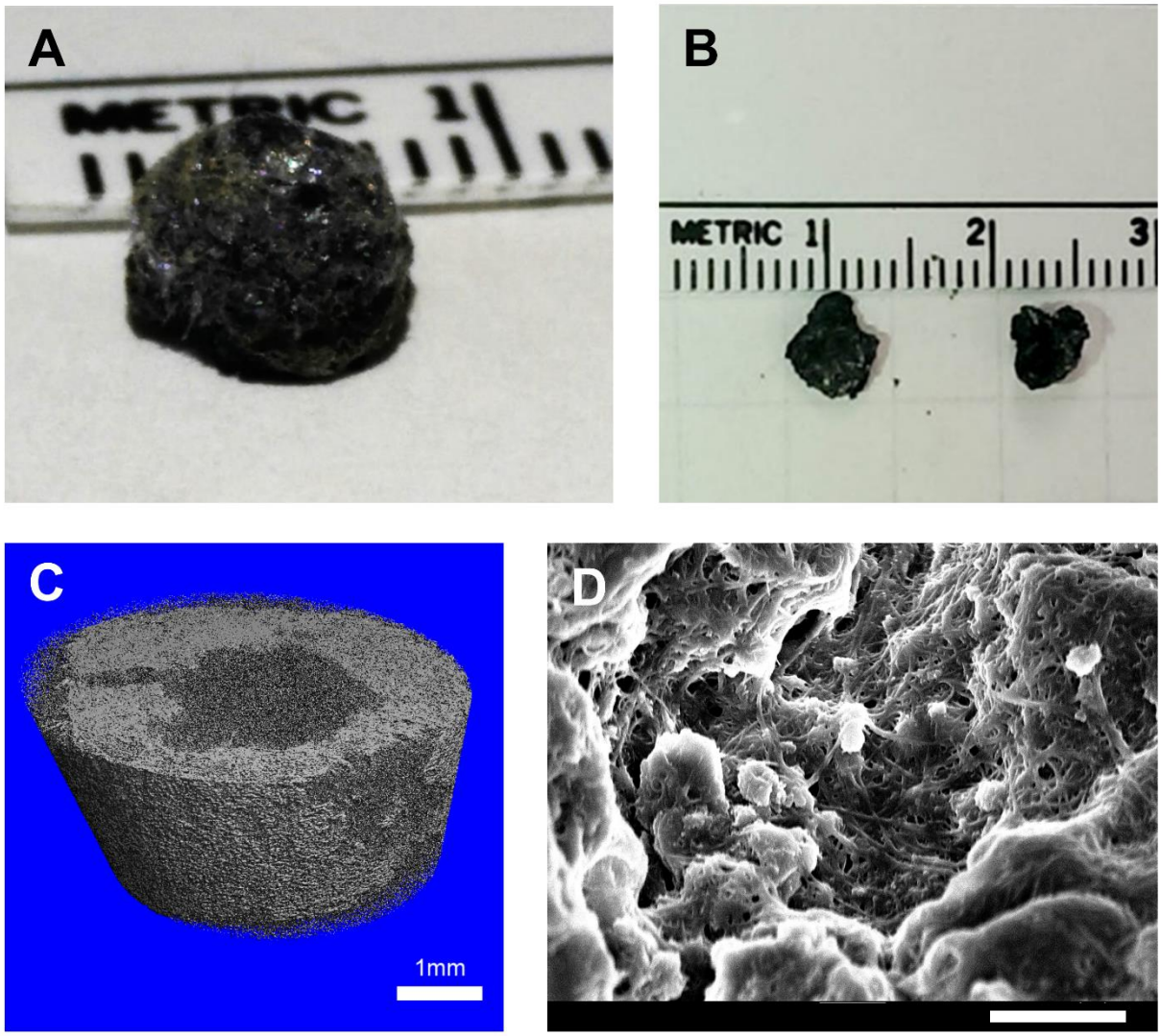

Figure 3.6. (A) Photographs of a free standing, three-dimensional, chemically crosslinked, layer-on-layer assembled SWCNT structure and (B) fragmented macroscopic pieces of the crosslinked SWCNT structure. (C) 3D image reconstructions from μCT analysis of three dimensional SWCNT structures. Each slice of the reconstruction is approximately 6μm in thickness (scale bar: 1mm). (D) SEM image from inside a pore of a 3D chemically crosslinked SWCNT structures (scale bar: 2μm).

structure. The mean porosity of the 3D SWCNT assemblies was approximately 68% (s.d.=9.3%) as measured by μCT. SEM analysis of the 3D SWCNT assembly (Figure 3.6d) was performed, revealing a network of crosslinked, interconnected bundles of SWCNT.

In a previous report we have shown the ability to fabricate 3D, chemically crosslinked, all carbon scaffolds from graphene and carbon nanotubes.[43] In our previous work, we have fabricated scaffolds in a cylindrical mold by pouring a saturated dispersion of the carbon nanoparticles and free radical initiator. The porosity of the carbon nanotube scaffolds were tunable from ~20% to 85% depending on the radical initiator.[43] Tuning porosity by this layer-on-layer approach may be possible by decreasing the concentration of the nanoparticle dispersion to make thinner layers due to the fewer amount of nanoparticles per spray coating pass.

To analyze overall functionalization and the chemistry of the 3D SWCNT assemblies, we performed TGA on the SWCNT architectures (Figure 3.7). Three major weight loss peaks were observed, when plotting the second derivative of the TGA plot, at ~ 210°C, 425°C, and 530°C. At 210°C, a total of 19.31% weight loss was observed. At 425°C and 530°C, a total of 24.56% and 22.41% weight loss was observed, respectively. By 550°C only 29.65% of the total weight remained in the aluminum crucible. The thermal stability of SWCNTs has been previously reported to have weight loss deflections between 350-425°C[44,45] and ~570°C.[31] Therefore we believe that the weight loss deflection at ~ 210°C of approximately 19.31% is attributed to defect sites on the carbon nanotubes formed during crosslinking and radical reactions from the BP as well as any amorphous, degraded carbon in the sample. Therefore we estimate that more than 80% of the carbon nanotube material of the 3D carbon nanotube structures is intact SWCNT and any trace metal catalyst from the nanotube growth process.[31]

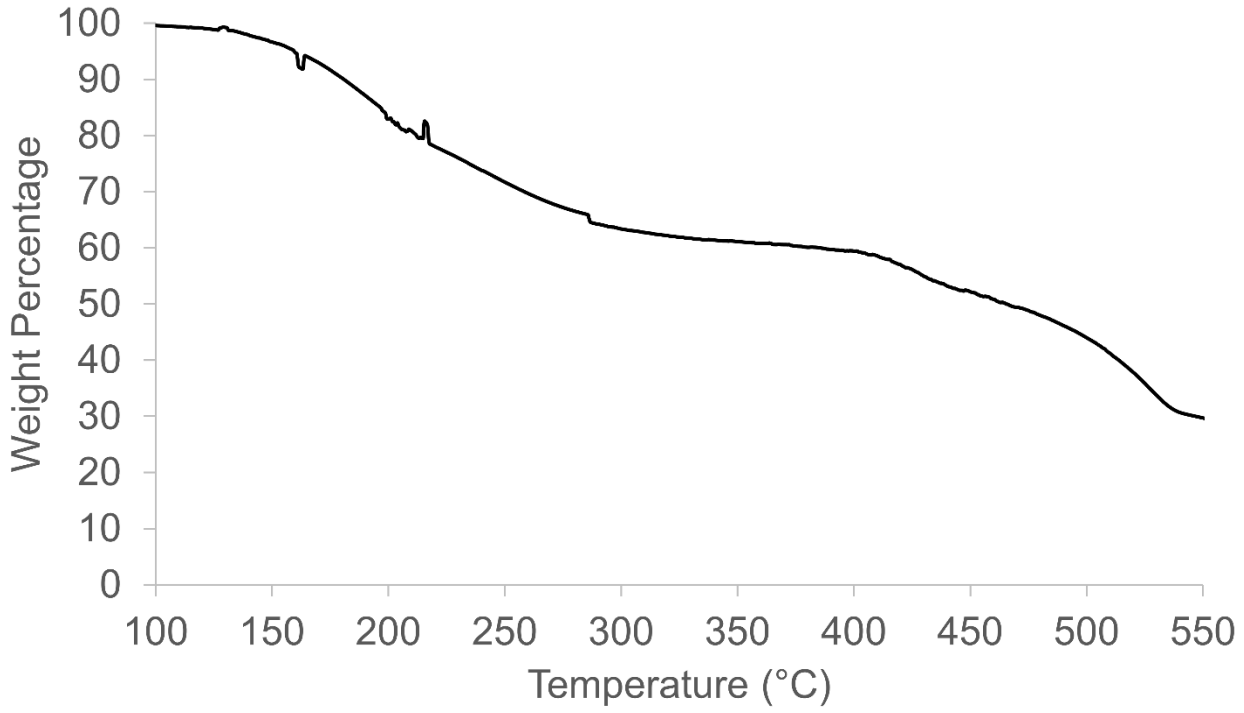

Figure 3.7. TGA plot of layer-on-layer assembled 3D crosslinked SWCNT architectures.

This work builds on our previous work[25,43] to enable all-carbon nanomaterial based 3D printing. To the best of our knowledge, currently, 3D printing with carbon nanomaterials is limited to inkjet printing of graphene and carbon nanotube[46-49] suspensions as well as commercially available graphene/polymer 3D printing filament (3D Graphene Labs). While inkjet printing provides films of carbon nanotubes or graphene, expanding the structures three dimensionally would require a method for the nanoparticles to be interconnected for mechanical stability and robustness. Graphene/polymer blends for 3D printing can potentially provide robust 3D structures but would lack some of the fundamental properties of graphitic materials such as limiting the sites for chemical functionalities[50] or binding adsorbents[51] to the sp^2 hybridized graphitic backbone. Another method to create porous graphene or carbon nanotube structures is via aerogel formation.[52-54] Unlike these assemblies, aerogels can be made to be compressible and have porosity of over 99%.[52] Typically these materials have small pores, from nanometer to a few micrometer

size range[54] which can be advantageous for applications in gas storage[55] or electrochemical cells.[56] However they do not provide macropores which are required in many applications for porous membranes,[57,58] bioreactors,[59,60] or scaffolding in tissue repair[61,62] which are all potential applications suggested for assemblies of carbon nanomaterials.

Conclusions

Layer-on-layer assembly of chemically crosslinked carbon nanoparticles (SWCNT, MWCNT, GONP, and GONR) allows for fabrication of thick carbon nanomaterial coatings. The method produces more uniform coatings then a previously reported airbrush method. The crosslinking method does not largely damage the carbon nanomaterial sp^2 hybridized backbone as observed by Raman spectroscopy. The coatings are robust and show some viscoelastic behavior as shown by nanoDMA. The method has also been adapted for fabricating chemically crosslinked, free standing, macroscopic, three dimensional structures from SWCNTs. The method proves to be a proof of concept for 3D printing of all-carbon nanoparticle macroscopic assemblies. The method opens avenues for scalable fabrication of robust carbon nanomaterial assemblies with control of coating thickness, surface roughness and three dimensional architectures.

Acknowledgements

This work was sponsored by a National Institutes of Health grants (1DP2OD007394 and AR61821). SEM, TEM, and TGA were conducted at Center for Functional Nanomaterials at BNL, supported by the U.S. Department of Energy, Office of Basic Energy Sciences, under Contract No. DE-AC02-98CH10886. We would also like to acknowledge Kamal James for helping in collecting Raman spectroscopy data.

References

1 Gogotsi, Y. & Presser, V. *Carbon nanomaterials*. (CRC Press, 2013).

2 Dai, L., Chang, D. W., Baek, J. B. & Lu, W. Carbon nanomaterials for advanced energy conversion and storage. *Small* **8**, 1130-1166 (2012).

3 Bonaccorso, F., Sun, Z., Hasan, T. & Ferrari, A. Graphene photonics and optoelectronics. *Nature photonics* **4**, 611-622 (2010).

4 Feng, L. & Liu, Z. Graphene in biomedicine: opportunities and challenges. *Nanomedicine* **6**, 317-324 (2011).

5 Dong, X. *et al.* 3D graphene foam as a monolithic and macroporous carbon electrode for electrochemical sensing. *ACS applied materials & interfaces* **4**, 3129-3133 (2012).

6 Kang, I., Schulz, M. J., Kim, J. H., Shanov, V. & Shi, D. A carbon nanotube strain sensor for structural health monitoring. *Smart materials and structures* **15**, 737 (2006).

7 Wang, X., Zhi, L. & Müllen, K. Transparent, conductive graphene electrodes for dye-sensitized solar cells. *Nano letters* **8**, 323-327 (2008).

8 Xu, H., Hu, L., Anlage, S. M. & Gruner, G. Microwave shielding of transparent and conducting single-walled carbon nanotube films. *arXiv preprint cond-mat/0611755* (2006).

9 Cao, M.-S., Wang, X.-X., Cao, W.-Q. & Yuan, J. Ultrathin graphene: electrical properties and highly efficient electromagnetic interference shielding. *Journal of Materials Chemistry C* **3**, 6589-6599 (2015).

10 Maiyalagan, T., Dong, X., Chen, P. & Wang, X. Electrodeposited Pt on three-dimensional interconnected graphene as a free-standing electrode for fuel cell application. *Journal of Materials Chemistry* **22**, 5286-5290 (2012).

11 Li, N. *et al.* Three-dimensional graphene foam as a biocompatible and conductive scaffold for neural stem cells. *Scientific reports* **3** (2013).

12 Wang, Y. *et al.* Electrochemical delamination of CVD-grown graphene film: toward the recyclable use of copper catalyst. *ACS nano* **5**, 9927-9933 (2011).

13 Obraztsov, A. N. Chemical vapour deposition: making graphene on a large scale. *Nature nanotechnology* **4**, 212-213 (2009).

14 Wu, Z. *et al.* Transparent, conductive carbon nanotube films. *Science* **305**, 1273-1276 (2004).

15 Tenent, R. C. *et al.* Ultrasmooth, Large-Area, High-Uniformity, Conductive Transparent Single-Walled-Carbon-Nanotube Films for Photovoltaics Produced by Ultrasonic Spraying. *Advanced materials* **21**, 3210-3216 (2009).

16 Tait, J. G. *et al.* Spray coated high-conductivity PEDOT: PSS transparent electrodes for stretchable and mechanically-robust organic solar cells. *Solar Energy Materials and Solar Cells* **110**, 98-106 (2013).

17 Pham, V. H. *et al.* Fast and simple fabrication of a large transparent chemically-converted graphene film by spray-coating. *Carbon* **48**, 1945-1951, doi:http://dx.doi.org/10.1016/j.carbon.2010.01.062 (2010).

18 Ramasamy, E., Lee, W. J., Lee, D. Y. & Song, J. S. Spray coated multi-wall carbon nanotube counter electrode for tri-iodide reduction in dye-sensitized solar cells. *Electrochemistry Communications* **10**, 1087-1089, doi:http://dx.doi.org/10.1016/j.elecom.2008.05.013 (2008).

19 Nayak, T. R. *et al.* Thin Films of Functionalized Multiwalled Carbon Nanotubes as Suitable Scaffold Materials for Stem Cells Proliferation and Bone Formation. *ACS Nano* **4**, 7717-7725, doi:10.1021/nn102738c (2010).

20 Alver, U. *et al.* Optical and structural properties of ZnO nanorods grown on graphene oxide and reduced graphene oxide film by hydrothermal method. *Applied Surface Science* **258**, 3109-3114, doi:http://dx.doi.org/10.1016/j.apsusc.2011.11.046 (2012).

21 Steirer, K. X. *et al.* Ultrasonic spray deposition for production of organic solar cells. *Solar Energy Materials and Solar Cells* **93**, 447-453 (2009).

22 Kim, B. C., Jeong, H. T., Higgins, M. J., Yu, K. H. & Wallace, G. G. Dynamic Electrochemical Properties of Extremely Stretchable Electrochemical Capacitor Using Reduced Graphene Oxide/Single-Wall Carbon Nanotubes Composite. *Journal of The Electrochemical Society* **162**, A2351-A2355 (2015).

23 Tutak, W. *et al.* Toxicity induced enhanced extracellular matrix production in osteoblastic cells cultured on single-walled carbon nanotube networks. *Nanotechnology* **20**, 255101 (2009).

24 King, D., Quintana, M., Kratochvil, J., Ellibee, D. & Hansen, B. Photovoltaic module performance and durability following long-term field exposure. *Progress in Photovoltaics Research and Applications* **8**, 241-256 (2000).

25 Patel, S. C., Lalwani, G., Grover, K., Qin, Y.-X. & Sitharaman, B. Fabrication and cytocompatibility of in situ crosslinked carbon nanomaterial films. *Scientific Reports* **5** (2015).

26 Wang, W.-N. *et al.* Investigation on the correlations between droplet and particle size distribution in ultrasonic spray pyrolysis. *Industrial & Engineering Chemistry Research* **47**, 1650-1659 (2008).

27 Ozcivici, E., Ferreri, S., Qin, Y.-X. & Judex, S. in *Osteoporosis* 323-334 (Springer, 2008).

28 Li, X. & Bhushan, B. A review of nanoindentation continuous stiffness measurement technique and its applications. *Materials Characterization* **48**, 11-36, doi:http://dx.doi.org/10.1016/S1044-5803(02)00192-4 (2002).

29 Xiaodong, L. *et al.* Nanomechanical characterization of single-walled carbon nanotube reinforced epoxy composites. *Nanotechnology* **15**, 1416 (2004).

30 Eslamian, M. Spray-on thin film PV solar cells: Advances, potentials and challenges. *Coatings* **4**, 60-84 (2014).

31 Xie, S. X. *et al.* Effect of synthesis and acid purification methods on the microwave dielectric properties of single-walled carbon nanotube aqueous dispersions. *Applied Physics Letters* **103**, 133114 (2013).

32 Suk, J. W. *et al.* Transfer of CVD-grown monolayer graphene onto arbitrary substrates. *ACS nano* **5**, 6916-6924 (2011).

33 Mattia, D. *et al.* Effect of graphitization on the wettability and electrical conductivity of CVD-carbon nanotubes and films. *The Journal of Physical Chemistry B* **110**, 9850-9855 (2006).

34 Franklin, N. R. & Dai, H. An enhanced CVD approach to extensive nanotube networks with directionality. *Advanced Materials* **12**, 890-894 (2000).

35 Eda, G., Fanchini, G. & Chhowalla, M. Large-area ultrathin films of reduced graphene oxide as a transparent and flexible electronic material. *Nature nanotechnology* **3**, 270-274 (2008).

36 Ci, L., Manikoth, S. M., Li, X., Vajtai, R. & Ajayan, P. M. Ultrathick freestanding aligned carbon nanotube films. *ADVANCED MATERIALS-DEERFIELD BEACH THEN WEINHEIM*- **19**, 3300 (2007).

37 Dresselhaus, M. S., Dresselhaus, G., Saito, R. & Jorio, A. Raman spectroscopy of carbon nanotubes. *Physics Reports* **409**, 47-99 (2005).

38 Ferrari, A. C. Raman spectroscopy of graphene and graphite: disorder, electron–phonon coupling, doping and nonadiabatic effects. *Solid state communications* **143**, 47-57 (2007).

39 Gojny, F. H., Wichmann, M. H., Fiedler, B. & Schulte, K. Influence of different carbon nanotubes on the mechanical properties of epoxy matrix composites–a comparative study. *Composites Science and Technology* **65**, 2300-2313 (2005).

40 Lahiri, D., Das, S., Choi, W. & Agarwal, A. Unfolding the damping behavior of multilayer graphene membrane in the low-frequency regime. *ACS nano* **6**, 3992-4000 (2012).

41 Agrawal, R., Nieto, A., Chen, H., Mora, M. & Agarwal, A. Nanoscale Damping Characteristics of Boron Nitride Nanotubes and Carbon Nanotubes Reinforced Polymer Composites. *ACS Applied Materials & Interfaces* **5**, 12052-12057, doi:10.1021/am4038678 (2013).

42 Kosynkin, D. V. *et al.* Longitudinal unzipping of carbon nanotubes to form graphene nanoribbons. *Nature* **458**, 872-876 (2009).

43 Lalwani, G. *et al.* Fabrication and characterization of three-dimensional macroscopic all-carbon scaffolds. *Carbon* **53**, 90-100 (2013).

44 Hu, H., Zhao, B., Itkis, M. E. & Haddon, R. C. Nitric Acid Purification of Single-Walled Carbon Nanotubes. *The Journal of Physical Chemistry B* **107**, 13838-13842, doi:10.1021/jp035719i (2003).

45 Shi, Z. *et al.* Purification of single-wall carbon nanotubes. *Solid State Communications* **112**, 35-37, doi:http://dx.doi.org/10.1016/S0038-1098(99)00278-1 (1999).

46 Le, L. T., Ervin, M. H., Qiu, H., Fuchs, B. E. & Lee, W. Y. Graphene supercapacitor electrodes fabricated by inkjet printing and thermal reduction of graphene oxide. *Electrochemistry Communications* **13**, 355-358, doi:http://dx.doi.org/10.1016/j.elecom.2011.01.023 (2011).

47 Tölle, F. J., Fabritius, M. & Mülhaupt, R. Emulsifier-Free Graphene Dispersions with High Graphene Content for Printed Electronics and Freestanding Graphene Films. *Advanced Functional Materials* **22**, 1136-1144 (2012).

48 Kordás, K. *et al.* Inkjet printing of electrically conductive patterns of carbon nanotubes. *Small* **2**, 1021-1025 (2006).

49 Small, W. R. Inkjet Printing of Transparent, Electrically Conducting Single-Walled Carbon-Nanotube Composites. *Small* **3**, 1500-1503 (2007).

50 Georgakilas, V. *et al.* Functionalization of graphene: covalent and non-covalent approaches, derivatives and applications. *Chemical reviews* **112**, 6156-6214 (2012).

51 Ramesha, G., Kumara, A. V., Muralidhara, H. & Sampath, S. Graphene and graphene oxide as effective adsorbents toward anionic and cationic dyes. *Journal of colloid and interface science* **361**, 270-277 (2011).

52 Hu, H., Zhao, Z., Wan, W., Gogotsi, Y. & Qiu, J. Ultralight and highly compressible graphene aerogels. *Advanced materials* **25**, 2219-2223 (2013).

53 Worsley, M. A. *et al.* Synthesis of Graphene Aerogel with High Electrical Conductivity. *Journal of the American Chemical Society* **132**, 14067-14069, doi:10.1021/ja1072299 (2010).

54 Bryning, M. B. *et al.* Carbon nanotube aerogels. *ADVANCED MATERIALS-DEERFIELD BEACH THEN WEINHEIM-* **19**, 661 (2007).

55 Worsley, M. A. *et al.* Synthesis of graphene aerogel with high electrical conductivity. *Journal of the American Chemical Society* **132**, 14067-14069 (2010).

56 Bordjiba, T., Mohamedi, M. & Dao, L. H. New Class of Carbon-Nanotube Aerogel Electrodes for Electrochemical Power Sources. *Advanced materials* **20**, 815-819 (2008).

57 Park, S. H. & Xia, Y. Macroporous Membranes with Highly Ordered and Three-Dimensionally Interconnected Spherical Pores. *Advanced Materials* **10**, 1045-1048 (1998).

58 Park, S.-H. *et al.* Spray-assisted deep-frying process for the in situ spherical assembly of graphene for energy-storage devices. *Chemistry of Materials* **27**, 457-465 (2015).

59 Wang, Y. & Caruso, F. Macroporous zeolitic membrane bioreactors. *Advanced Functional Materials* **14**, 1012-1018 (2004).

60 Xie, X. *et al.* Three-dimensional carbon nanotube− textile anode for high-performance microbial fuel cells. *Nano letters* **11**, 291-296 (2010).

61 Murphy, W. L., Dennis, R. G., Kileny, J. L. & Mooney, D. J. Salt fusion: an approach to improve pore interconnectivity within tissue engineering scaffolds. *Tissue engineering* **8**, 43-52 (2002).

62 Goenka, S., Sant, V. & Sant, S. Graphene-based nanomaterials for drug delivery and tissue engineering. *Journal of Controlled Release* **173**, 75-88 (2014).

Chapter 4

Osteogenic Differentiation of Human Adipose Derived Stem Cells on Chemically Crosslinked Carbon Nanomaterial Coatings

Contributions by: Sunny C. Patel, Owais Alam, Balaji Sitharaman

Abstract

Carbon nanomaterial coatings have been widely investigated for many biomedical applications including bone tissue engineering. Current methods to fabricate carbon nanomaterial coatings are limited by specific substrate requirements and the lack of strong bonds between the nanomaterials. Furthermore, few studies compare the effect of carbon nanoparticle architecture on stem cell differentiation and mineralization for osteogenic differentiation. Herein we report a study comparing chemically crosslinked carbon nanotubes (of various diameters), graphene nanoplatelets, and graphene nanoribbons coatings for adipose derived stem cell differentiation towards an osteogenic lineage. We observed greatest auto-deposition of calcium on graphene nanoribbon surfaces, while multiwalled carbon nanotubes of high diameter had the greatest influence on stem cell fate (by alkaline phosphatase activity, calcium deposition, and osteocalcin measurements). Studies indicate the cause for multiwalled carbon nanotube related stem cell differentiation, may be related to early timepoint toxicity as indicated by lactose dehydrogenase release. These results indicate suggestions for orthopedic tissue engineering applications for carbon nanomaterial coatings.

Introduction

Biomedical research of carbon nanomaterials (fullerenes, carbon nanotubes, graphene, etc.) includes studies on bioimaging,[1,2] cancer therapeutics,[3,4] biosensor development,[5,6] tissue engineering,[7,8] and other biomedical applications.[9,10] Stem cell interactions with carbon nanomaterials have been widely investigated for mainly neuronal,[11,12] muscular,[13,14] and bone tissue engineering. Both, graphene and carbon nanotube assemblies of coatings and films have been investigated for bone tissue engineering applications. These films and coatings are fabricated by a variety of methods including spray coating, chemical vapor deposition, and vacuum filtration. For such applications, it is important to understand the interface of the nanomaterial assembly to native bone tissue and its cellular components.

Carbon nanotube coatings and films have been previously assembled for bone tissue engineering applications. Bone cell proliferation and viability have been previously investigated on spray coated single walled (SWNCT) and multi-walled (MWCNT) carbon nanotube substrates.[15] They found nanotube charge neutrality was the key for greatest osteoblastic growth and proliferation.[15] Carbon nanotubes have also been investigated for their interactions with mesenchymal stem cells (MSCs).[16] Patterned monolayers of SWCNT can control the shape and adhesion of MSCs, which is closely related to the lineage MSCs differentiate into.[16] Spray coated thin films of MWCNT have shown the ability to differentiate MSCs towards bone progenitor cells.[17] Other than MSCs, adipose derived stem cells (ADSCs) have also been investigated for bone cell differentiation on carbon nanotube substrates.[18] Due to the lack of availability and low count of MSCs in bone marrow, ADSCs derived from lipoaspirates, may be a more viable option than MSCs.[19]

Graphene substrates have also been investigated for bone tissue engineering applications. Graphene substrates have been shown to be suitable for both human osteoblasts and MSC growth and proliferation.[20] Chemical vapor deposition (CVD) formed graphene substrates have shown the ability to accelerate osteogenic differentiation of MSCs and produce comparable calcium deposition to bone morphogenic protein-2 (positive control) treated groups.[21] Lee, et al. reported a possible reason for the enhanced stem cell growth and differentiation on graphene can be attributed to the adhesion of growth factors and osteogenic induction agents.[22]

While graphene and carbon nanotube coatings and films have shown promise in bone tissue engineering applications, there are many limitations in the techniques used to fabricate these assemblies.[23] One of the key limitations to CVD, vacuum filtration, and spray coating methods, is the lack of chemical bonding between the nanoparticles. This can lead to loose nanoparticle related toxicity and wear debris small enough to enter cells or other organs such as the brain. Also there are no current studies, to the best of our knowledge, that cross compare various carbon nanotubes and graphene architecture substrates for their effectiveness in stem cell differentiation.

We have recently developed a technique to create *in situ* chemically crosslinked carbon nanomaterial coatings on titanium substrates by ultrasonic spray deposition. We have leveraged this method to fabricate chemically crosslinked carbon nanotube coatings (of various diameters) and graphene coatings (nanoplatelets and nanoribbons). We aim to assess the effect of the nanotopography of the nanomaterials, surface chemistry, and roughness of the coatings on ADSC differentiation towards osteogenic lineages.

Materials and Methods

Materials

Both multiwalled carbon nanotubes, of high diameter (MWCNT-H) and low diameter (MWCNT-L), benzoyl peroxide (BP), and anhydrous ethyl acetate were purchased from Sigma Aldrich (St. Louis, MO USA). Single-walled carbon nanotubes (SWCNT) and graphene oxide nanoplatelets (GONP) were purchased from CheapTubes (Cambridgeport, VT. USA). Graphene oxide nanoribbons (GONR) were generously provided by AZ Electronic Materials (Branchburg, NJ, USA).

Crosslinked Carbon Nanomaterial Coatings

Carbon nanoparticle dispersions were prepared for SWNCT, MWCNT-L, MWCNT-H, GONP and GONR in ethyl acetate at 0.4 – 1.0 mg/mL. All dispersions were subsequently bath sonicated for 1 hour to separate aggregates. BP, a free radical initiator, was added at a 1:4 mass ratio (nanomaterial: BP) shortly before spraying. Spray coating was conducted in a rastering pattern utilizing an automated XYZ gantry with an attached ultrasonic spray nozzle (Sonear Ultrasonics, Farmingdale, NY USA). The nanomaterial and BP dispersion was fed to into the spray nozzle by a syringe pump and deposited onto heated titanium discs (commercially pure grade-2) mounted on an aluminum vacuum chuck. The hotplate temperature was set at 135°C and the approximate temperature at the titanium was measured to be ~ 90°C as measured by an infrared heat gun (Fluke, Everett, WA USA). Inert nitrogen gas, at 2 psi, was fed into the spray nozzle to form a conical spray shape.

Scanning Electron Microscopy

Scanning electron microscopy (SEM) was performed at the Center for Functional Nanomaterials, Brookhaven National Lab (Upton, NY) using a JEOL 7600 high-resolution SEM. Carbon nanomaterial films on titanium discs were sputter coated with 3nm of silver to assist with charge dissipation and provide higher resolution imaging.

Atomic Force Microscopy

Atomic force microscopy (AFM) was conducted using a Nanosurf FlexAFM (Nanoscience Instruments Inc., USA) using a V-shaped cantilever tip (APP Nano ACL − 10, frequency fc = 145−230 kHz, L = 225 μm, W= 40 μm, tip radius < 10 nm, spring constant k = 20−95 N/m) on a 10 x 10μm scan head. Surface roughness (r.m.s.) was measured using the NanoSurf Easy Scan 2 software over 5 regions on each coating.

Raman Spectroscopy

Point Raman spectra were acquired using a 40x objective and a 532nm laser source (Enwave Optronics, Irvine, CA) in five regions for each group. Raman spectral scanning from 100 to 3,100 cm^{-1}, at room temperature, were acquired for analysis. All data was normalized to the G band of the carbon nanomaterials for comparisons.[24]

Protein Adsorption Assay

Protein adsorption of bovine serum albumin (BSA) was measured using Pierce Bicinchoninic acid (BCA) Protein Assay Kit (Thermo Scientific, Grand Island, NY USA). Crosslinked carbon nanoparticle coatings of SWCNT, MWCNT-L, MWCNT-H, GONP, and GONR were treated with 1 ml of 2mg/mL bovine serum albumin in water inside a 24 well non-tissue culture treated plate. The plates were left for 48 hours in a 37°C incubator, 99% humidity, and 5% CO_2 after which plates were removed for the assay. The plates where placed on a shaker to mix the BSA in solution and the solution was removed for analysis. The BCA working reagent was added to each standard (for creating a concentration curve), baseline (24 well plate), and experimental group in a 96 well microplate. The microplate was shaked in the plate reader and solution was protected from light for 30 minutes after which absorbance was read at 562nm (Molecular Devices, Sunnyvale, CA, USA). BSA adsorbed was reverse calculated from the amount of BSA which had remained in the solution.

Cell Culture

Primary human adipose derived stem cells (ADSCs) were cultured to passages 3-5 in ADSC basal media (Lonza, Allendale, NJ USA) with heat-inactivated fetal bovine serum and ADSC Growth Media Bulletkit™ (Lonza, Allendale, NJ USA). Cells were grown in tissue culture treated polystyrene flasks at 95% humidity, 5% CO_2, and 37°C with media changes every two to three days.

Crosslinked carbon nanoparticle-coated titanium discs (12mm diameter) and clean titanium discs (control) was treated with 70% ethanol for two hours and treated with UV for 15 minutes to sterilize the samples. Each disc was then washed with sterile phosphate buffered saline (PBS) solution (Gibco, Grand Island, NY USA). The discs were pre-treated with cell culture

media, as described above, supplemented with 10mM β-glycerophosphate (Sigma Aldrich), 50μM ascorbic acid-2-phosphate (Sigma Aldrich), and 0.1μM dexamethasone (Sigma Aldrich). Each group was pre-treated for two days and transferred to new non-adherent 24 well polystyrene plates. Cells were plated onto the discs and tissue culture polystyrene, as another control, (n=6) at a density of $2x10^4$ cells per well. The cells were given 24 hours to adhere after which the media was removed and each well was washed with sterile PBS. After this, cells were kept for two timepoints; day 14 and day 21. Every three days, the media was changed with fresh media. At the terminal timepoints, we either fixed the cells in 4% paraformaldehyde or lysed the cells in 1 mL of deionized water using repetitive freeze thaw (4 cycles at -20°C and room temperature) for assays. Cell lysate was removed from the 24 well plate and placed in sterile conical tubes for analysis.

Lactose Dehydrogenase Release Assay

Cytotoxicity of ADSCs on crosslinked carbon nanomaterial coatings on titanium substrates was assessed by lactate dehydrogenase (LDH) release from cells (Sigma Aldrich). Media was collected from each coating and titanium substrates, as controls, at day 5. For each sample (n=6), 50μL of the media or the NADH standards were added to a 96 well plate in triplicates followed by 50μL of the combined LDH assay buffer and substrate mix. The plate was incubated in the dark at 37°C for 20 minutes and the plate absorbance was read at 450 nm in a plate reader (Molecular Devices). Positive control of 100% dead cells was performed by adding 10 μl of kit-supplied lysis buffer to the positive control groups.

DNA Quantification

DNA quantification was performed using QuantiFluor® dsDNA assay (Promega, Madison, WI USA). Briefly, triplicates of cell lysate or DNA standards (100µL) were diluted with 100µL of TE buffer in a 96 well plate, followed by adding 100 µL of QuantiFluor® working reagent. The 96 well plates were then incubated at room temperature, protected from light, for 15 minutes after which fluorescence was measured in a plate reader with λ_{ex}=504 nm and λ_{em}=531 nm (Molecular Devices).

Alkaline Phosphatase Activity Assay

Alkaline phosphatase enzyme activity was assessed using p-nitrophenyl phosphate liquid substrate (Sigma Aldrich). In a 96 well plate, 100 µL of the p-nitrophenyl substrate was added to 100 µL of cell lysate or 4-nitrophenol standards in triplicates. Protected from light, the 96 well plates were incubated in a 37°C incubator for 45 minutes. The reaction was stopped with 0.1 M sodium hydroxide and absorbance was read at 405 nm in a plate reader (Molecular Devices).

Calcium Deposition Assay

Carbon nanomaterial coated titanium substrates with cell lysate, at day 14 and day 21, were mixed with equal volume 1M acetic acid for two days to digest any extracellular matrix and biological components and dissolve calcium ions into solution. For assessment of auto-deposition of calcium, carbon nanomaterial substrates without cells seed on it, were digested in 1M acetic acid after 21 days. In a 96 well plate 75µL of the lysate mix or standards (calcium chloride) were

added in triplicates to 75 µL of calcium-chelating Arsenazo III dye (FisherScientific). Absorbance at 650nm was read in a plate reader (Molecular Devices).

Immunofluorescent Staining and Quantification

Live cells on titanium or crosslinked carbon nanomaterial coatings at day 21, were washed with PBS three times to remove residual media. Cells were fixed with 4% paraformaldehyde for 15 minutes followed by three PBS washes. Cells were permeabilized using a 0.5% Triton X-100 solution for 20 minutes. Non-specific binding was blocked using 1% BSA for 60 minutes at room temperature followed by a gentle PBS wash. For actin staining, rhodamine phalloidin (Molecular Probes, Thermo Scientific) was added to cover the titanium discs at a concentration of 2µL/mL in PBS for 30 minutes followed by 3 PBS washes. For immunofluorescent imaging of osteocalcin (OCN), titanium discs were immersed in monoclonal anti-osteocalcin antibody (Novus Biologicals, Littleton, CO USA) raised in mouse (2µL/mL in PBS) for one hour at room temperature followed by 3 washes in PBS. Following, the discs were incubated with anti-mouse FITC secondary antibody (FisherScientific) at 5µg/mL for 1 hour at room temperature. Samples were imaged with a Leica TCS SP5 confocal microscope at 10x. Actin and OCN fluorescence quantification was performed in FIJI, an open source ImageJ based image processing software (http://fiji.sc/). For image analysis, all imaging data was collected with the same microscope, gain settings, and parameters. Integrated density was subtracted from the background fluorescence from each image (n=5) and OCN expression was normalized to actin content.

Statistical Analysis

All statistical analysis was performed in GraphPad Prism 4, using one way ANOVA, for all cell studies and protein adsorption, followed by Tukey-Kramer post hoc analysis for comparisons. A 95% confidence interval was chosen for all statistical analysis and significant differences with $p < 0.05$ are reported.

Results and Discussions

Pure, grade-2 titanium was used as substrates for the crosslinked carbon nanomaterial coatings. Commercially available carbon nanomaterials of varying nanoarchitectures were selected including SWCNT (1-4nm diameter), MWCNT-L (40-70nm diameter), MWCNT-H (110-170nm diameter), GONP (few layer, 1-2μm grain size), and GONR (~400-700nm in width). Grade 2 titanium substrates were chosen as the underlying material and control groups since they are widely used in orthopedic implants, bone screws and plates.[25,26] The nanomaterials, along with the benzoyl peroxide were dispersed in ethyl acetate and coated onto heated titanium to form *in situ* crosslinks between the materials.

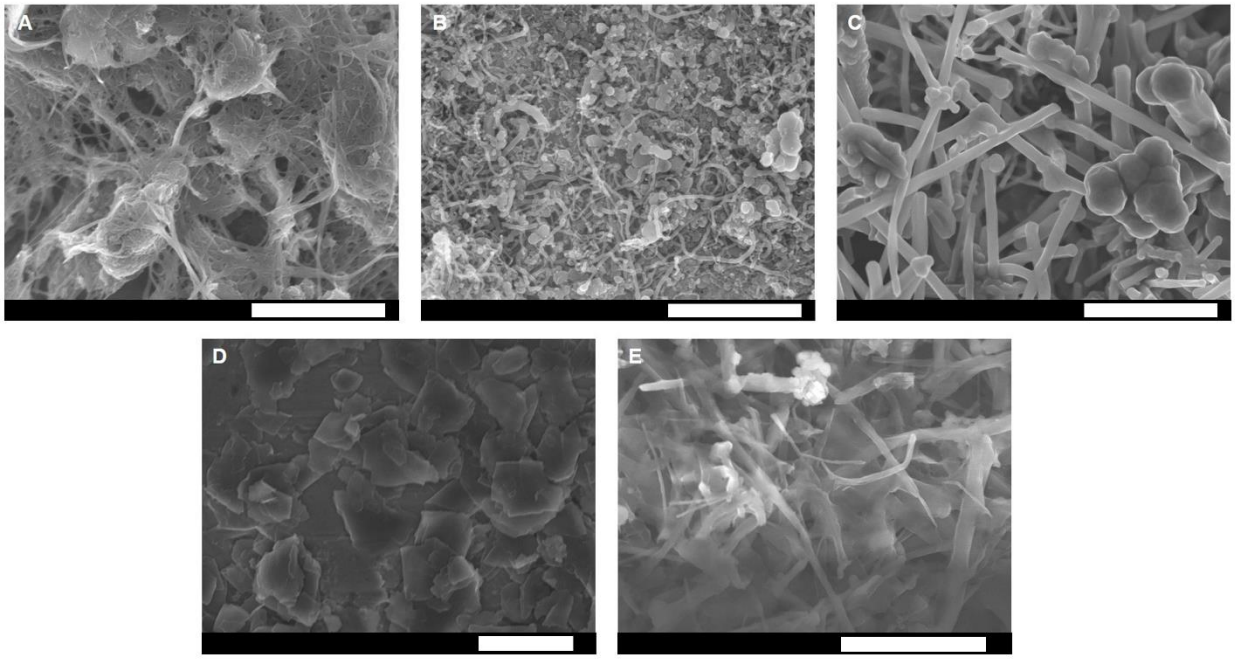

Figure 4.1. Scanning electron microscopy images of chemically crosslinked (A) SWCNT, (B) MWCNT-L, (C) MWCNT-H, (D) GONP, and (E) GONR coatings on titanium substrates. Each scale bar is 2μm in width.

The microstructure of the carbon nanomaterial coatings were studied by SEM analysis (Figure 4.1). SWCNT were found in densely packed ropes (Figure 4.1a) while MWCNT-L and

MWCNT-H (Figure 4.1b, 1c respectively) were found as more individual particles. GONP are flat planar structures (Figure 4.1d) appearing to be stacked upon each other on their planar axis. GONR (Figure 4.1e) are similar to both the MWCNT-H coatings, where the particles are observably more individualized, and GONP coatings, where the particles are stacked on their planar axis. AFM reveals the topographical features of titanium substrates and the crosslinked carbon nanomaterial coatings (Figure 4.2). Titanium substrates (Figure 4.2a) exhibited the lowest r.m.s. surface roughness (μ=114.4 nm, sd = 43.4 nm). Coating with carbon nanoparticles increased the surface roughness for each group. Increasing nanotube diameter from SWCNT to MWCNT-H increased the surface roughness from 136.1 nm (s.d. = 73.2nm) to 186.1 nm (s.d. = 24.5), respectively. SWCNT (Figure 4.2b) had more nested peaks in its line plot, compared to MWCNT-L (Figure 4.2c) and MWCNT-H (Figure 4.2d), likely due to the smaller diameter tubes being probed in the larger SWCNT ropes. The surface roughness of MWCNT-L coatings however, 123.7 nm (s.d = 46.5 nm), was not greater than SWCNT coatings. SWCNT, as seen in Figure 4.1a, were visibly bundled and tangled into ropes. It is well reported that SWCNT, if not separated by oxidizing, acid-wash treatment, form dense and tangled ropes.[27] Surface oxidation on the nanotubes would also limit the amount of sp^2 hybridized, double bonded carbons, for free-radical initiated crosslinking. GONP (μ=162.6 nm, sd = 78.66 nm) and GONR (μ=168.4 nm, sd = 36.3 nm) both had similar surface roughness. The line plot of GONP coatings (Figure 4.2e) shows large area, flat structures while line plots for GONR coatings (Figure 4.2f) show some of the flat ribbon-like, folded structures.

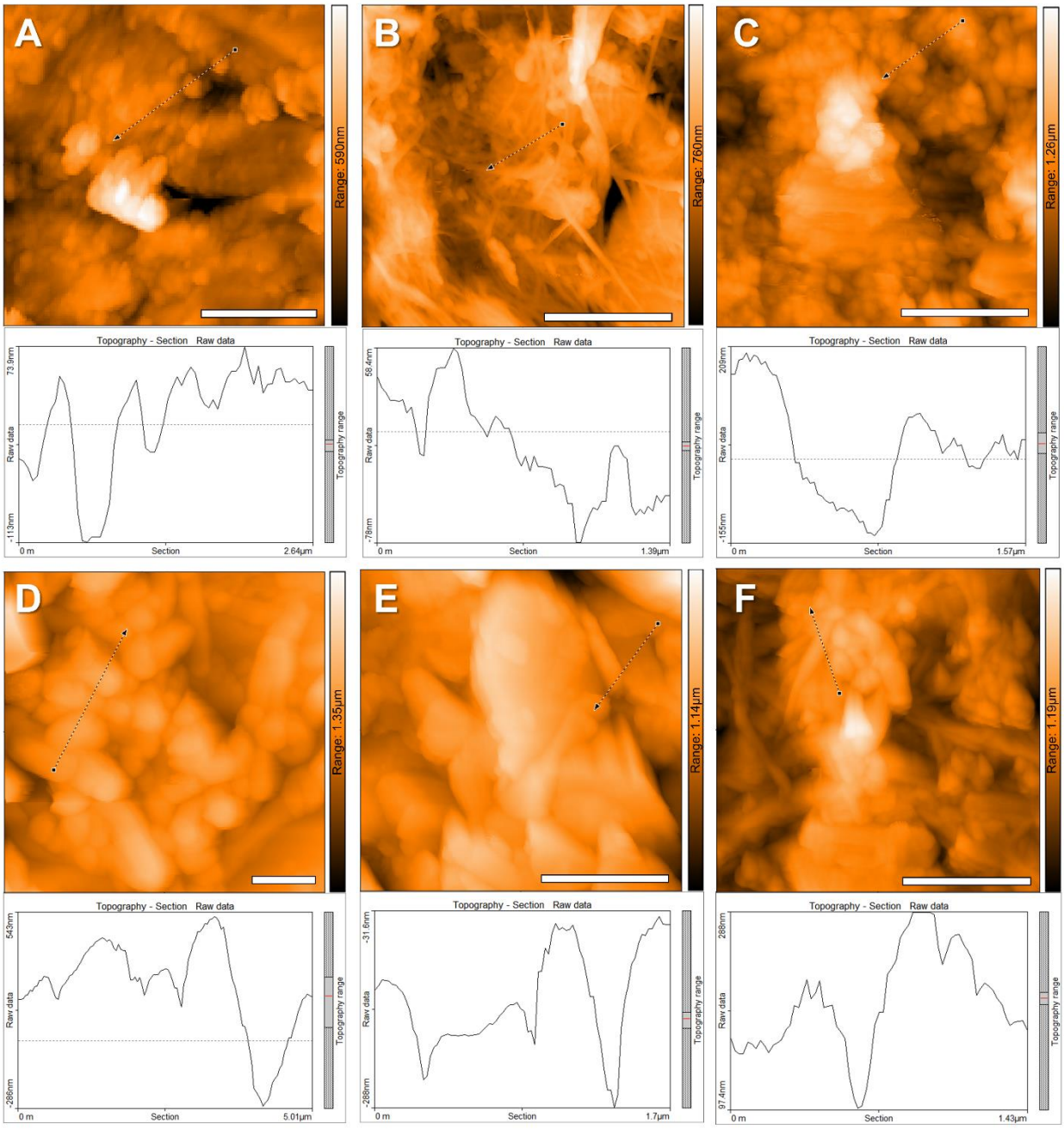

Figure 4.2. Representative AFM images and line plots showing regions of interest on (A) titanium substrates as well as chemically crosslinked (B) SWCNT, (C) MWCNT-L, (D) MWCNT-H, (E) GONP, and (F) GONR coatings on titanium substrates. Each scale bar is 2µm in width.

Chemical properties of the crosslinked carbon nanomaterial coatings on the titanium substrates (n=5 per group) were assessed by Raman spectroscopy. The primary Raman peaks of

carbon nanomaterials which were investigated were at ~ 1345 cm^{-1}, 1560 cm^{-1}, identified as the D, G, bands, respectively.[28] All sp^2 hybridized carbon nanomaterials present a characteristic peak noted as the 'G' band, caused by in-plane vibrations of the sp^2 hybridized carbon atoms.[24] Another prominent peak presented in most carbon nanomaterials is the 'D' band, caused by structural and chemical disorder in the sp^2 hybridized network.[28] Therefore, to compare differences in structural and chemical defects between groups, we can normalize the intensity of the defect structures (D band) by the intensity of the sp^2 hybridized carbon (G band). Figure 4.3 presents the Raman spectrographs for crosslinked carbon nanomaterial substrates from 500 cm^{-1} to 3000 cm^{-1}. The relative, mean D/G ratio of SWCNT, MWCNT-L and MWCNT H was 0.085 (sd = 0.02), 1.10 (sd = 0.10), and 0.16 (sd = 0.04), respectively. The high D/G ratio of the MWCNT-L can be attributed to any combination of amorphous carbon in the MWCNTs, kinks in the tubes caused by heptagon and pentagon shaped carbon rings in the nanotube structure, and graphitic regions in the nanotube walls.[29] GONP had a D/G ratio of 0.34 (sd = 0.04), with oxidation being the most likely and prominent cause for the D band formation. Similar to GONP, oxidation on GONR can partially explain a D/G ratio of 1.01 (sd = 0.03). Since GONR are fabricated by

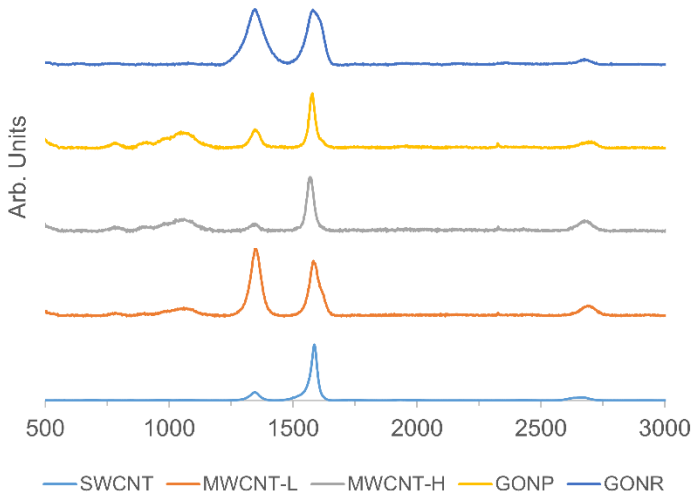

Figure 4.3. Representative Raman spectrographs of chemically crosslinked SWCNT, MWCNT-L, MWCNT-H, GONP, and GONR coatings on titanium substrates.

oxidative unzipping of MWCNT,[30] other defect structures which can originate are similar to those described for MWCNT-L.

Protein adsorption was measured using a BCA assay to measure bovine serum albumin (BSA) adsorption on the crosslinked carbon nanomaterial substrates. BSA is a plasma protein found in high concentrations in blood and a common model protein for assessment of nonspecific protein adsorption on materials.[31] Protein adsorption on the crosslinked carbon nanomaterial substrates (n=6) after 48 hours is presented in Figure 4.4. Both MWCNT-H ($p<0.01$) and GONP ($p<0.05$) showed statistically significant increases in BSA adsorption than SWCNT, MWCNT-L, and GONR.

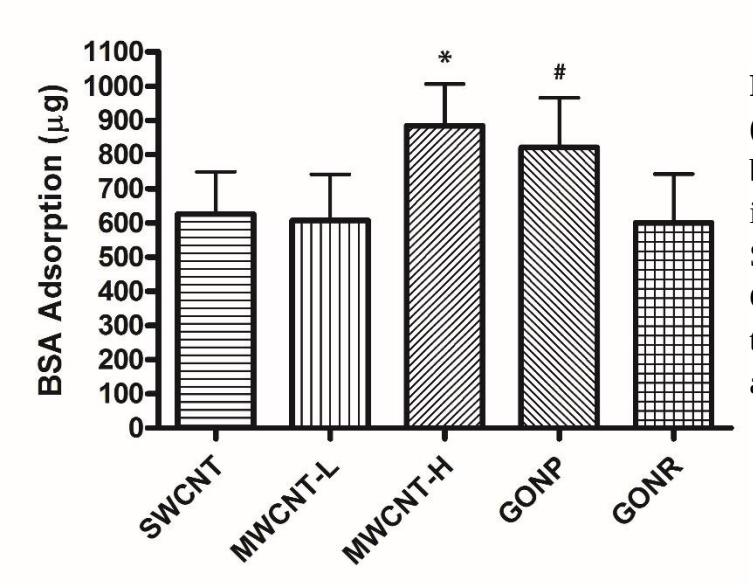

Figure 4.4. Bovine serum albumin (BSA) protein adsorption measured by BCA assay at 48 hours (n=6) of incubation for chemically crosslinked SWCNT, MWCNT-L, MWCNT-H, GONP, and GONR coatings on titanium substrates. (*denotes $p<0.01$ and #denotes $p<0.05$)

Cellular toxicity, at day 5, was studied by measuring lactose dehydrogenase (LDH) release from ADSCs seeded on crosslinked carbon nanomaterial coatings. Nanoparticle toxicity has been widely studied and a tool validated to study nanoparticle toxicity is the LDH release assay.[32,33] LDH released into cell culture media, through damaged cell membranes, was collected and assayed (Figure 4.5). SWCNT and MWCNT-H groups showed significant increases ($p<0.05$) in LDH release compared to titanium controls (8% and 10% respectively). No significant differences were

observed in LDH release for MWCNT-L, GONP, GONR groups compared to titanium substrates. Although some toxicity was observed in SWCNT and MWCNT-H groups, many cells were observed on the surface of both groups during imaging at day 21 timepoints.

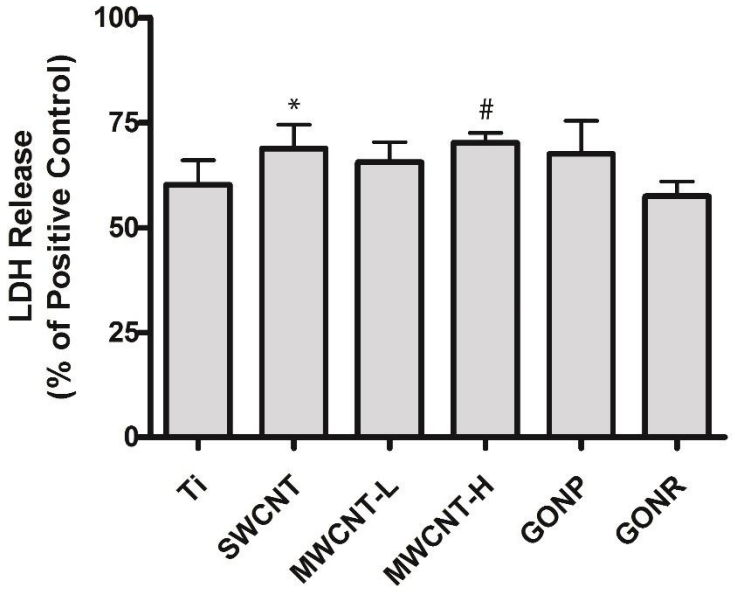

Figure 4.5. Lactose dehydrogenase release, at day 5, as a measure for cytotoxicity for ADSCs on tissue culture titanium substrates (Ti), and chemically crosslinked SWCNT, MWCNT-L, MWCNT-H, GONP, and GONR coatings on titanium substrates. (* and # represent statistical significant increases in LDH release ($p<0.05$)).

Alkaline phosphatase (ALP) activity, an early stage marker for stem cell differentiation to osteogenic lineages,[34] was assessed for each group at day 14 (Figure 4.6a) and day 21 (Figure 4.6b). ALP activity was normalized to DNA content to account for the number of cells on each substrate. At day 14, MWCNT showed a significantly greater ALP activity compared to the titanium substrates ($\Delta\mu = 0.0013$, $p<0.01$), GONP ($\Delta\mu = 0.0011$, $p<0.05$), and GONR ($\Delta\mu = 0.0012$, $p<0.01$). Tissue culture polystyrene controls also indicated significant increases in ALP activity compared to all groups ($p<0.001$) at day 14, however expressed no significant differences at day 21. ALP activity at day 21 was greatest in GONR ($\mu=0.0199$, sd = 0.0072) followed by MWCNT-H ($\mu=0.0188$, sd = 0.015), though not statistically different. We observed a trend in ALP activity for increasing carbon nanotube diameters from SWCNT ($\mu=0.0161$, sd = 0.0030) to

MWCNT-L (μ=0.0181, sd = 0.0081) to MWCNT-H, but no significant differences. The differences in ALP activity for GONP compared to GONR were mild and not significant (Δμ = 0.0018).

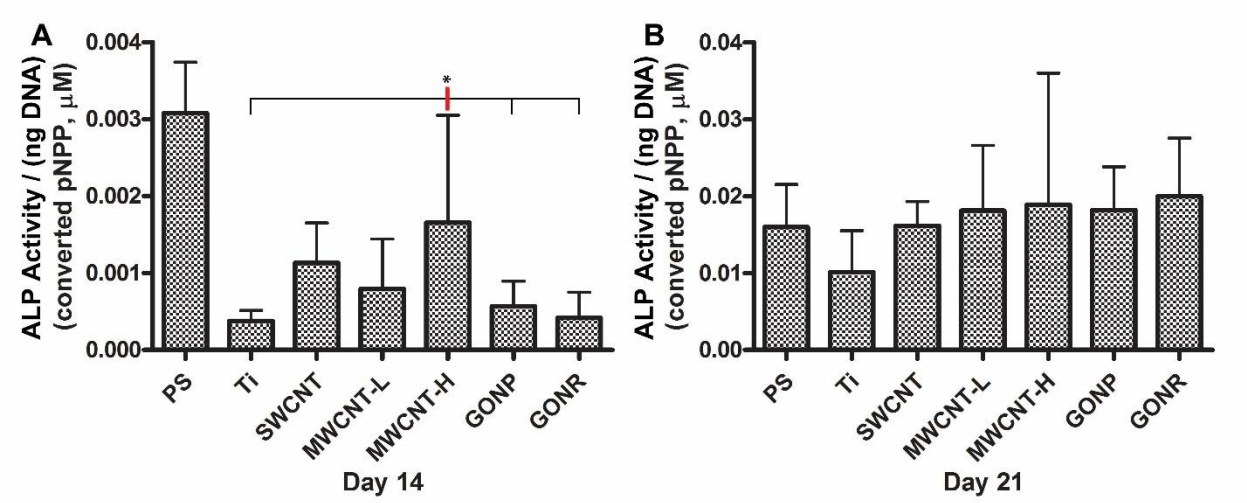

Figure 4.6. Alkaline phosphatase (ALP) activity assay as an early marker for ADSC differentiation at (A) day 14 and (B) day 21 timepoints for tissue culture polystyrene (PS), titanium substrates (Ti), and crosslinked carbon nanomaterial substrates. All values are normalized to the DNA content in the group.

Calcium deposition from ADSCs were studied for day 14 and day 21 timepoints (Figure 4.7a) and auto-deposition, without cells, was studied at day 21 (Figure 4.7b). Calcium is a late-stage marker for stem cell differentiation towards osteogenic lineages as calcium phosphate is the inorganic phase found in bone tissue[35] and can be quantified using calcium chelating agents like Arsenazo III.[36] At day 14, no appreciable differences were observed between the nanoparticle coated groups and the titanium substrates however it is notable that tissue culture polystyrene showed less Ca^{2+} deposition than all other groups. An increasing trend in calcium deposition was observed at day 21 when comparing SWCNT (μ= 0.135 mg, sd= 0.023 mg), MWCNT-L (μ= 0.201 mg, sd= 0.116 mg), and MWCNT-H (μ=0.497 mg, sd = 0.224mg). At day 21, calcium deposition from cells seeded on MWCNT-H was significantly greater ($p<0.01$) than GONR (μ= 0.351 mg,

sd= 0.0274 mg), MWCNT-L, SWCNT, and titanium substrates (μ= 0.236 mg, sd= 0.0422). Calcium deposition was also significantly greater ($p<0.05$) on GONR and GONP substrates (μ= 0.424 mg, sd= 0.0565 mg) compared to MWCNT-L, SWCNT, and titanium substrates.

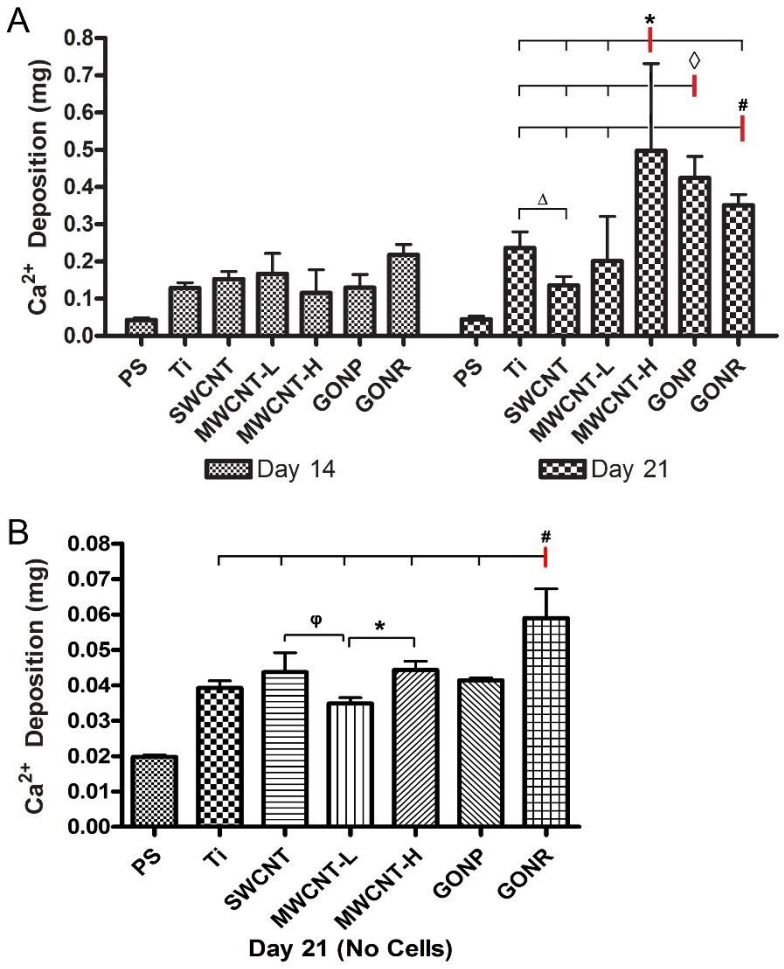

Figure 4.7. (A) Ca^{2+} quantification on substrates seeded with ADSCs at 14 and 21 days after seeding. (B) Ca^{2+} quantification on substrates treated with only cell culture media for 21 days to assess auto-calcium deposition. Symbols denotes comparisons where each substrate ($^{\Delta}$Ti, $^{\varphi}$SWCNT, *MWCNT-H, $^{\Diamond}$GONP, and $^{\#}$GONR) is significantly greater ($p<0.05$) than other indicated groups. All day 21 groups, for both (A) cell seeded and (B) no cells, are significantly greater than PS controls ($p<0.05$).

Assessment of auto-deposition of calcium, without cells, is a measure of bioactivity of the material surface.[37] As expected, tissue culture polystyrene showed significantly less deposition than all other groups ($p < 0.001$). Auto-deposition of calcium was significantly greater ($p<0.001$) on GONR coatings (μ= 0.0589 mg, sd= 0.008 mg) then all other coatings and control titanium substrates (μ=0.0392 mg, sd=0.006 mg). The least amount of auto-deposition of calcium was observed on MWCNT-L coatings (μ=0.0437 mg, sd= 0.005 mg), significantly less ($p<0.01$) than

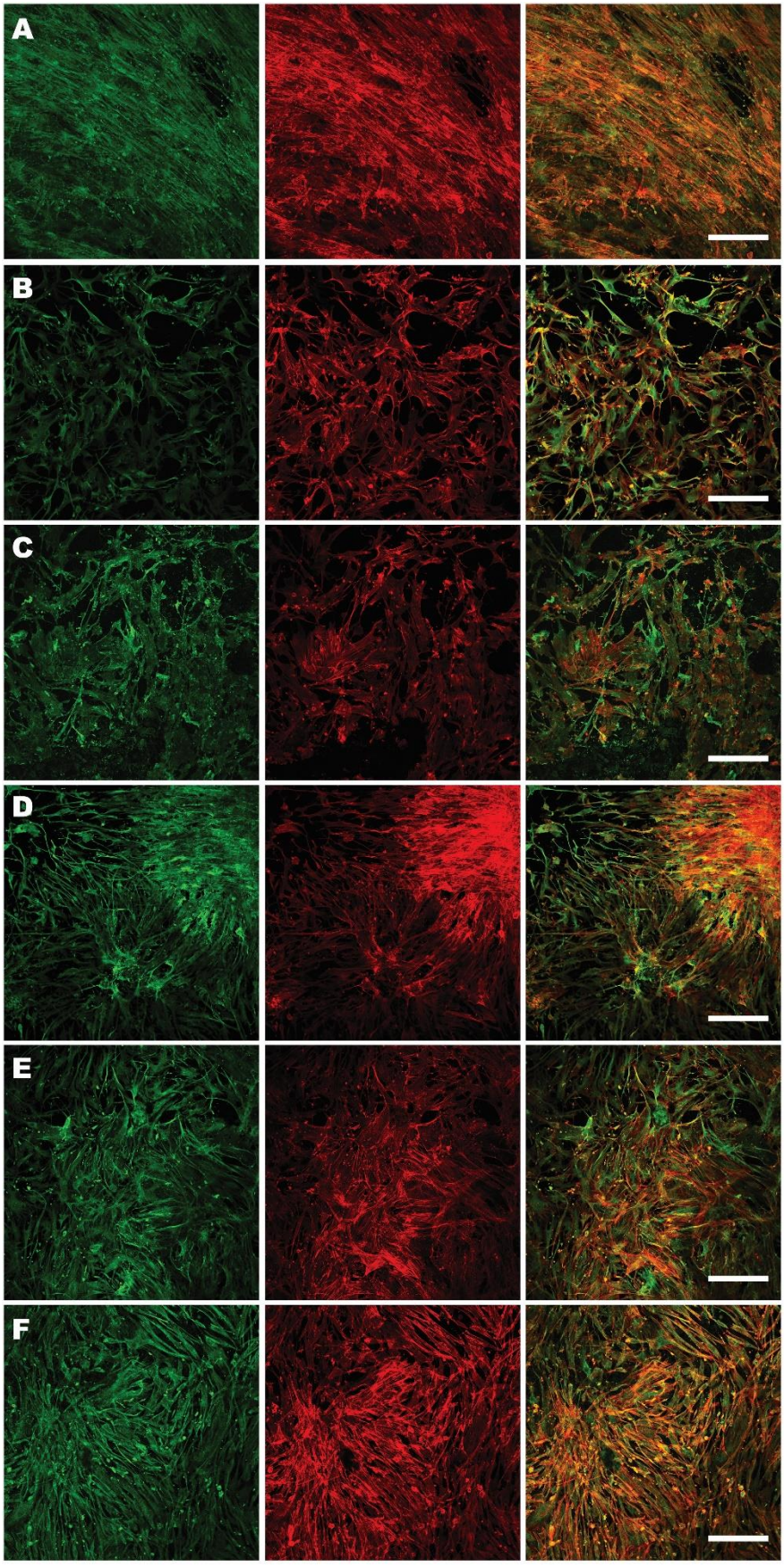

Figure 4.8. FITC-osteocalcin immunofluorescent stating (left panel, green), rhodamine phallodin-based actin staining (middle panel, red), and merged imaged images (right panel, multi-colored) for ADSC grown on (A) titanium substrates, and chemically crosslinked (B) SWCNT, (C) MWCNT-L, (D) MWCNT-H, (E) GONP, and (F) GONR coatings on titanium substrates.

Calcium deposition on GONP (μ= 0.0414 mg, sd= 0.002 mg) was also greater than titanium and MWCNT-L, though not significantly.

Osteocalcin (OCN) immunofluorescence staining was performed on the day 21 ADSCs to further assess the differentiation of the stem cells to osteogenic linages (Figure 4.8, left panel). OCN is one of the most abundant, non-collagenous proteins found in bone[38] and stem cell marker for differentiation towards osteogenic lineages.[39,40] Substrates stained with OCN antibodies were also stained with rhodamine phalloidin to visualize actin filaments in the cells (Figure 4.8, center panel). Merged images can be seen in Figure 4.8 (right panel). OCN was observed near and around cells as seen in the merged images. Actin staining revealed elongated and well spread cells with stress fiber formation in each group. OCN fluorescence, normalized to actin fluorescence, was quantified between groups and presented in Figure 4.9. MWCNT-H showed significantly greater ($p<0.05$) OCN fluorescence compared to titanium substrates, MWCNT-L, GONP, and GONR. SWCNT showed significantly ($p<0.01$) higher OCN fluorescence compared to GONP and non-statistically significant increases compared to MWCNT-L and GONR. GONR showed 60% more fluorescence then GONP, though not statistically significantly different.

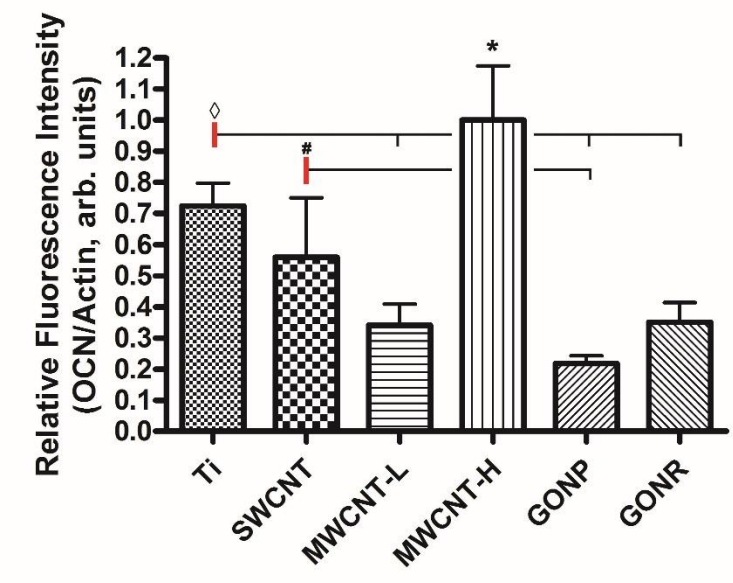

Figure 4.9. Fluorescence quantification of osteocalcin (OCN), normalized to actin fluorescence, for titanium substrates (Ti), and chemically crosslinked SWCNT, MWCNT-L, MWCNT-H, GONP, and GONR coatings on titanium substrates.

While the nanoparticle crosslinking, does introduce a structural and chemical variation in the nanomaterial, the nanoparticles remained mainly intact and possessed features of their pristine nanotopography as well. One goal of this study was to elucidate the effect of the nanoparticle/ coating topography and chemistry on stem cell differentiation towards osteogenic lineages for bone tissue engineering applications.

An informative tool for studying cell-material interaction is to assess protein adsorption on the surface of the material.[41] Protein adsorption on a biomaterial can happen within milliseconds of interaction, depending on its affinity, and can play an important role in cell attachment, migration, and extracellular matrix deposition.[41,42] While for some proteins like fibrinogen, increased surface roughness has correlated to increased protein adsorption,[43] BSA adsorption does not always share the same effect as shown in multiple studies.[43,44] Small changes in surface roughness, from 2 – 32.9 nm r.m.s., does not change BSA adsorption on tantalum surfaces while there is increased fibrinogen adsorption. This was attributed to the globular nature of BSA where the changes in the surface roughness did not affect the ability for the protein to bind to the surface.[43] However, significantly larger surface roughness, such as MWCNT-H coatings compared to SWCNT and MWCNT-L may lead to appreciable increases in surface area for increased BSA adsorption.

BSA adsorption on graphitic surfaces has been previously explored. One group found BSA adsorption onto graphite led to spreading of the BSA onto the graphite substrate.[31] While this may be a good indication for the biocompatibility for implanted graphitic constructs, assessment of other proteins, such as fibronectin, also needs to be assessed for cell-based tissue engineering applications. Multiple groups have studied protein adsorption on carbon nanotube substrates.[45] One group found increased adsorption of proteins from fetal bovine serum leads to better myocyte

attachment on MWCNT substrates.[46] Other studies found nanostructured materials increase cell binding site availability from vitronectin and fibronectin by unfolding the proteins upon adsorption.[47] Unfolding or changing confirmation of proteins, however does not always reflect positive outcomes. One study found conformational changes after enzyme adsorption of α-chymotrypsin and soybean peroxidase on SWCNT resulted in only 1% and 30% of the native enzyme activity, respectively.[48] In our studies, we also observed that GONP showed greater protein adsorption compared to GONR, likely due to the increased oxidation on GONR leading to fewer hydrophobic binding sites for the BSA molecules.

All cell studies were performed using human adipose derived stem cells (ADSCs). A common strategy utilized in bone tissue engineering methods is to create surfaces which enhance osteogenic differentiation from adult stem cells; either bone marrow derived[35] or adipose tissue derived.[19] There is a significant disparity in the number of stem cells that can be harvested from bone compared to adipose tissue. Bone marrow derived mesenchymal stem cells (MSCs) yields about 2.4×10^4 stem cells per local anesthetized procedure while under the same conditions ADSCs yield orders of magnitude more ($\sim 1 \times 10^6$) stem cells.[19] Therefore, with the correct treatment strategy, ADSCs can prove to be a more viable and safer alternative to MSC therapies.

Lee et al., reports potential reasons for increased stem cell differentiation on graphene substrates.[22] They found graphene substrates better adsorb β-glycerophosphate while graphene oxide better adsorbs ascorbic acid on its surface. Also differentiation of the MSCs towards adipogenic lineages is greatly reduced due to the denaturing of insulin (regulator for fatty acid deposition) upon π-bonding to the graphitic carbon.[22] This is particularly important to approaches utilizing ADSCs for orthopedic tissue engineering to minimize adipogenic tissue growth in place of bone.

It should be noted that cell-related calcium deposition can not only be inferred by subtracting auto-deposition of calcium from total calcium. The most intuitive reason for this is the surface area available for auto-deposition when cells are not present is more than when cells occupy the nanomaterial surface. In addition, calcium deposition which occurs during pre-treatment with cell culture media and during cell growth may also lead to a similar and favorable surface for cell growth and mineralization such as decellualarized matrix[49,50] and pre-treated substrates with hydroxyapatite.[51] Therefore, even though GONR coating exhibited greatest calcium deposition, MWCNT-H substrates may have other factors leading to greater calcium deposition, as explained below. Calcium deposition may also be governed by surface chemistry. Auto-deposition was observed most on GONR substrates, the most oxidized substrates as suggested by Raman spectroscopy. While MWCNT-L also exhibited a high D/G ratio, low calcium deposition on MWCNT-L substrates may be due to presence of amorphous carbon in the MWCNT-L samples. Future studies require simulated body fluid based bioactivity assessment of GONR and other carbon nanomaterial coated substrates.

While stem cell fate can be determined by chemically induced differentiation, mechanical cues from substrate stiffness also can determine differentiation lineages.[52] Diffuse organization of actin can be observed in less stiff substrates (for neurogenic differentiation), while in stiffer substrates actin organizes into stress fibers (for osteogenic differentiation).[52] For titanium substrates and each crosslinked carbon nanomaterial coating, we observed actin stress fiber formation suggesting the coatings are suitable substrates for stem cell differentiation towards osteoblasts.

Alkaline phosphatase activity, calcium assay, OCN immunofluorescence, and actin staining provide corroboratory evidence that MWCNT-H coatings provide the optimal surface for

stem cell differentiation of ADSCs towards osteogenic lineages. However the bioactivity of the GONR coatings may be more attractive than MWCNT-H coatings because of the toxicity of MWCNT-H coatings measured by LDH release. The increased LDH release from cells seeded on SWNCT and MWCNT-H coatings also correlates to the increased OCN expression at day 21 for both groups. Previous reports with murine preosteoblasts suggest toxicity of loose particles in SWCNT films (made by vacuum filtration) are responsible for enhanced matrix deposition.[53] However, here SWCNT groups did not have increased calcium deposition but did have increased OCN expression. Cells seeded on MWCNT-H, however, did show increased LDH release, increased calcium deposition and increased OCN expression. Tutak, et al. reported carbon nanotube substrates enhance pre-osteoblast (MC3T3 cells) activity in a two-step process.[53] First, loose nanomaterial is uptaken by cells and the release of endogenous factors from those cells boosts activity in the remaining cells causing increased matrix deposition.[53] Therefore, the causation of increased calcium deposition and OCN expression on MWCNT-H substrates needs to be further investigated.

Conclusions

This study compared the osteogenic differentiation capability of human adipose derived stem cells on chemically crosslinked carbon nanomaterial substrates. Carbon nanomaterial coatings of SWCNT, MWCNT-L, MWCNT-H, GONP, and GONR by an *in situ* chemical crosslinking method performed by ultrasonic spray coating. Coating surface roughness was mostly governed by nanomaterial dimensions and supramolecular structures formed by the nanomaterials. Protein adsorption of BSA on the carbon nanomaterial coatings suggests surface roughness and chemistry govern BSA adsorption on these materials. MWCNT-H substrates showed the greatest stem cell differentiation potential, as evaluated by ALP activity, calcium deposition, and OCN fluorescence. However, this may have been caused by cytotoxic effects at early timepoints. GONR showed greatest bioactivity and may be a candidate substrate for bioactive carbon nanomaterial coatings.

Acknowledgements

This work was sponsored by a National Institutes of Health grant (1DP2OD007394). SEM was conducted at Center for Functional Nanomaterials at BNL, supported by the U.S. Department of Energy, Office of Basic Energy Sciences, under Contract No. DE-AC02-98CH10886.

References

1 Sitharaman, B. *et al.* Gadofullerenes as nanoscale magnetic labels for cellular MRI. *Contrast media & molecular imaging* **2**, 139-146 (2007).

2 Ray, S., Saha, A., Jana, N. R. & Sarkar, R. Fluorescent carbon nanoparticles: synthesis, characterization, and bioimaging application. *The Journal of Physical Chemistry C* **113**, 18546-18551 (2009).

3 Kostarelos, K., Bianco, A. & Prato, M. Promises, facts and challenges for carbon nanotubes in imaging and therapeutics. *Nature Nanotechnology* **4**, 627-633 (2009).

4 Cho, K., Wang, X., Nie, S. & Shin, D. M. Therapeutic nanoparticles for drug delivery in cancer. *Clinical cancer research* **14**, 1310-1316 (2008).

5 Wu, L., Chu, H., Koh, W. & Li, E. Highly sensitive graphene biosensors based on surface plasmon resonance. *Optics express* **18**, 14395-14400 (2010).

6 Shao, Y. *et al.* Graphene based electrochemical sensors and biosensors: a review. *Electroanalysis* **22**, 1027-1036 (2010).

7 Harrison, B. S. & Atala, A. Carbon nanotube applications for tissue engineering. *Biomaterials* **28**, 344-353 (2007).

8 Goenka, S., Sant, V. & Sant, S. Graphene-based nanomaterials for drug delivery and tissue engineering. *Journal of Controlled Release* **173**, 75-88 (2014).

9 Shen, H., Zhang, L., Liu, M. & Zhang, Z. Biomedical applications of graphene. *Theranostics* **2**, 283 (2012).

10 Bianco, A., Kostarelos, K., Partidos, C. D. & Prato, M. Biomedical applications of functionalised carbon nanotubes. *Chemical Communications*, 571-577 (2005).

11 Jan, E. & Kotov, N. A. Successful differentiation of mouse neural stem cells on layer-by-layer assembled single-walled carbon nanotube composite. *Nano Letters* **7**, 1123-1128 (2007).

12 Chao, T.-I. *et al.* Carbon nanotubes promote neuron differentiation from human embryonic stem cells. *Biochemical and biophysical research communications* **384**, 426-430 (2009).

13 Martinelli, V. *et al.* Carbon nanotubes promote growth and spontaneous electrical activity in cultured cardiac myocytes. *Nano letters* **12**, 1831-1838 (2012).

14 Lee, T.-J. *et al.* Graphene enhances the cardiomyogenic differentiation of human embryonic stem cells. *Biochemical and biophysical research communications* **452**, 174-180 (2014).

15 Zanello, L. P., Zhao, B., Hu, H. & Haddon, R. C. Bone Cell Proliferation on Carbon Nanotubes. *Nano Letters* **6**, 562-567, doi:10.1021/nl051861e (2006).

16 Park, S. Y. *et al.* Carbon nanotube monolayer patterns for directed growth of mesenchymal stem cells. *ADVANCED MATERIALS-DEERFIELD BEACH THEN WEINHEIM-* **19**, 2530 (2007).

17 Nayak, T. R. *et al.* Thin Films of Functionalized Multiwalled Carbon Nanotubes as Suitable Scaffold Materials for Stem Cells Proliferation and Bone Formation. *ACS Nano* **4**, 7717-7725, doi:10.1021/nn102738c (2010).

18 Li, X. *et al.* The use of carbon nanotubes to induce osteogenic differentiation of human adipose-derived MSCs in vitro and ectopic bone formation in vivo. *Biomaterials* **33**, 4818-4827 (2012).

19 Bunnell, B. A., Flaat, M., Gagliardi, C., Patel, B. & Ripoll, C. Adipose-derived stem cells: isolation, expansion and differentiation. *Methods* **45**, 115-120 (2008).

20 Kalbacova, M., Broz, A., Kong, J. & Kalbac, M. Graphene substrates promote adherence of human osteoblasts and mesenchymal stromal cells. *Carbon* **48**, 4323-4329, doi:http://dx.doi.org/10.1016/j.carbon.2010.07.045 (2010).

21 Nayak, T. R. *et al.* Graphene for controlled and accelerated osteogenic differentiation of human mesenchymal stem cells. *ACS nano* **5**, 4670-4678 (2011).

22 Lee, W. C. *et al.* Origin of Enhanced Stem Cell Growth and Differentiation on Graphene and Graphene Oxide. *ACS Nano* **5**, 7334-7341, doi:10.1021/nn202190c (2011).

23 Patel, S. C., Lalwani, G., Grover, K., Qin, Y.-X. & Sitharaman, B. Fabrication and cytocompatibility of in situ crosslinked carbon nanomaterial films. *Scientific Reports* **5** (2015).

24 Ferrari, A. C. Raman spectroscopy of graphene and graphite: disorder, electron–phonon coupling, doping and nonadiabatic effects. *Solid state communications* **143**, 47-57 (2007).

25 Carlsson, L., Regner, L., Johansson, C., Gottlander, M. & Herberts, P. Bone response to hydroxyapatite-coated and commercially pure titanium implants in the human arthritic knee. *Journal of orthopaedic research* **12**, 274-285 (1994).

26 Rack, H. & Qazi, J. Titanium alloys for biomedical applications. *Materials Science and Engineering: C* **26**, 1269-1277 (2006).

27 Xie, S. X. *et al.* Effect of synthesis and acid purification methods on the microwave dielectric properties of single-walled carbon nanotube aqueous dispersions. *Applied Physics Letters* **103**, 133114 (2013).

28 Dresselhaus, M. S., Dresselhaus, G., Saito, R. & Jorio, A. Raman spectroscopy of carbon nanotubes. *Physics Reports* **409**, 47-99 (2005).

29 Datsyuk, V. *et al.* Chemical oxidation of multiwalled carbon nanotubes. *Carbon* **46**, 833-840 (2008).

30 Kosynkin, D. V. *et al.* Longitudinal unzipping of carbon nanotubes to form graphene nanoribbons. *Nature* **458**, 872-876 (2009).

31 Mücksch, C. & Urbassek, H. M. Molecular Dynamics Simulation of Free and Forced BSA Adsorption on a Hydrophobic Graphite Surface. *Langmuir* **27**, 12938-12943, doi:10.1021/la201972f (2011).

32 Han, X. *et al.* Validation of an LDH assay for assessing nanoparticle toxicity. *Toxicology* **287**, 99-104, doi:http://dx.doi.org/10.1016/j.tox.2011.06.011 (2011).

33 Chowdhury, S. M. *et al.* Cell specific cytotoxicity and uptake of graphene nanoribbons. *Biomaterials* **34**, 283-293 (2013).

34 Owen, M. & Friedenstein, A. Stromal stem cells: marrow-derived osteogenic precursors. *Cell and molecular biology of vertebrate hard tissues* **136**, 42-60 (1988).

35 Pittenger, M. F. *et al.* Multilineage potential of adult human mesenchymal stem cells. *science* **284**, 143-147 (1999).

36 Bauer, P. J. Affinity and stoichiometry of calcium binding by arsenazo III. *Analytical biochemistry* **110**, 61-72 (1981).

37 Rezwan, K., Chen, Q., Blaker, J. & Boccaccini, A. R. Biodegradable and bioactive porous polymer/inorganic composite scaffolds for bone tissue engineering. *Biomaterials* **27**, 3413-3431 (2006).

38 Price, P. A., Otsuka, A., Poser, J. W., Kristaponis, J. & Raman, N. Characterization of a gamma-carboxyglutamic acid-containing protein from bone. *Proceedings of the National Academy of Sciences* **73**, 1447-1451 (1976).

39 Zuk, P. A. *et al.* Human adipose tissue is a source of multipotent stem cells. *Molecular biology of the cell* **13**, 4279-4295 (2002).

40 Hung, S. C. *et al.* Isolation and Characterization of Size-Sieved Stem Cells from Human Bone Marrow. *Stem cells* **20**, 249-258 (2002).

41 Liu, H. & Webster, T. J. Nanomedicine for implants: A review of studies and necessary experimental tools. *Biomaterials* **28**, 354-369, doi:http://dx.doi.org/10.1016/j.biomaterials.2006.08.049 (2007).

42 Schmidt, D., Waldeck, H. & Kao, W. in *Biological Interactions on Materials Surfaces* (eds David A. Puleo & Rena Bizios) Ch. 1, 1-18 (Springer US, 2009).

43 Rechendorff, K., Hovgaard, M. B., Foss, M., Zhdanov, V. & Besenbacher, F. Enhancement of protein adsorption induced by surface roughness. *Langmuir* **22**, 10885-10888 (2006).

44 Deligianni, D. D. *et al.* Effect of surface roughness of the titanium alloy Ti–6Al–4V on human bone marrow cell response and on protein adsorption. *Biomaterials* **22**, 1241-1251 (2001).

45 Tran, P. A., Zhang, L. & Webster, T. J. Carbon nanofibers and carbon nanotubes in regenerative medicine. *Advanced Drug Delivery Reviews* **61**, 1097-1114, doi:http://dx.doi.org/10.1016/j.addr.2009.07.010 (2009).

46 Li, X. *et al.* Effect of carbon nanotubes on cellular functions in vitro. *Journal of Biomedical Materials Research Part A* **91**, 132-139 (2009).

47 Webster, T. J., Schadler, L. S., Siegel, R. W. & Bizios, R. Mechanisms of enhanced osteoblast adhesion on nanophase alumina involve vitronectin. *Tissue engineering* **7**, 291-301 (2001).

48 Karajanagi, S. S., Vertegel, A. A., Kane, R. S. & Dordick, J. S. Structure and function of enzymes adsorbed onto single-walled carbon nanotubes. *Langmuir* **20**, 11594-11599 (2004).

49 Grayson, W. L., Martens, T. P., Eng, G. M., Radisic, M. & Vunjak-Novakovic, G. in *Seminars in cell & developmental biology.* 665-673 (Elsevier).

50 Grayson, W. L. *et al.* Effects of initial seeding density and fluid perfusion rate on formation of tissue-engineered bone. *Tissue Engineering Part A* **14**, 1809-1820 (2008).

51 Hahn, B.-D. *et al.* Mechanical and in vitro biological performances of hydroxyapatite–carbon nanotube composite coatings deposited on Ti by aerosol deposition. *Acta Biomaterialia* **5**, 3205-3214 (2009).

52 Engler, A. J., Sen, S., Sweeney, H. L. & Discher, D. E. Matrix Elasticity Directs Stem Cell Lineage Specification. *Cell* **126**, 677-689, doi:http://dx.doi.org/10.1016/j.cell.2006.06.044 (2006).

53 Tutak, W. *et al.* Toxicity induced enhanced extracellular matrix production in osteoblastic cells cultured on single-walled carbon nanotube networks. *Nanotechnology* **20**, 255101 (2009).

Chapter 5

Conclusions and Future Work

Conclusions

Carbon nanomaterial assemblies possess unique physicochemical properties which can be utilized and engineered for many biomedical applications including biosensors, protective coatings, antibacterial surfaces, and tissue engineering. In Chapter 1, we have reviewed the promise and prospect of each of these applications along with the challenges which need to be resolved for each. Of these applications, the most studied of the applications is tissue engineering, particularly bone tissue engineering. However, to utilize these materials in tissue engineering applications, robust assemblies into larger scale structures are required. Two-dimensional coatings and films can provide distinct advantages for bone tissue engineering, being an osteoconductive surface for stem cells to grow and differentiate as well as support osteoblast growth and mineralization. Previous studies utilizing carbon nanomaterial substrates for bone tissue engineering have utilized many different fabrication techniques to make the substrates. Commonly used techniques include chemical vapor deposition, vacuum filtration, and spray coating. Although these techniques provide promising results, there are many challenges in the assembly and fabrication of robust two dimensional architectures which hinders carbon nanomaterial coatings in clinical tissue engineering applications. While the lack of strong nanomaterial bonding in these assemblies is a challenge for tissue engineering applications, it is also a major challenge to the other applications of two-dimensional carbon nanomaterial substrates. Also, while there are many studies which directly compared carbon nanomaterial surface chemistry or utilize unique allotropes of graphene, there are no studies directly comparing the efficacy of various carbon materials (including carbon nanotubes of different diameters and various forms of graphene) for bone tissue engineering applications.

In Chapter 2 we reported and demonstrated a first of its kind, proof of concept study which shows carbon nanotubes can be *in situ* chemically crosslinked into macroscopic coatings via a spray coating technique. The method resulted in more robust multiwalled carbon nanotube coatings while maintaining the sp^2 hybridized architecture of the nanomaterial. This also resulted in maintaining good electrical conductivity in the macroscopic coatings. The coatings were also cytocompatible to human adipose derived stem cells, a multi-potent stem cell capable of differentiation into osteogenic lineages. However the coatings fabricated in this study were highly inhomogeneous, in regards to the surface roughness and the technique not being automated therefore, the airbrush coating method used cannot make batch-to-batch reproducible coatings. Furthermore, the high pressure at the inlet of the airbrush can also disrupt the coating as we build larger layer-on-layer structures. Therefore we needed to optimize a method to fabricate *in situ* chemically crosslinked films in a reproducible, automated manner (to reduce user errors) with more uniform surface roughness.

In Chapter 3 we describe work where we optimized and developed an automated, ultrasonic spray coating system to fabricate reproducible, *in situ* chemically crosslinked carbon nanotube (single walled and multi walled, with different diameters) and graphene (nanoplatelets and nanoribbons) coatings on titanium substrates. While the technique we developed here can easily be adapted for multiple applications, our primary focus for these studies were for bone tissue engineering applications. Therefore we used titanium substrates as they are commonly used in many orthopedic implant applications. The coatings produced in this method were more uniform then the previously employed airbrushing method with lower surface roughness for the multiwalled carbon nanotube substrates. Another advantage to the ultrasonic spray technique, over the airbrush technique, is the ultrasonic nozzle which simultaneously creates uniformly sized

droplets and disperses the nanomaterial by sonication. With different diameter nanotubes and the different graphene substrates we observed unique quasi-static elastic modulus and hardness values dependent on the nanoarchitecture. The carbon nanomaterial coatings also showed interesting viscoelastic mechanical properties as shown by nanoscale dynamic mechanical analysis. Furthermore we demonstrated, as proof of concept, *in situ* chemical crosslinking can layer-on-layer create free standing, porous, three dimensional structures of carbon nanotubes while maintaining more than 80% of the carbon nanotube architecture, as determined by thermogravimetric analysis.

Lastly, we utilized these coatings and studied the effects of nanotopography and surface chemistry on stem cell differentiation towards osteogenic lineages. We found carbon nanotubes provide the most osteoconductive surface, while graphene particles lead to greatest auto-mineralization of calcium. The insights gained from this study provides a basis for comparing carbon nanomaterial related efficacy in bone tissue engineering applications.

Future Work

This worked has opened many avenues for future studies. While in the aforementioned work, we have described a novel fabrication method for crosslinked carbon nanomaterial coatings and films, the technology can significantly benefit with many improvements. Furthermore, for clinical application in bone tissue engineering, there a many studies which need to be completed before clinical studies are performed. Below we have summarize a few of the studies which would further expand and develop the fabrication technique and the application as an osteoconductive coating for bone tissue engineering.

1) Further improvements can be made on the chemical crosslinking method to create more robust coatings. To increase the elastic modulus and hardness of the coatings, we hypothesize that we need to increase the crosslinking efficiency. We predict this can be done in a few ways. A) We can include a chemical crosslinker to bridge between nanomaterials to reduce steric hindrances which may be encountered by crosslinking pristine carbon nanomaterials. B) Since the *in* situ crosslinking process is a short process when the droplet of nanomaterial and initiator reaches the heated surface, utilizing a radical accelerators to catalyze free radical generation can increase the crosslinking efficiency. C) Using an inert chamber (N_2 purged) to perform the spray coating can alleviate quenching of the free radical initiators and would therefore require less concentration of the radical initiator in the dispersion.
2) While we provide some *in vitro* assessment of biocompatibility for these coatings, further investigation of the *in vitro* and *in vivo* biocompatibility is required. For *in vitro* cytocompatibility assessment, further assessment of toxicity mechanism should be

identified for SWCNT and MWCNT substrates. This includes, but not limited to, apoptosis, necrosis, genotoxicity, wear particle toxicity, and toxicity assessment using more cell types (including pre-osteoblasts, osteoblasts, fibroblasts, etc.). For *in vivo* biocompatibility, both subcutaneous pocket and in-bone assessment of toxicity needs to be performed in small animal rat models. For both small and large animal models, we would also be required to determine the outcome of effective bone growth on these substrates.

3) The sp^2 hybridized chemistry of carbon nanomaterials allows for many functionalization to improve application specific properties of the nanomaterials. These can be functional groups like carboxyl, carbonyl, amines, etc. which affect the surface charge of the nanomaterials. Macromolecular functionalization with synthetic (e.g. poly ethylene glycol) or natural (e.g. collagen) polymers can impart bio-inertness or improve cell adhesion. The crosslinked carbon nanomaterial substrates can provide an excellent platform for functionalization with peptides for cell growth or osteogenic inducing agents (e.g. bone morphogenic protein-2) which may further accelerate stem cell differentiation. Furthermore, the carbon nanomaterial substrates can also be a platform for loading drugs to help improve bone growth in defect sites, such as bisphosphonates.
4) Three dimensional carbon nanomaterial assemblies may also have many applications. While we showed a proof of concept study for 3D, layer-on-layer assembled crosslinked carbon nanomaterials, further optimization is required. To fabricate larger scale 3D structures we need even heat distribution of the 3D structure for efficient crosslinking. Furthermore, we need to implement a method to correctly move the z-axis of the spray coating system since we are layering materials with nanosized dimensions. Furthermore,

to print 3D structures with controlled substructures, similar to extrusion 3D printing technologies, would open avenues for fabricating complex carbon nanomaterial frameworks.